Effects of Confining Pressure and Static Shear on Liquefaction Resistance of Fraser River Sand

By

James David Stedman

B.A.Sc. University of British Columbia, 1994

A THESIS SUBMITTED IN PARTIAL FULFILMENT OF

THE REQUIREMENTS FOR THE DEGREE OF

MASTER OF APPLIED SCIENCE

in

THE FACULTY OF GRADUATE STUDIES

Department of Civil Engineering

We accept thesis as conforming

To the required standards

THE UNIVERSITY OF BRITISH COLUMBIA

September 1997

In presenting this thesis in partial fulfilment of the requirements for an advanced degree at the University of British Columbia, I agree that the Library shall make it freely available for reference and study. I further agree that permission for extensive copying of this thesis for scholarly purposes may be granted by the head of my department or by his or her representatives. It is understood that copying or publication of this thesis for financial gain shall not be allowed without my written permission.

Department of Civil Engineering

The University of British Columbia
Vancouver, Canada

Date 10/11/1997

DE-6 (2/88)

ABSTRACT

A comprehensive investigation into the effects of confining stress and static shear levels on the resistance to liquefaction of Fraser river sand is presented. A wide range of initial states characterized by static shear, confining stress and relative density levels are considered. It is shown that both K_σ and K_α factors that are used to modify the cyclic resistance value at a reference confining stress of 100 kPa and no static shear to account for higher confining stresses and static shear depend on all initial state parameters; density, confining stress and static shear levels. The currently used modifying factors K_σ, K_α proposed by Seed and Harder (1990) grossly underestimate the cyclic resistance of Fraser river sand regardless of the magnitude of confining stress, static shear and relative density. The under prediction is the largest for loose density states for which the greatest potential for liquefaction exists.

TABLE OF CONTENTS

LIST OF FIGURES

LIST OF SYMBOLS

CRR	Cyclic resistance ratio
CSR	Critical stress ratio
D_r, D_{rc}	Relative density after consolidation
e_c	Void ratio after consolidation
e_i	Void ratio after pluviation, $\sigma'_v \approx 1$ kPa
e_{20}	Void ratio after consolidation to 20 kPa
ESR	Effective stress ratio, σ'_1/σ'_3
K_c	Consolidation stress ratio, σ'_v / σ'_h
K_α	Empirical correction factor for static shear stress
K_σ	Empirical correction factor for confining stress
N	Number of loading cycles
α	Static shear stress to normal stress ratio
ΔU	Change in pore water pressure
ε_a	Axial strain
Φ_{csr}	Friction angle at critical stress ratio
Φ_{PT}	Friction angle at phase transformation
σ'_1	Effective major principal stress
σ'_3	Effective minor principal stress
$\sigma'_{d,cy}$	Cyclic deviator stress

σ'_h	Horizontal effective stress
σ'_{nc}	Effective normal stress on 45° plane at the end of consolidation
σ'_v	Vertical effective stress
τ_{cy}/σ'_{3c}	Cyclic stress ratio (= $\sigma'_{d,cy}/2\sigma'_{3c}$)

ACKNOWLEDGEMENTS

The author wishes to express his thanks to his supervisor for guidance in all things including this work. Without the insight and encouragement of Professor Y. P. Vaid none of this would have been possible. The author would also like to thank Dr. Byrne, Dr. Finn, Dr. Campanella and Dr. Fannin for advancing his knowledge of soil mechanics.

The assistance of the civil engineering machine shop personnel and in particular, Mr. Harald Schremp and Mr. Dick Postgate for the fabrication of testing equipment is gratefully acknowledged. The camaraderie and insight provided by fellow students Siva Sivathayalan, Ali Eldorani Akbar and Anthony Fuller made the years at the University of British Columbia rewarding in a professional and personal manner.

Chapter 1

INTRODUCTION

Earth structures comprised of saturated sands and superstructures founded on such materials have suffered extensive damage during earthquakes (e.g. Alaska, 1964; Niigata, 1964 and Kobe, 1995). This damage has been attributed to the phenomenon of sand liquefaction. The term liquefaction signifies all phenomena involving excessive deformation of saturated cohesionless materials.

Earthquake loading, being of short duration causes saturated sands to undergo shear deformation under undrained conditions. This causes the pore pressure to rise, and the accompanied decrease in effective stress could trigger excessive deformation. These deformations may be caused by either a reduction in shear strength or a progressive reduction in the stiffness of sand with cycles of loading.

Most of the fundamental understanding of sand liquefaction has been derived from controlled laboratory studies. The cyclic simple shear test is considered ideal for simulating earthquake loading of horizontal elements of sand under level ground. The complexity of this device has however resulted in the use of the cyclic triaxial test on hydrostatically consolidated specimens. This substitution assumes that the stress conditions on 45° planes in the triaxial specimen are equivalent to those on horizontal

planes in the simple shear, and further, empirical reduction factors are applied to the triaxial results to account for the different stress conditions in the two types of tests.

Initial static shear stress conditions on horizontal soil elements under sloping ground are simulated in the triaxial test by using anisotropically consolidated specimens with principal stresses σ'_{1c} and σ'_{3c} ($K_c = \sigma'_{1c} / \sigma'_{3c}$). On the 45° plane therefore the static shear stress to normal stress ratio, $\alpha = \frac{\sigma'_{1c} - \sigma'_{3c}}{\sigma'_{1c} + \sigma'_{3c}}$. α is regarded as a measure of the initial static shear stress level.

The resistance to liquefaction in a cyclic triaxial test is defined as the uniform amplitude cyclic stress ratio $CRR = \frac{\sigma_{dcy}}{2\sigma'_{3c}}$ (σ_{dcy} = cyclic deviator stress) that causes a specified level of axial strain in a specified number of load cycles. Laboratory studies have revealed that for a given sand $CRR = f(D_r, \sigma'_{nc}, \alpha)$ in which D_r = relative density of the sand and σ'_n is a measure of the initial confining stress. For the simple shear conditions, there is no ambiguity regarding the specification of σ'_n, which is taken as the initial vertical effective confining stress σ'_{vo}. In the triaxial tests $\sigma'_{nc} = \frac{(\sigma'_{1c} + \sigma'_{3c})}{2}$, it's value on the 45° plane.

In practice the cyclic loading resistance of sand is often assessed by cyclic triaxial tests on isotropically consolidated specimens $\alpha = 0$, at generally one value of the confining stress σ'_{nc} level. The resistance at an arbitrary σ'_{nc} and α is then estimated by applying empirical modifying factors K_σ and K_α as

$$(CRR)_{\sigma'_n,\alpha} = (CRR)_{\sigma'_n=100kPa,\alpha=0} \times K_\alpha \times K_\sigma \qquad (1)$$

in which $(CRR)_{\sigma'_n=100kPa,\alpha=0}$ represents the cyclic resistance of initially hydrostatically consolidated specimens at $\sigma'_n = \sigma'_{3c}$ = 100 kPa and $K_{\sigma'_n} = \frac{(CRR)_{\sigma'_n,0}}{(CRR)_{100,0}}$ and $K_\alpha = \frac{(CRR)_{\sigma'_n,\alpha}}{(CRR)_{\sigma'_n,0}}$. $K_{\sigma'_n}$ depends on the level of σ'_{nc} and a relationship between $K_{\sigma'_n}$ and σ'_{nc} has been proposed by Seed and Harder (1990). In general $K_{\sigma'_n}$ decreases substantially with increase in σ'_n, but no dependence of $K_{\sigma'_n}$ on D_r has been suggested. Recent experimental data (Vaid and Thomas, 1995) together with earlier simple shear data by Vaid et al. (1985) however suggests a strong dependence of $K_{\sigma'_n}$ on D_r. Furthermore, although not clear in the literature, the $K_{\sigma'_n}$ - σ'_{nc} relationship data apparently corresponds mostly to initially hydrostatic stress conditions (i.e. $\alpha = 0$) in the triaxial test. It is not known whether $K_{\sigma'_n}$, in addition, depends on the level of α.

K_α has been suggested to depend both on D_r and α. The proposed relationship (Seed 1990), however, represents a very large K_α range for a given α value for loose and medium D_r states. The relationship suggested are for σ'_{nc} < 300 kPa, and thus no dependence of K_α on σ'_{nc} has been implied.

The research reported in this thesis is aimed at a systematic investigation of the dependence of $K_{\sigma'_n}$ and K_α on D_r, σ'_{nc} and α. The effect of each variable is assessed independently by holding all others constant. Thus CRR under site specific D_r, σ'_{nc} and α conditions can be assessed. These measured CRR values are then compared with those implied by the current practice (eqn. 1) using suggested $K_{\sigma'_n}$ and K_α factors and

the situations where such extrapolations should not be used pointed out. Considering that the sand behaviour at a given density state is profoundly affected by the levels of σ'_{nc} and for a given σ'_{nc} by the level of α, the use of $K_{\sigma'_n}$ and K_α as independent factors for modifying the $(CRR)_{100,0}$ may not be completely sound.

Fraser River sand, which underlies the heavily populated Fraser Delta in B.C., was used for the investigations. Cyclic loading resistance was assessed for a range of D_r, σ'_{nc} and α values in order to explicitly define dependence of $K_{\sigma'_n}$ and K_α on these variables.

Chapter 2

LITERATURE REVIEW

Saturated cohesionless soils are susceptible to excessive deformations under undrained loading, and catastrophic damage has been caused as a result of such loading in the 1964 earthquakes in Alaska and Niigata. Since then, the undrained behaviour of saturated sands has been of interest to several researchers. Transient undrained state is induced in soil masses when they are subjected to sudden or dynamic loads, such as a shock or an earthquake.

Under a level ground the occurrence of liquefaction is on account of the high induced pore pressures. Under a sloping ground however, flow failure may develop as a consequence of static gravity stresses. The interest in the static undrained response has essentially focused on potential failure leading to flow failures. Under cyclic loading, however, the interest has been related to the accumulation of large strains, due to a progressive reduction in shear stiffness on account of the increase in pore pressure.

Monotonic loading behaviour

Monotonic (static) loading behaviour of saturated sands under triaxial loading conditions had been studied by several researchers (e.g. Castro 1969, Lee and Seed 1980, Chern 1985, Vaid and Thomas, 1994). The range of typical undrained response

of isotropically consolidated saturated sands in triaxial compression is shown in Fig. 2.1. Sand exhibiting strain softening type of response (type 1 & type 2) is termed contractive and the sand that strain hardens (type 3) is called dilative.

The type of response is primarily dependent upon the initial state of sand, represented by its relative density, confining and shear stresses, and the loading mode. Starting from a given initial stress state, the undrained response changes from a type 1 to type 3 with decreasing void ratio (increasing relative density), for a given loading mode.

Type 1 response has been called liquefaction by Castro (1969), Casagrande (1975) and Seed (1979) and true liquefaction by Chern (1985). The characteristic of this type of behaviour is unlimited continued deformation at constant stresses and void ratio, called flow failure or steady state deformation. The constant shear stress at which the sand undergoes unlimited deformation is called the steady state strength or residual strength.

Type 2 response which transforms in to a strain hardening type after the initial contractive type, has been called limited liquefaction by Chern (1985). In this type of response, there exists a finite range of strain over which the sand deforms at essentially constant void ratio and stresses.

For a given sand, contractive response is exhibited over a large range of void ratios in triaxial extension than in triaxial compression mode of loading (Vaid et al., 1989). This implies that at a given initial state, the sand may be dilative, and hence strain hardening in compression, but could be contractive, and hence strain softening in extension.

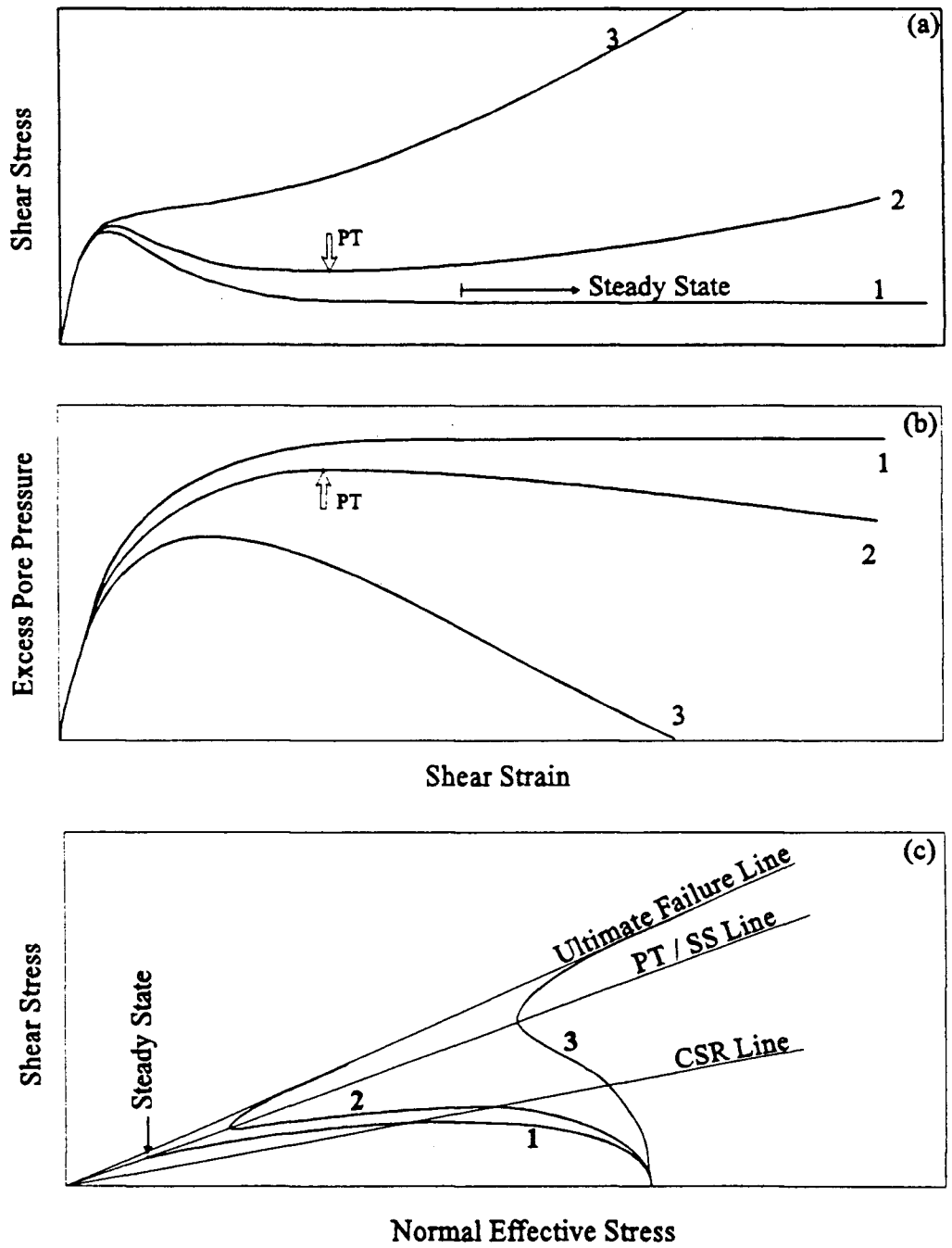

Fig. 2.1 Typical undrained behaviour of saturated sands (After Chern, 1985)

Initiation of Strain Softening

The instance of peak deviator stress in types 1 and 2 responses indicate the initiation of strain softening. The effective stress ratio corresponding to this peak shear stress has been termed the critical stress ratio (CSR) by Vaid and Chern (1983). The critical stress ratio is dependent on the loading mode. Chern (1985), Vaid et al. (1990), Kuerbis (1989) and Vaid and Chern (1985) concluded that CSR is unique for water pluviated sand in triaxial compression. However, Castro (1969) and Sladen et al (1985) have reported that CSR varies with the void ratio and confining stress level in triaxial compression for moist tamped specimens. This apparently is a manifestation of the effect of different specimen preparation techniques. CSR has been found to be dependent upon the deposition void ratio in triaxial extension (Vaid and Thomas, 1994) and in simple shear (Vaid and Sivathayalan, 1996) loading modes. The CSR values in triaxial extension and simple shear are considerably smaller than those in triaxial compression. This is an indication of the influence of loading mode on the undrained response, due to the inherently anisotropic fabric of sand that ensues on water pluviation.

Phase Transformation and Steady States

Considerable interest has been paid to the study of the true liquefaction behaviour. Most of the understanding of this phenomena has come from monotonic triaxial compression tests (Castro 1969, Castro et al., 1982; Casagrande, 1975). Based on tests on moist tamped specimens, Castro (1969) has shown that the effective

confining stress, shear stress and void ratio are uniquely related during steady state deformation.

The instance of maximum excess pore pressure in a type 2 response is called the state of phase transformation (Ishihara, 1975). The response of sand up to the instance of phase transformation (PT) is contractive and beyond PT is dilative. The termination of contractive behaviour is characterised by a sharp turnaround in the stress path. Many researchers have treated limited liquefaction response as steady state, ignoring the dilation of sand, beyond the PT state.

The angle of mobilised friction at steady state (for a type 1 response) is equal to that at phase transformation for a (type 2) response (Chern, 1985; Vaid and Thomas, 1994). The mobilised friction angle at phase transformation is found to be unique for a given sand, under a variety of loading conditions (Chern 1985; Vaid and Thomas, 1994). Neguessy et al. (1986) show that the friction angle at phase transformation is dependent only upon soil mineralogy and equal to the constant volume friction angle under drained conditions.

Ultimate failure envelope

On further straining beyond the PT state, the effective stress path rapidly approaches the line of maximum obliquity and any subsequent deformation progresses at a constant friction angle (Fig. 2.1). The angle of maximum obliquity has also been found to be unique for a water deposited sand (Vaid and Chern, 1985; Vaid and Thomas, 1994), regardless of relative density, stress levels, loading mode, sample

preparation technique or gradation (Kuerbis, 1989). Miura and Toki (1982), however, report that this angle varies somewhat with relative density and loading mode.

Cyclic Loading Behaviour

The undrained response of saturated sand under cyclic loading depends on a variety of factors; relative density, confining stress level and cyclic shear stress level being the most important. The stress conditions on a soil element in the field during an earthquake or wave loading are simulated in the laboratory by undrained cyclic simple shear tests or cyclic triaxial tests. The understanding of such response has mostly come from cyclic triaxial tests on isotropically consolidated specimens. Stress conditions in the field, however are invariably anisotropic. The initial anisotropic stress state has a profound impact in the manner in which strains develop during cyclic loading.

Mechanisms of Strain Development

Strain development during cyclic loading can either be due to true liquefaction, limited liquefaction or cyclic mobility -type1, type 2 or type 3 response shown in Fig. 2.2 (Castro, 1969; Vaid and Chern, 1985). Because of the different mechanisms that are responsible for strain development, the results of cyclic loading are generally assessed in terms of a fixed level of strain developed in a given number of cycles. The initial development of strain is associated with stiffness degradation with cycles of loading. Seed (1979) found that strain development is small until the excess pore pressure ratio $\Delta u/\sigma'_{3c}$ exceeds about 60%. In contractive sands (true or limited liquefaction type of response) however, large strains may develop without very high excess pore pressures.

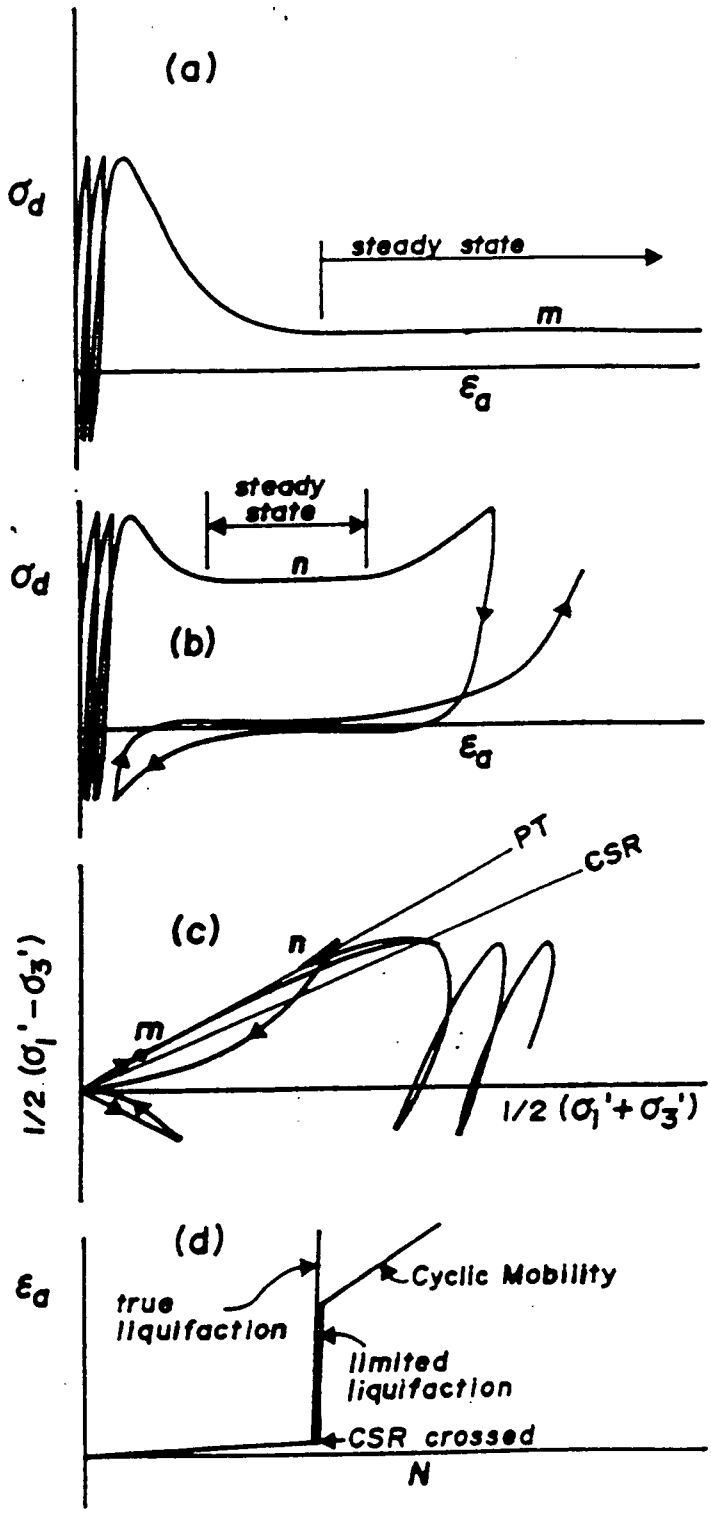

Fig. 2.2. Mechanisms of strain development during cyclic loading (After Chern, 1985)

A transient state of zero effective stress is normally a pre-requisite for large strain development due to cyclic mobility. Such a state of zero effective stress, however, will occur only if the cyclic stresses undergo stress reversal.

Castro (1969) and Vaid and Chern (1985) have demonstrated that true liquefaction and limited liquefaction type of responses develop in cyclic loading in the same manner as in monotonic loading. Vaid and Chern (1985) have also shown that contractive deformation in cyclic loading is triggered at the critical value of stress ratio, CSR observed under monotonic response. Upon the triggering of contractive deformation, unlimited strains occur in true liquefaction type of behaviour at finite stress levels. In limited liquefaction however, the strain development is associated with strain softening until the PT state and the stresses increase due to dilation, beyond the PT state. Subsequent unload cycle generally brings the sand to a state of zero effective stress $\sigma'_3 = 0$. Any further load cycles will take the sand through transient states of zero effective stress that cause strain accumulation.

No contractive deformation occurs in cyclic mobility type of response. But the continuous rise in pore pressure with increasing load cycles causes progressive stiffness degradation. Vaid and Chern (1985) observed that strain development is small until the sand reaches the PT state. Subsequent to PT state, the unloading pulse causes a large increase in excess pore pressure and takes the sample to very low effective stresses. Additional load cycles may take the sample through transient states of zero effective stress, that are responsible for strain accumulation.

Effect of confining stress

Castro (1969) recognised that Banding sand was more prone to true liquefaction failure under static loading as the confining stress increased. Vaid and Thomas (1994) demonstrate that at given density, increasing confining stress in triaxial compression loading promotes more contractive behaviour. However, increasing confining stress in triaxial extension loading was found to promote less contractive behaviour. The effect of confining stress was found to be less significance for the loosest deposited specimens (Vaid and Thomas, 1994).

The effect of increased confining pressures has been recognised to essentially decrease the cyclic resistance of a saturated sand. The extent of this effect, however, is not very well understood yet. Seed and Harder (1990) suggested the use of a correction factor K_σ, that is defined as the ratio between the cyclic stress ratio required to cause liquefaction at the given confining stress to that required to cause liquefaction at a reference stress state of $\sigma' = 100$ kPa. K_σ is always less than one for $\sigma' > 100$ kPa. The data presented by Seed and Harder (1990) show a large scatter in K_σ for a given confining stress (Fig. 2.3). This apparently indicates the dependency of K_σ on factors other than the confining stress. Vaid and Thomas (1994) show that K_σ depends, in addition, on the relative density of the sand, and is smaller in dense sand, than in most liquefaction prone loose sands. Comparative cyclic simple shear studies (Vaid and Sivathayalan, 1996) show that cyclic triaxial tests tend to over estimate K_σ at higher densities.

It is evident from the existing laboratory data that K_σ is dependent on relative density and loading mode, in addition to the level of confining stress. The influence of

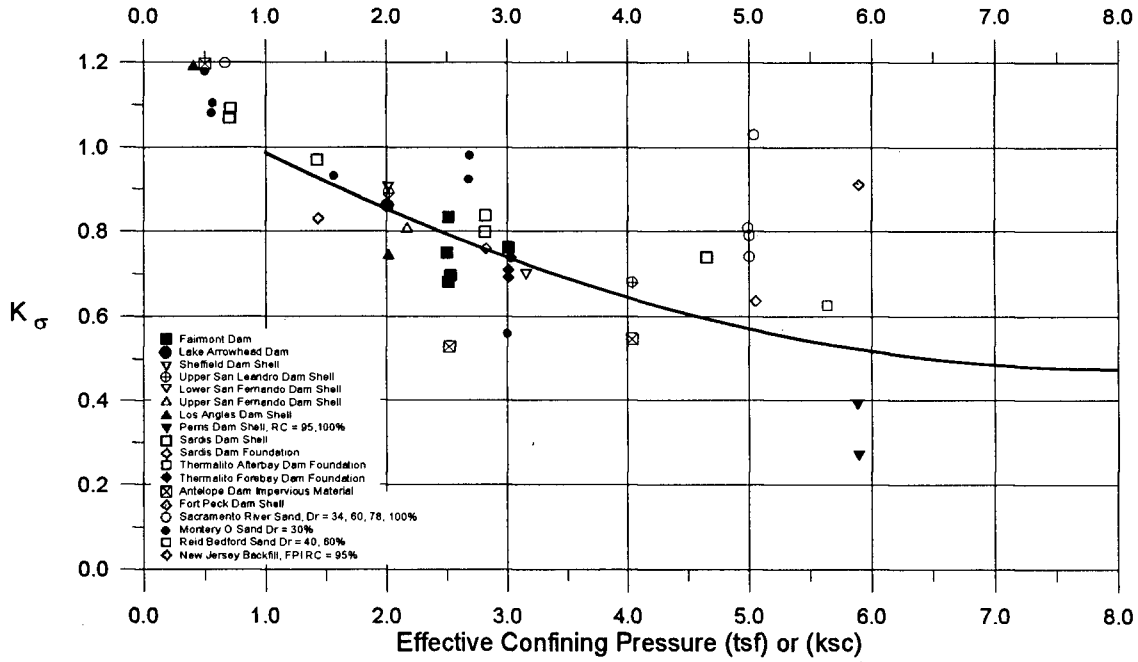

Fig. 2.3 Proposed Relationship between Vertical Effective Stress (σ'_o) and K_σ (Seed and Harder, 1990).

the presence of initial static shear (anisotropic initial conditions) however, is missing from all previous studies. It is very vital to know the effect of anisotropic initial stresses on K_{σ}, because the field stresses are invariably anisotropic.

Effect of Static Bias

Cyclic resistance of saturated sand deposits are commonly evaluated from cyclic triaxial tests on isotropically consolidated sand samples. Lee and Seed (1967) pioneered cyclic triaxial testing of anisotropically consolidated specimens. Studies by Lee and Seed (1967), Lee, et al. (1975), Seed, et al. (1975) and Seed (1983) conclude that the presence of static shear increases the cyclic resistance to liquefaction. Castro (1969, 1975), Casagrande (1976), Castro and Poulos (1977) and Castro, et al. (1982) have also performed cyclic triaxial tests on anisotropically consolidated saturated sands. They however, arrived at a conclusion that an increase in the static shear stress may decrease the cyclic resistance of sand to liquefaction. Studies by Vaid and Chern (1983) show that the effect of initial static shear on cyclic resistance depends on the relative density of the specimen and on the magnitude of the initial static shear together with the strain criterion used to define liquefaction.

Vaid and Finn (1978) and Vaid and Chern (1983, 1985) showed that without reference to the density state, the dependence of cyclic resistance on static shear was not rational. Contradiction in the past studies was explained by a systematic testing program controlling cyclic stress, confining and static shear stresses and densities resulted in the conclusion that the cyclic resistance of a given sand can either increase

or decrease depending on the density and the static bias, and is closely linked to the mechanism of strain development during cyclic loading.

Based on experimental information available at the time Seed and Harder (1990) incorporated the static bias effects into a convenient term K_α (Fig. 2.4). K_α represents the cyclic resistance under finite static shear when it is multiplied by level ground cyclic resistance. K_α is defined in Fig. 2.5.

Thus the current design approach estimates cyclic resistance at arbitrary σ' and α levels from the reference cyclic resistance at σ' = 100 kPa and α = 0 by the relation

$$(CRR)_{\sigma'_n,\alpha} = (CRR)_{\sigma'_n=100kPa,\alpha=0} \times K_\alpha \times K_\sigma \qquad (1)$$

The K_σ and K_α factors are treated as separable, despite some experimental evidence to the contrary. A clear understanding of the combined effect of confining stress and static shear would thus complement the present knowledge on the cyclic response of saturated sands as affected by the collective initial state. Such an understanding is essential in order to address any conservatism or unconservatism that may be present in the current empirical methods of estimating $(CRR)_{\sigma,\alpha}$ using factors K_σ and K_α.

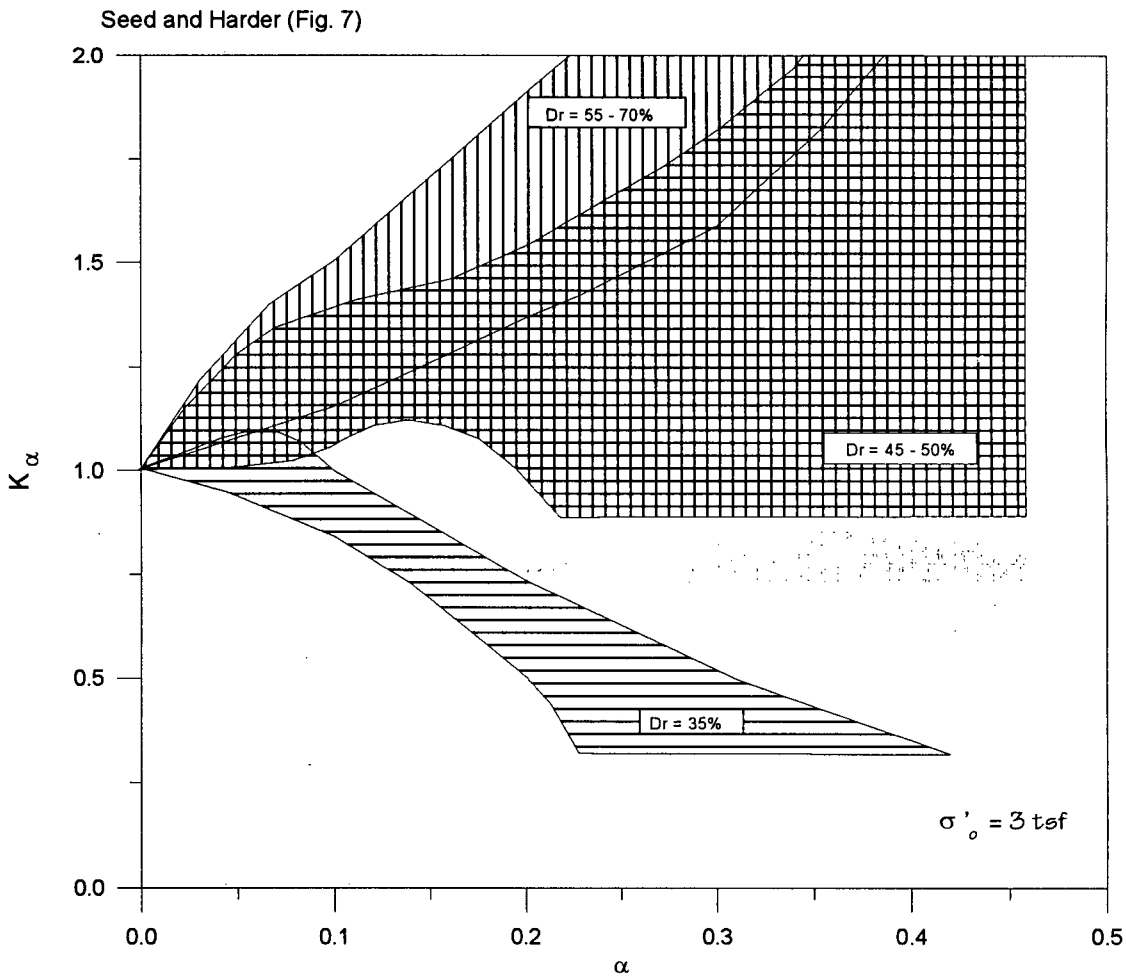

Fig. 2.4 Seed and Harder (1990) K_α Correction Factor.

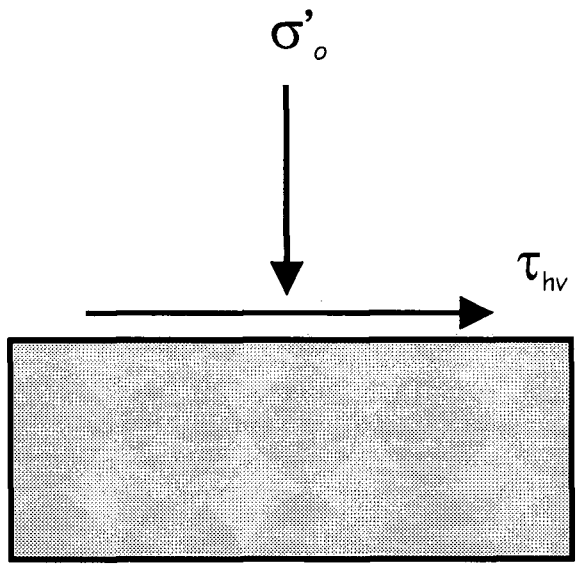

$$\alpha = \left| \frac{\tau_{hv}}{\sigma'_o} \right|$$

Fig. 2.5 Seed and Harder (1990) Definition of α.

Chapter 3

EXPERIMENTAL WORK

Material Tested

Sand, dredged from the Fraser River and stock piled at the south foot of No. 5 road in Richmond B.C., was used throughout the experimental work. Sand of this type underlies large portions of the heavily populated Fraser Delta and hence forms the strata of interest for liquefaction susceptibility. The material obtained was wet washed through a 1.00 mm sieve and the material retained was discarded. Similarly, the sand was then wet washed through a 0.10 mm sieve and the material passing discarded. The fraction coarser than 1.00 mm was about 3% and the finer than 0.10 mm only about 1.5%

The material tested visually conforms to a determination of the composition of Fraser River Sand made by Garrison et al. (1969), which was further confirmed by Tomlinson (1996). This analysis determined that the sand had a composition of 40% quartz, quartzite and chert 11% feldspar, 45% unstable rock fragments and the remaining 4% described as other. The grains are described as angular to sub rounded. A close visual inspection reveals grey sand with small but noticeable quantities of muscovite and biotite mica flakes. A grain size curve was produced and is shown in

Figure 3.1 together with photomicrograph. The average particle size (D_{50}) was determined to be 0.30 mm and the coefficient of uniformity (C_u) (ASTM D 2487) was found to be 1.85. The maximum and minimum void ratios determined according to ASTM 4254 and ASTM 4253 were found to be 0.926 and 0.605 respectively. The specific gravity was also determined to be 2.70 according to ASTM 854.

Testing Apparatus

All tests were performed in a triaxial loading frame with a pneumatic device being used for the anisotropic consolidation and cyclic loading stages. The integral mechanical linkage was utilised for the monotonic post cyclic and pre cyclic loading. A schematic diagram of the testing apparatus is shown in figure 3.2. All triaxial specimens had a nominal diameter of 63 mm and a nominal length of 130 mm. End restraint was minimised by caps and pedestals of polished and anodised aluminium with a central 21mm drainage stone. All pressures, force, displacement and volume changes were measured using electronic transducers interfaced to a computer via a signal conditioner.

The triaxial cells used for this program were standard cells and consisted of solid bases and a low friction (less than 0.1N) air bleed bushing seal for the loading ram. The reduction of the friction to a negligible amount is achieved by balancing the cell pressure against an equal pressure in the clearance between the ram and the bushing. This permits accurate measurement of axial forces outside of the cell.

The physical continuity of the loading ram from the sample, thence in series through the vertical loading piston permits the engagement of the strain controlled mechanism after either consolidation for the pre cyclic monotonic loading or post cyclic

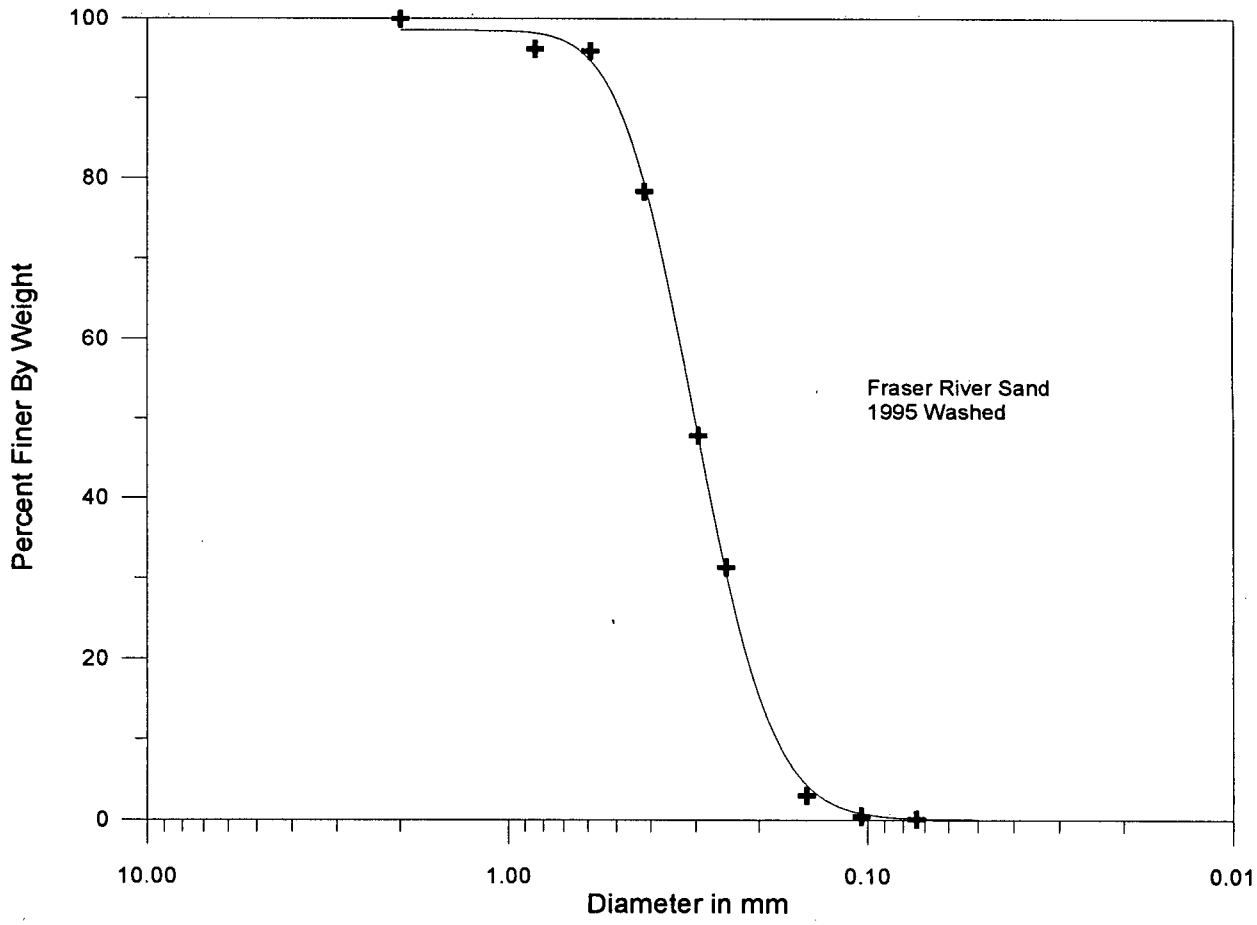

Fig. 3.1(a) Grain Size Distribution Curve for Fraser River Sand F95T

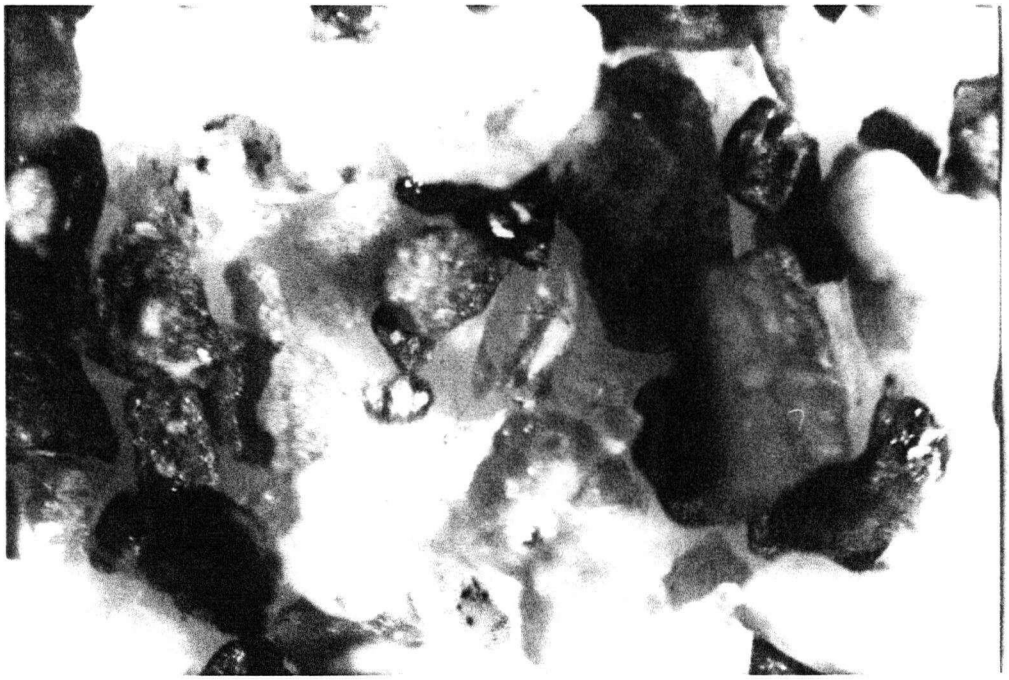

Figure 3.1(b) Photomicrograph of Fraser River Sand

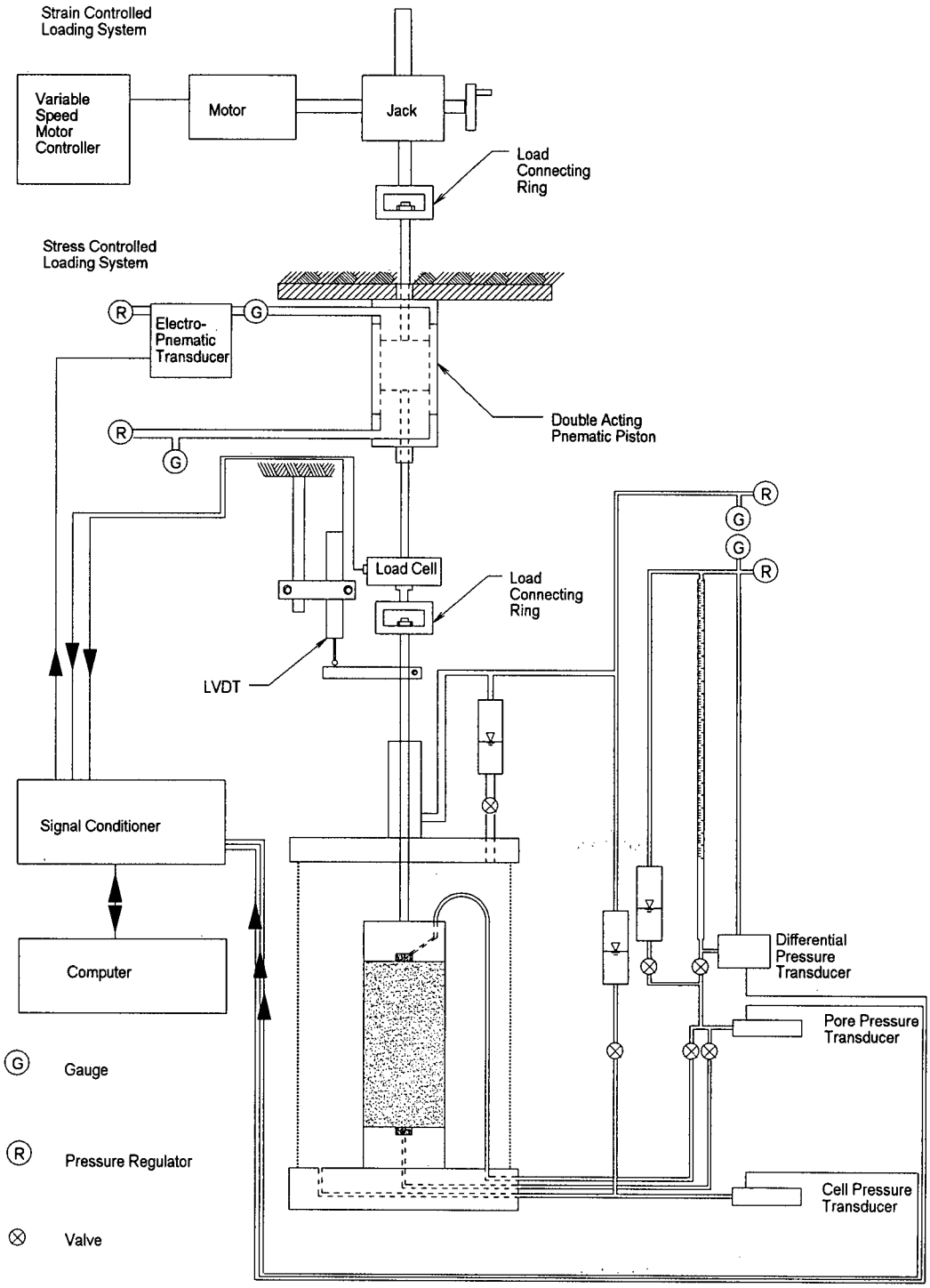

Fig. 3.2 Schematic diagram of cyclic and monotonic loading system for triaxial tests

monotonic loading without undue disturbance to the specimen. The piston also permits compressive force to be applied to the ram during consolidation to compensate for the uplift during hydrostatic consolidation or the desired deviatoric stress during anisotropic consolidation

Consolidation

Test samples were consolidated to the targeted confining stress - hydrostatic or anisotropic state after ensuring full saturation by B value measurement. The consolidation procedure consisted of setting the back pressure to it's post B Value, opening the drainage valve, bringing the sample to the required stress ratio K_c by increasing the vertical stress and then moving smoothly either up a constant K_c line, or horizontally (K_c = 1) across the mean normal stress axis until the targeted mean effective stress σ'_{nc} was reached by altering the cell pressure (Fig. 3.3).

Precyclic Monotonic Static Loading

Specimens, isotropically or anisotropically consolidated, were sheared under static strain controlled loading in extension or compression. A range of initial states (e_c, K_c, σ'_{3c}) was used to determine the spectrum of static undrained behaviour of the sand, and thus assess its possible impact on the mechanism of strain development during cyclic loading.

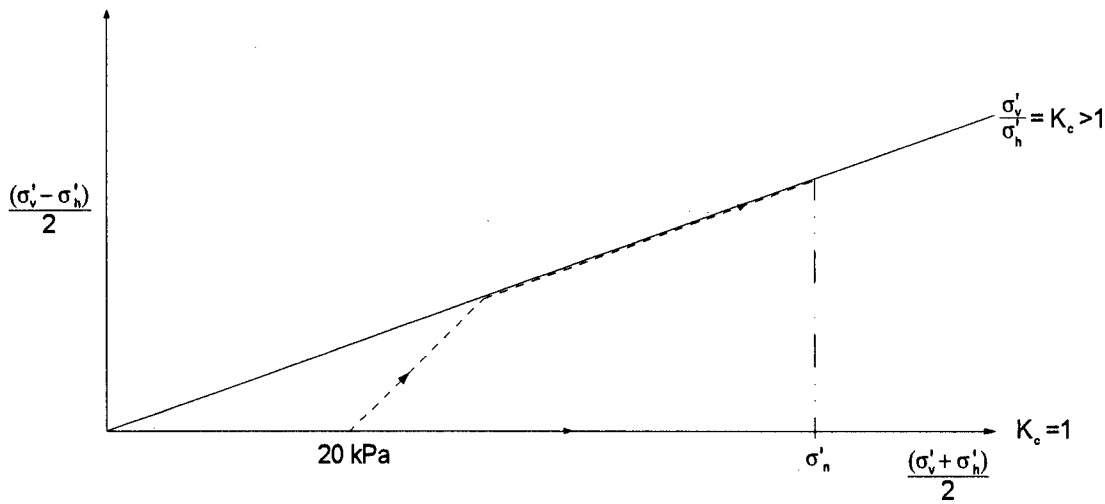

Fig. 3.3 Isotropic and anisotropic consolidation paths

Cyclic Loading

Cyclic axial loads were applied by changing the pressure on one side of the double acting piston shown in Fig. 3.2. In the normal configuration, the piston is freely floating with equal pressures on both sides. The pressure on the top is controlled by the electro pneumatic transducer. Changes in axial stress may be made by variations in the signal voltage supplied by the signal conditioner to the electropneumatic transducer. The determination of the cyclic stress level required for each sample was based on the sample area and the targeted cyclic stress ratio. This was accomplished by first calibrating the system with the aid of a dummy solid bar in place of the sample. The electrical signal to the electro pneumatic transducer consisted of a sine wave variation in the voltage, and hence load, with the first quarter pulse being in the triaxial compression mode. This applied cyclic stress was superimposed on top of the vertical stress already applied either to overcome the hydrostatic ram uplift or the force necessary to achieve anisotropic consolidation. The frequency of the cyclic loading pulse was 0.1 Hz; this was used to achieve a reasonable degree of resolution from the instruments. The frequency of loading however has been shown to have little influence on the undrained response of sand (Yoshimi and Oh-Oka 1975). The data was recorded at a rate of 48 points per cycle.

If the drainage line to the cell pressure reservoir (see Fig. 3.2) is too narrow; the rapid movement of the loading ram into and out of the cell would introduce pressure fluctuation in the cell when the sample was straining. This problem was avoided by opening the valve at the top of the cell which leads directly into a Plexiglas reservoir having the same pressure as the cell pressure supply. This arrangement permits a

much greater exchange rate of water into and out of the cell and hence does not cause any appreciable fluctuation in the cell pressure. This valve was kept closed except during cyclic loading in order to retard the diffusion of air into the cell fluid.

Post Cyclic Loading

Following cyclic loading the strain-controlled drive was connected to the loading ram on the upper end of the piston without straining the sample. The sample was then first unloaded to zero deviatoric stress, if initially anisotropically consolidated, and then loaded in compression or extension, or loaded directly in extension or compression, if initially isotropically consolidated. Numerous samples were subjected to load/unload or unload/load cycles in a strain controlled manner with the loading reversed either at the start of shear band formation in the extension loading phase, or at the limits of the equipment in the compression loading phase. All strain controlled testing, whether post or precyclic, was conducted at an axial strain rate of about 0.5 % per minute.

Instrumentation and Measurement Resolutions

Data acquisition was performed by a National Instrument 16 bit high-speed A/D card and high accuracy transducers. Appropriate corrections were applied to axial and radial stresses due to factors such as; membrane stiffness (Vaid and Kuerbis, 1989), half the sample weight, buoyant weight of the loading cap and ram and hydrostatic uplift on the ram. The measured pressures were accurate to ± 0.25 kPa. The volumetric strain was determined to have a resolution of 0.001% and the axial strain a resolution of

0.01%. The load cell resolution was 4 grams, which for an average area of 30 cm^2 represents a resolution of deviator stress of ± 0.01 kPa, this value being much lower than the cell pressure resolution can be disregarded.

Sample Preparation

All triaxial samples were prepared by water pluviation directly into the membrane lined cavity created by the forming split mold. This technique has been well established by several researchers (e.g. Vaid and Negussey, 1988) to yield consistently repeatable test samples. The ensuing fabric has been shown to duplicate the fabric of natural alluvial sands, such as Fraser River Sand, and hydraulic fills (Oda 1972). The method of depositing the sand in place through water also ensures complete elimination of air and hence yields saturated samples. Consistent loosest void ratios can be achieved by a careful elimination of vibrations during sample preparation. These void ratios reflect the loosest possible state for a given sand at a given effective stress level. Denser states can easily be achieved by applying vibration vertical to the cell base during and after pluviation of the sand. Water pluviation techniques for reconstituting homogenous specimens are restricted to poorly graded sands. Particle segregation would occur with this technique if the sand is well graded, and alternative techniques of water deposition are needed (Vaid and Kuerbis, 1989).

The sand was first boiled, cooled to room temperature under vacuum, and then pluviated through standing deaired water into the membrane lined mold cavity. Consistent deposition density was achieved by moving the tip of the flask in a circular or spiral manner while allowing the sand to rain out of the flask into the mold cavity. A 60

mm by 150 mm membrane, 0.3 mm thick was employed. During deposition, the tip of the flask was kept submerged until all of the sand had passed out of the flask. The top of the sample was then levelled with the aid of a siphon to ensure minimal disturbance to the fabric. Samples that required a slight increase in density were subjected to external vertical vibration after placing the top cap that provided a small seating load. Samples that required higher densities were subjected to external vibration both prior to siphoning and after placing the top cap.

The mold cavity internal mean area was determined prior to the start of the testing program and checked from time to time by the use of a differential pressure transducer and the mass of the water expelled from the cavity. This method removes the potential error of circumferencial measurement and minimises errors in void ratio computations (Vaid and Sivathayalan, 1996). Determination of the initial loosest deposition void ratio, e_i was made in all cases as soon as the top cap was placed. Loosest void ratios were close to the ASTM e_{max} as previously stated. After placement of the top cap and densification if required, the latex membrane was carefully rolled up onto the cap and sealed by an O-ring around the perimeter of the cap. The samples were then subjected to a vacuum of about 20 kPa in order to develop some effective stress. This permitted the removal of the mold without collapsing the sample. During the exposure to vacuum, the volume of water expelled from the sample was recorded by permitting flow only into a graduated burette. This coupled with the height of the sample (measured using a reference dial indicator) and the mean area of the mold permitted an accurate value for the sample volume to be determined at any point in the preparation and testing phase. The void ratio of the sample was determined after

exposure to vacuum and recorded as e_{20} for all samples. The lowest and e_i and e_{20} found were 0.929 and 0.880 respectively. The act of passing the sand from the flask directly into the water in the mold cavity resulted in consistently high B values, which indicate a high degree of saturation. No samples were tested at a B value of less than 0.98.

After the sample was prepared and the cell assembled, the cyclic load pulse was calibrated based on the area of the sample at this point for cyclic tests. The cell was then moved to the loading frame and securely clamped in place under the loading ram. Application of a slight cell pressure to overcome the previously applied vacuum permitted a small bead of water to exit the drainage lines to expel any air. Determination of the degree of saturation followed by increasing the confining pressure and measuring the pore pressure response under undrained conditions. As soon as a suitable B value had been achieved the sample was then consolidated incrementally either isotropically or anisotropically. Drainage was permitted to continue under the final increment, until no further volume change was noticed. This was further confirmed by temporarily closing the drainage line and briefly monitoring the pore pressure for any increase above the pre-set back pressure.

Testing Program

Monotonic Response

Loosest deposited samples were tested undrained monotonically in compression and extension at all selected initial stress conditions used in the cyclic testing program.

This information delineated the material properties of the sand, in particular the type of response - contractive or dilative - at each initial condition and permitted the relationship between monotonic and cyclic behaviour to be examined. Additionally, isotropically consolidated and low K_c value samples were tested in undrained extension, over a range of depositional densities and at the same mean confining stresses σ'_{nc} as the cyclic testing, to determine the effect of density and confining stress on the development of contractive behaviour. The restriction to isotropically consolidated and low K_c value states only was adopted because these initial states will develop strain defined as liquefaction in extension. At higher K_c values, compressive mode became susceptible to contractive response, if any, during cyclic loading.

Cyclic Loading Response

Cyclic tests were performed on both isotropically consolidated and anisotropically consolidated initial states. Samples were prepared at a variety of densities under a given initial confining pressure and K_c value. A series of such specimens were then loaded with fixed cyclic stress amplitude. Such data enabled the construction of a set of curves showing D_r as a function of the number of cycles, at several constant $\sigma_{dcy}/2\sigma'_{3c}$ levels. These in turn permitted the development of a set of curves for each set of conditions showing CRR as a function of D_r for liquefaction in a fixed number, say, 10 stress cycles (Fig. 3.4).

Similar data was generated at identical confining stresses but at other selected values of K_c. The information thus obtained at one confining stress was then developed at other mean confining stress levels. This experimental data was then used to develop

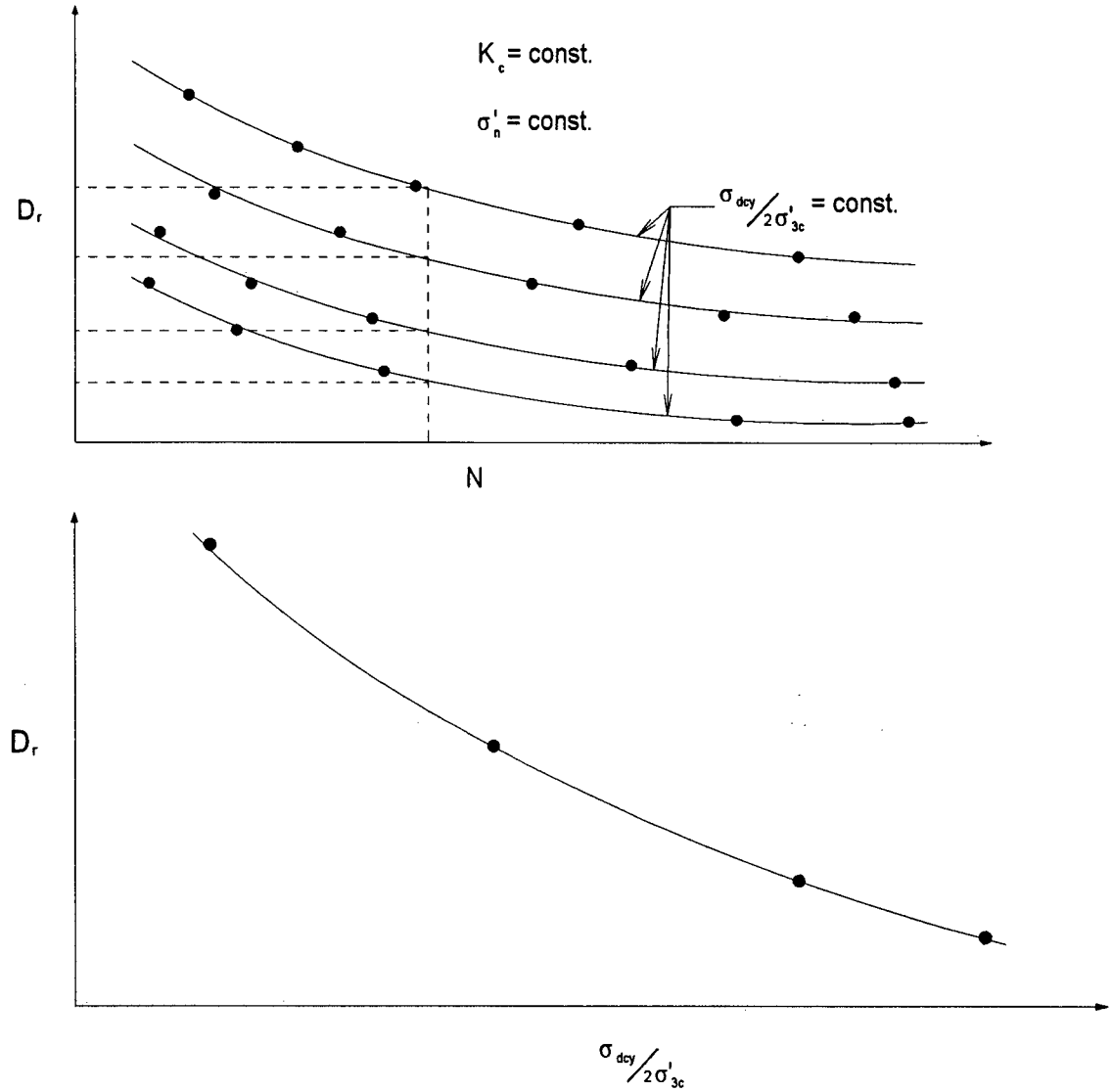

Fig. 3.4 Schematic Diagram of D_r Vs. Number of Cycles and D_r Vs. CRR showing cyclic resistance curve development at one σ'_{nc} and K_c.

a set of K_α versus α and $K_{\sigma'_n}$ versus σ'_n relations over a range of initial confining stresses and K_c values for a range of initial relative density states.

Post Cyclic Loading Response

Post cyclic monotonic loading tests were conducted on all cyclically loaded samples, after unloading the static deviator stress to zero, if any, under undrained conditions. They were then subjected to strain-controlled compression or extension monotonic loading to yield the post cyclic stress-strain behaviour of the sand. Many of the samples were subjected to a single load/unload or multiple unload/load cycles in order to asses the degradation in stiffness, both with increase in the amplitude of maximum strain as well as reversal in the mode of shearing.

Repeatability

Due to the limited supply of material and the large number of tests (over 300) required to complete this work, the material used in a tests at lower stresses was reused in the higher stress tests. Particle breakdown and other adverse affects on the material caused by the induced stresses affecting the results of the tests were addressed by performing monotonic loading tests on virgin and reused material. As can clearly be seen in Figs. 3.5 and 3.6 there is no detectable difference in either deviatoric stress or pore pressure response, and hence little effect on the material after one use.

The repeatability of the cyclic tests was also assessed by performing several tests, with identical initial conditions and identical cyclic stress ratio. Fig. 3.7 demonstrates excellent repeatability.

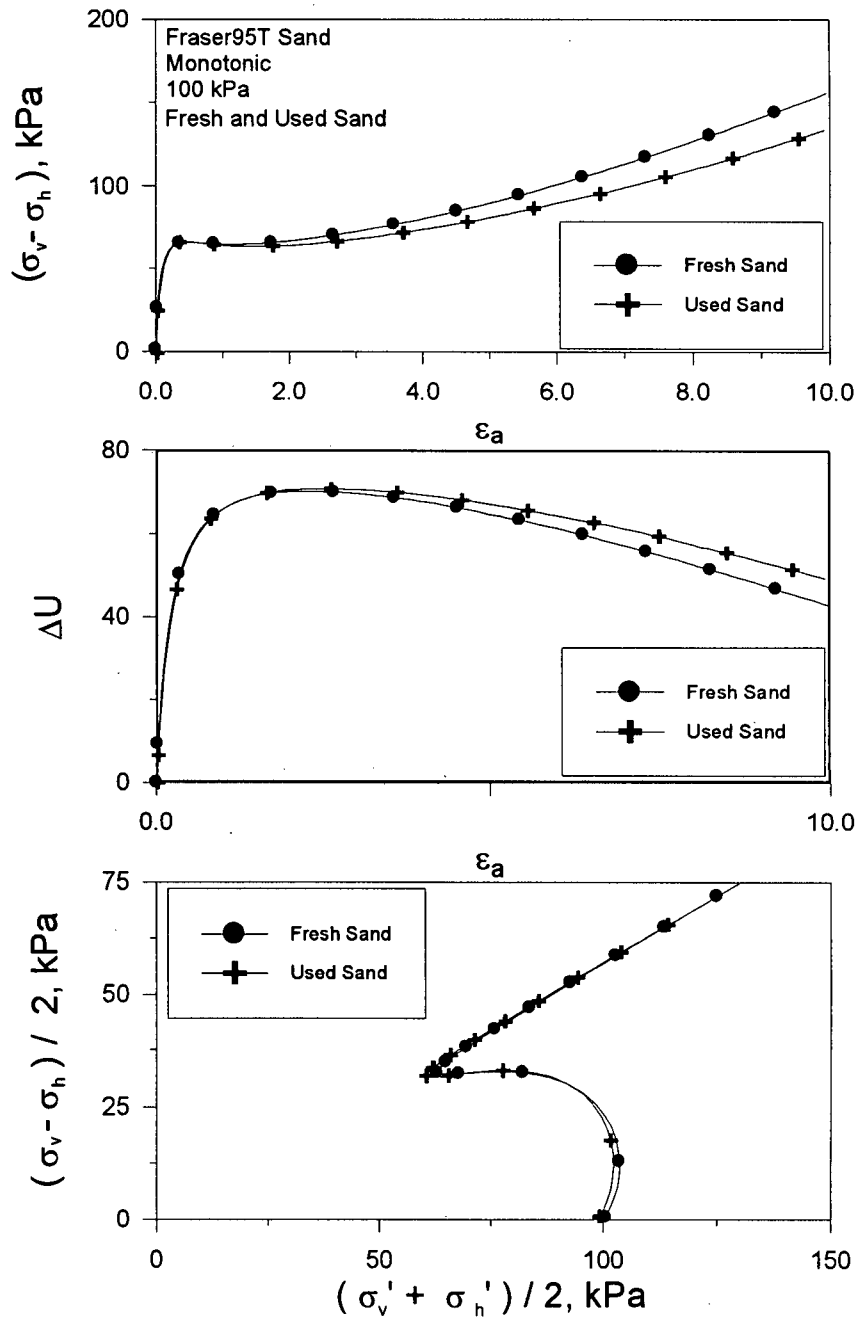

Fig. 3.5 Monotonic compression response of used and virgin sand at hydrostatic σ'_{nc} = 100 kPa

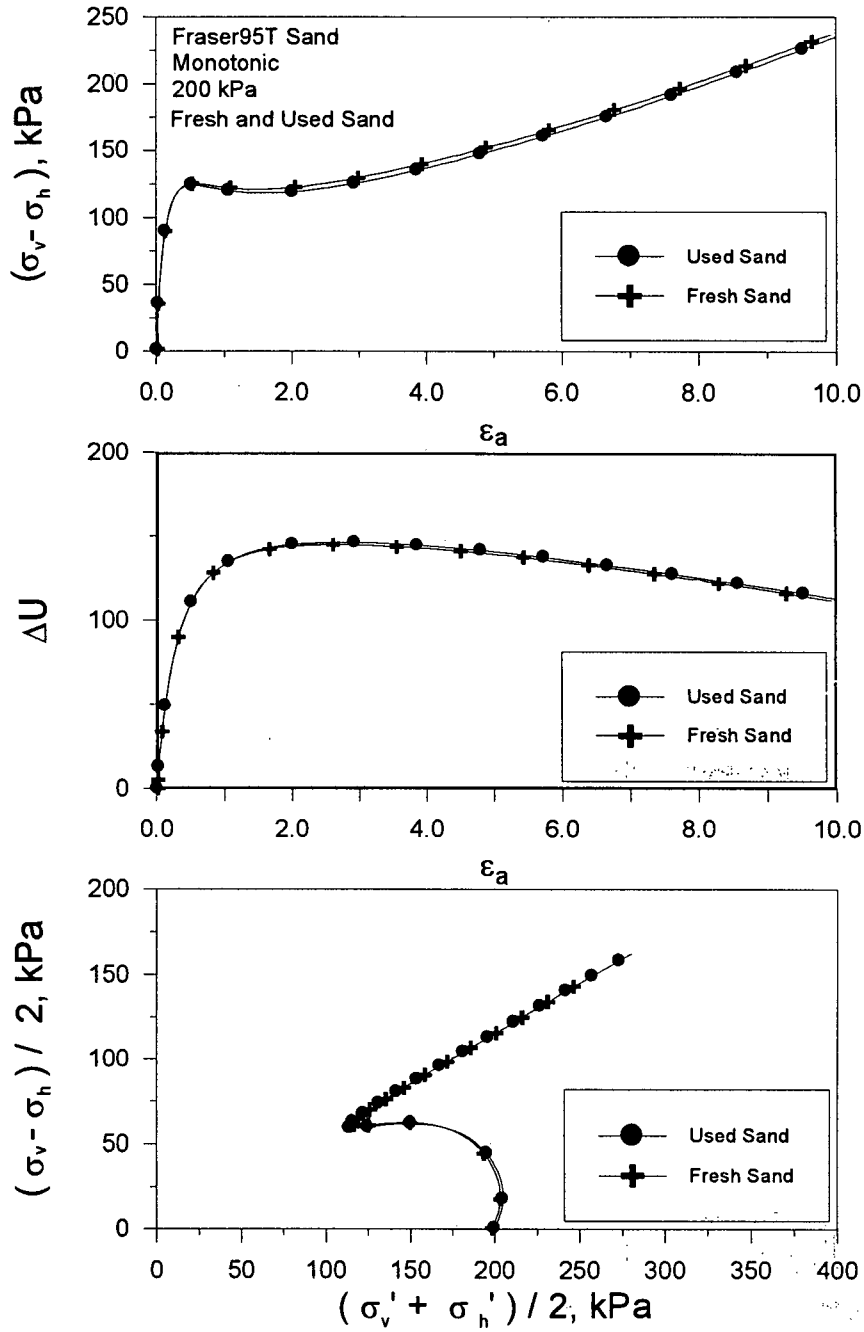

Fig. 3.6 Monotonic compression response of used and virgin sand at at hydrostatic σ'_{nc} = 200 kPa

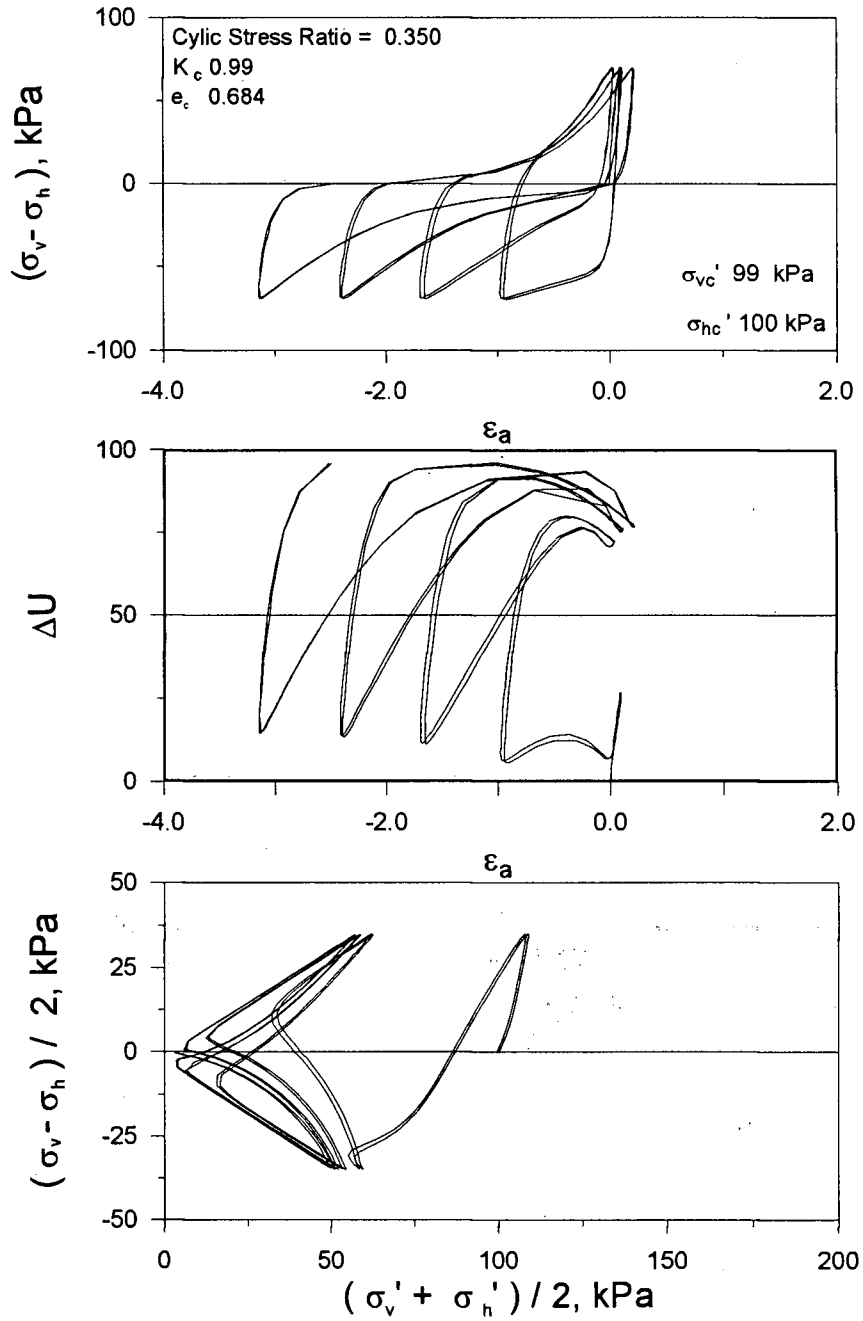

Fig. 3.7 Repeatability of cyclic response of hydrostatically consolidated sand at σ'_{nc} = 100 kPa.

Chapter 4

TEST RESULTS AND INTERPRETATIONS

Introduction.

This chapter presents the results of undrained static and cyclic triaxial tests on Fraser River sand. These tests encompass a range of initial states represented by the state variables e_c or relative density D_{rc}, confining pressure σ'_{nc} and static shear α. The bulk of the static tests in compression and extension were conducted on material in the loosest deposited state. This was done with the objective of delineating the initial states that may be susceptible to contractive deformation. Cyclic tests involving both stress reversal and non reversal were conducted, permitting the exploration of strain development to liquefaction by several different mechanisms: Contractive deformation, Cyclic mobility accompanied by excursions through states of transient $\sigma'_3 = 0$, or cyclic mobility without stress reversal and hence no transient $\sigma_3'=0$ states. Possible linkages between the cyclic and static behaviour are explored. Finally the cyclic resistance of the sand is characterised as influenced by the initial state variables. In particular, the effects of the static shear and confining stress on liquefaction resistance is examined or the premise that these variables influence behaviour collectively, and not independently, as currently assumed in practice, and further the nature of the influence depends on the initial density state.

In conventional triaxial testing σ_1' is vertical (perpendicular to the bedding planes) or horizontal. In order to distinguish between triaxial compression and extension the deviatoric stress will be expressed as $(\sigma'_v - \sigma'_h)$ instead of $(\sigma'_1 - \sigma'_3)$, thus positive deviator stress corresponds to compression and negative to extension mode of loading.

Accessible Density States

Fig 4.1 shows the compressibility characteristics of Fraser River Sand in the form of e log σ'_n relationships. Compressibility is shown at three different deposition void ratios - loosest to dense - loosest state e_{20} corresponds to deposition according to ASTM e_{max} (water pluviation) and a confinement of approximately 20 kPa following sample reconstitution. It may be noted that the loosest possible density states that are accessible depend on the mean effective confining stress level. They correspond respectively to 17%, 20%, and 24% corresponding to σ'_{nc} = 100, 200 and 400 kPa at which the tests were carried out. D_{rc} is thus not an independent variable but rather intimately linked to the stress state. The void ratio e_c is related to the mean confining stress and is essentially independent of K_c (Fig. 4.1).

Clearly, density states looser than D_{rc}=24% are not accessible to the sand at $\sigma'_{nc} \geq$ 400 kPa and states looser than D_{rc}=17% are not accessible to the sand at $\sigma'_{nc} \geq$ 100 kPa.

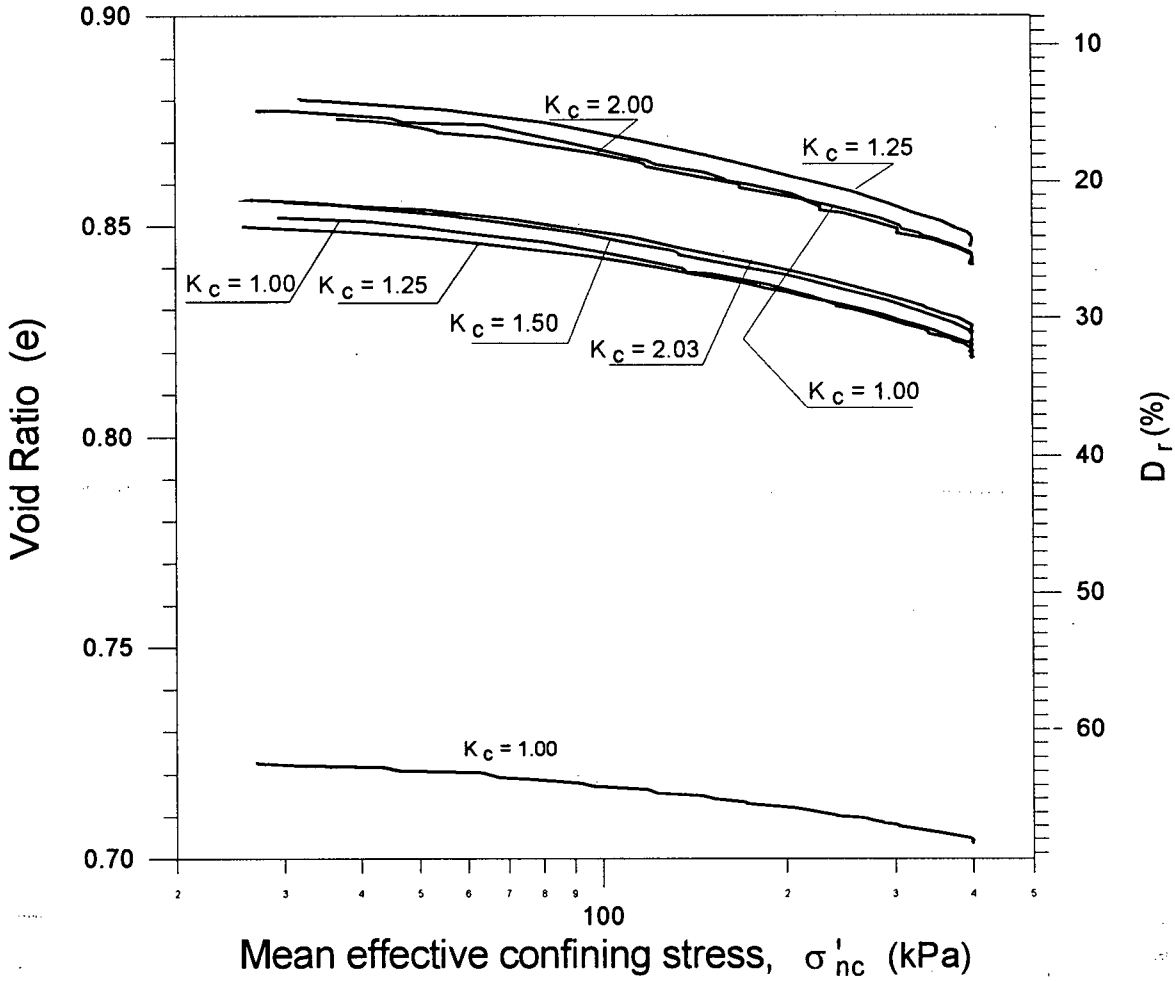

Fig 4.1 Compressibility of Fraser river sand at three different deposition densities

Static Behaviour

Fig. 4.2 shows the behaviour in compression for the loosest deposited sand at σ'_{nc} = 100, 200 and 400 kPa and K_c values of 1.0, 1.25, 1.5 and 2.0. It is apparent that the sand is only slightly contractive of the limited liquefaction type at all initial stress states considered. There is a slight tendency to increase the degree of contractivness with increasing σ'_{nc}, and for a given σ'_{nc} with an increase in the static shear. Both σ'_{nc} increase at constant K_c, and K_c increase at constant σ'_{nc} promote more contractive behaviour, despite the associated increase in density. At deposition void ratios denser than the loosest, the behaviour in compression was dilative, regardless of σ'_{nc} and K_c levels.

The behaviour in triaxial extension of the loosest deposited sand (Fig. 4.3) at initial states identical to those in compression reveals that at low σ'_{nc} the material exhibits contractive behaviour of the steady state type, regardless of the static shear level. At higher σ'_{nc} contractive deformation of the limited liquefaction type occurs. Thus, an increase in confining stress, σ'_{nc} at constant K_c decreases contractivness and an increase in K_c at constant σ'_{nc} increases contractivness somewhat, but only at higher σ'_{nc} levels. The effect of increasing σ'_{nc} is opposite of that found in compression loading at the same initial conditions. Vaid and Thomas (1995) have reported similar comparative behaviour in compression and extension on a slightly different batch of this sand.

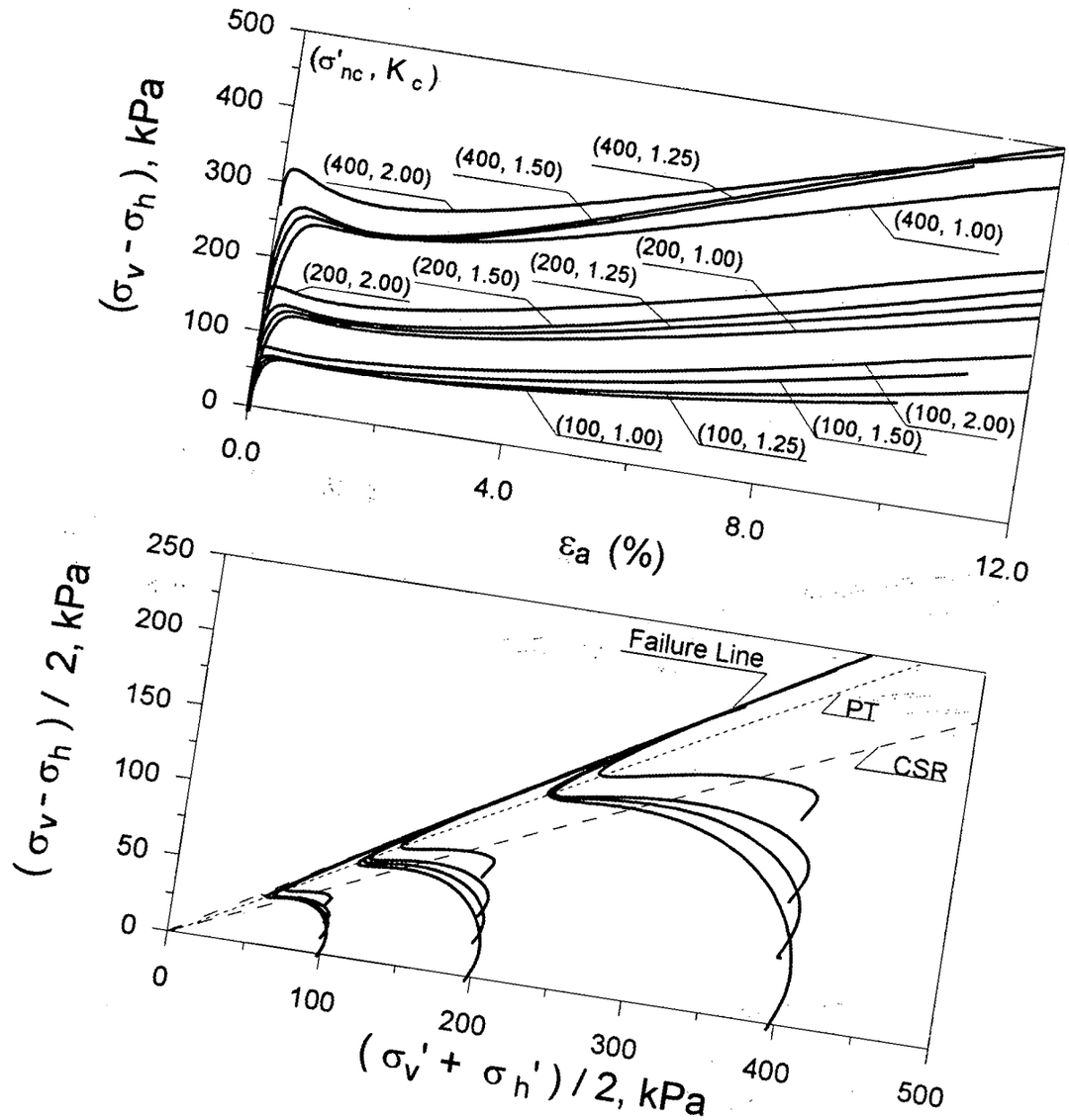

Fig 4.2 Behaviour of loosest deposited Fraser river sand in compression

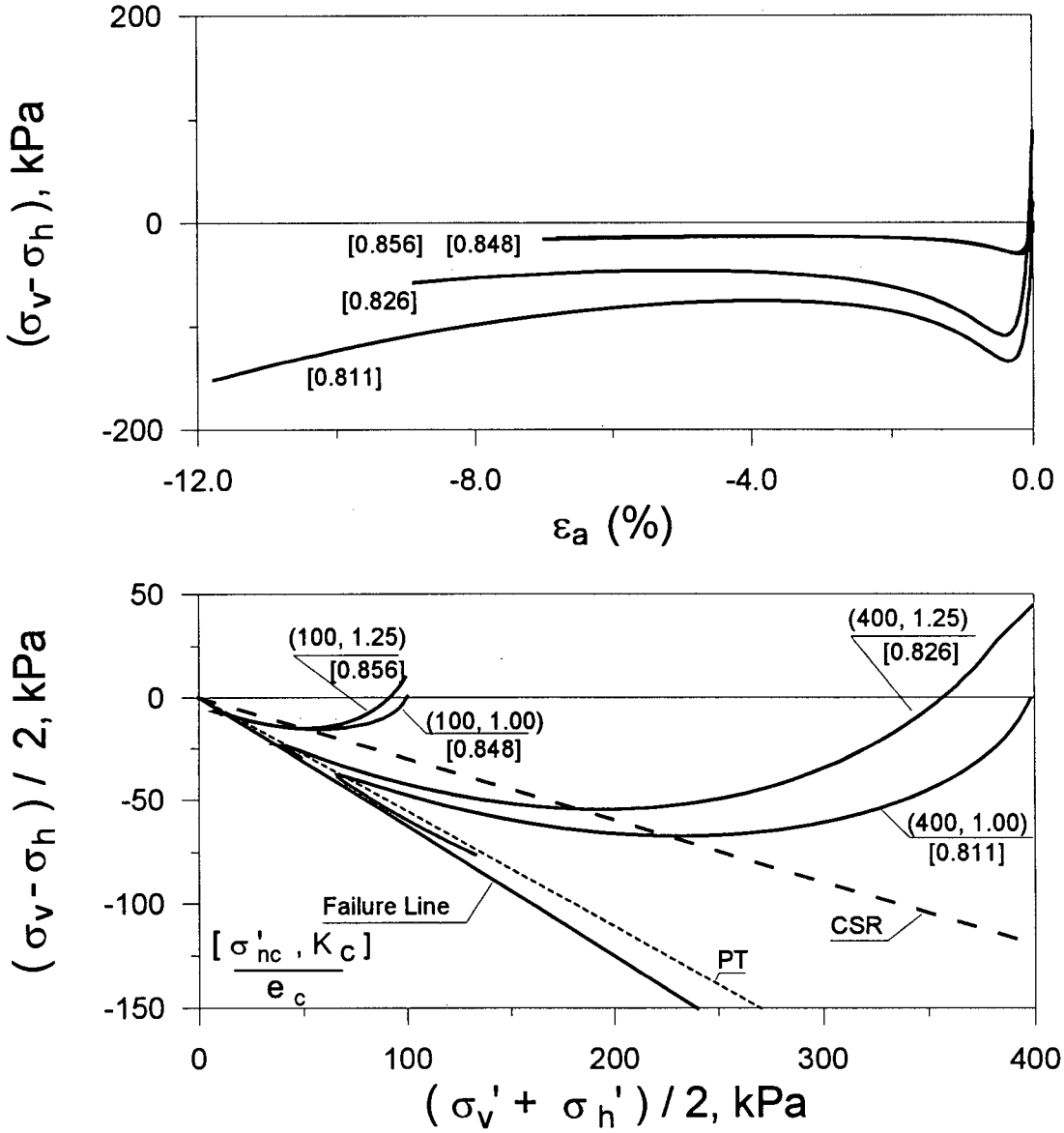

Fig 4.3 Extension behaviour of loosest deposited Fraser river sand

Extension behaviour at an initial denser depositional state is shown in Fig 4.4. It may be noted that a decrease in contractive tendency with increase in density at low σ'_{nc} levels, but once again a return to larger contractivness at higher σ'_{nc} despite initially denser states. This implies that the effect of increasing σ'_{nc} in increasing contractive behaviour is more than offset by the increase in D_{rc} and the tendency for this to reduce contractive behaviour.

Comparisons between Fig. 4.2 and 4.3 reveal that the contractive behaviour in extension is more severe than in compression for identical initial loosest deposited states. This marked difference in undrained behaviour depending on the loading direction has been attributed to the inherent anisotropy in water deposited sands (Oda, 1972). Fraser river sand is contractive in extension over a wide range of deposition densities; loosest to densest, but in compression it responds contractively only in the loosest depositional states. This has also been reported by Vaid and Thomas (1995). Similar behaviour of other sands has been reported by Vaid et al. (1989, 1990).

Triggering of contractive Deformation.

The locus of the peaks of deviator stress that manifest strain softening response may be noted to lie on a straight line (Fig 4.5) for each loading mode. This implies that triggering of contractive deformation occur at a constant value of effective stress ratio, termed herein as CSR, corresponding to the mobilised friction angle ϕ_{CSR}. Φ_{CSR} however, is dependent on the loading mode. For the loosest deposited states, the angle in compression is about $\phi_{csr} = 26^{o}$, independent of the initial stress state, but is

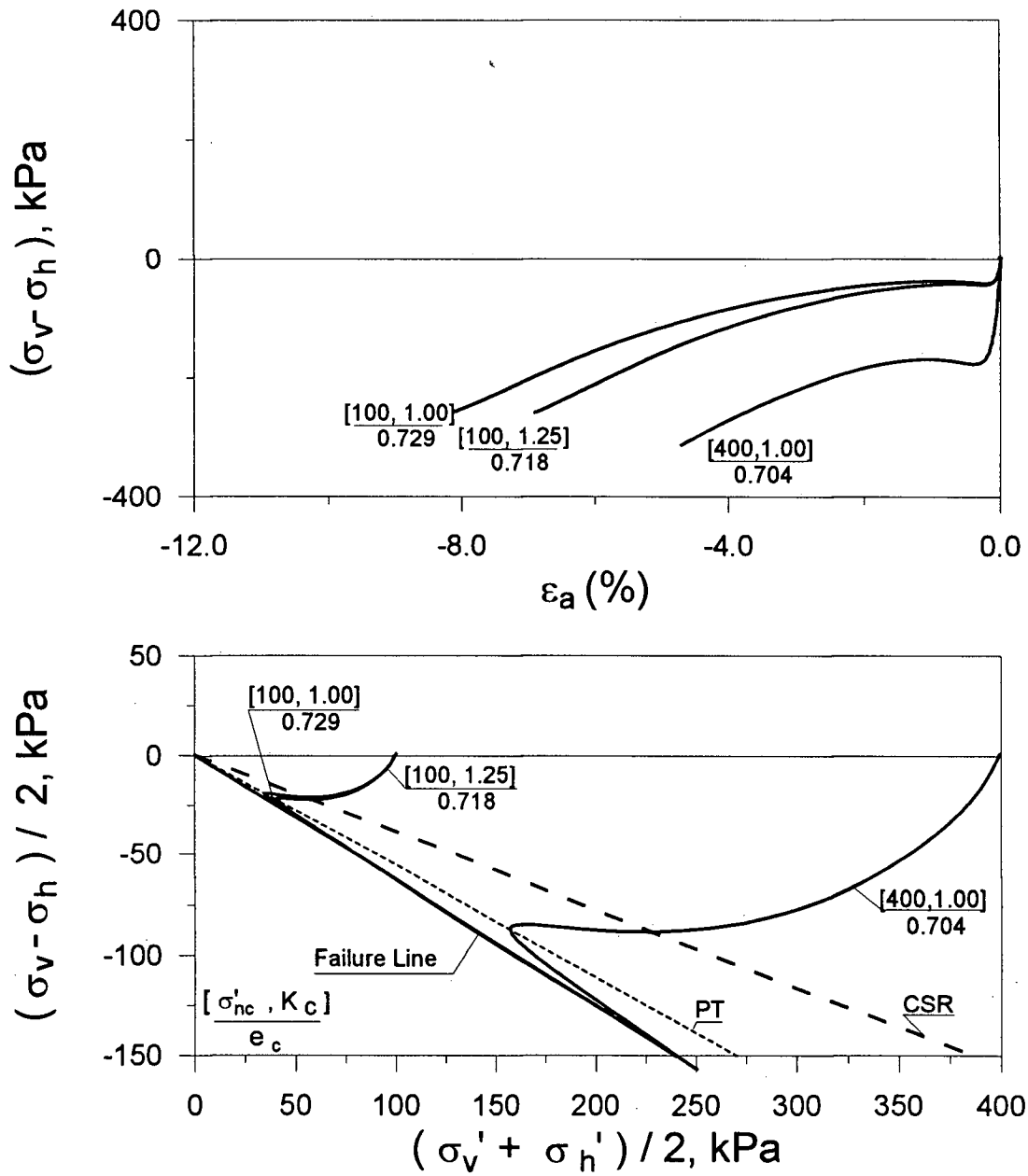

Fig 4.4 Extension behaviour of initially dense Fraser river sand

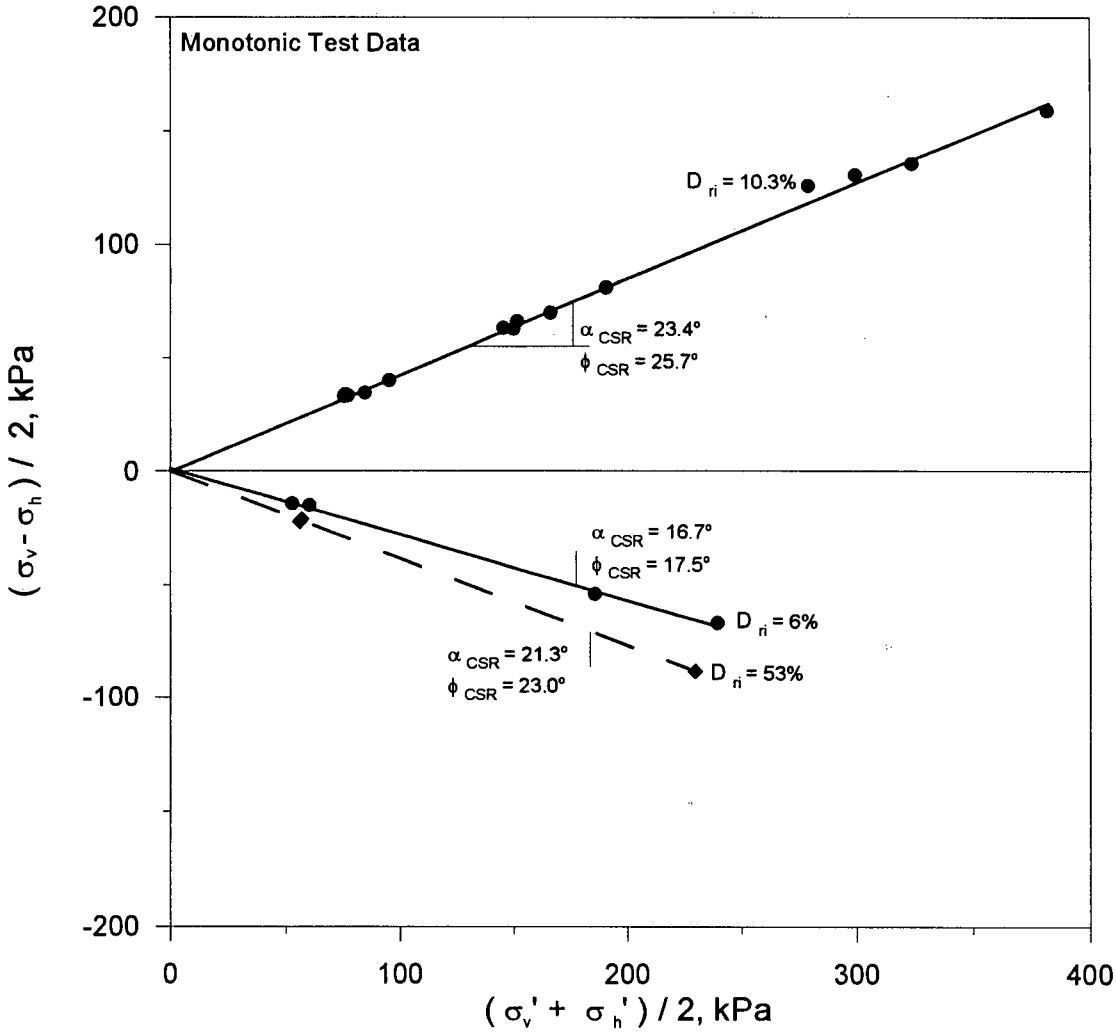

Fig 4.5 Effective stress states at triggering of strain softening in compression and extension

substantially smaller in extension at about 18°. In extension, it further depends on the deposition void ratio. In Fig. 4.5, $\phi_{csr} = 18^o$ in the loosest state, but it is larger at 23° for the denser e_{20} = 0.715. Similar results have been reported by Vaid and Thomas (1995) and Vaid et al (1990).

Phase Transformation and Steady State

Fig. 4.6 shows that the loci of phase transformation or steady states also lie on straight lines passing through the origin. The friction angle $\phi_{PT/SS}$ mobilised at these states is about 33.6° and is essentially identical in compression and extension. This uniqueness of $\phi_{PT/SS}$ has also been reported by Vaid and Thomas (1995) and Vaid and Chern (1985), regardless of the stress path and initial state prior to undrained loading.

Cyclic loading behaviour.

This was assessed at three levels of σ'_{nc} = 100, 200 and 400 kPa and for each σ'_{nc} at four levels of initial shear stress (K_c or α values). Depending on the initial state together with the value of cyclic shear stress amplitude τ_{cy}, the deformation level due to cyclic loading defined as liquefaction occurred by several different mechanisms. The development of a single amplitude axial strain of ±2.5% was taken as the definition of liquefaction.

Fig 4.7 shows contractive deformation in compression as the cause of liquefaction. The initial state of the specimen corresponds to σ'_{nc} = 100 kPa, K_c = 1.5, and D_{rc} = 23.6%. No cyclic shear stress reversal occurs, and contractive deformation

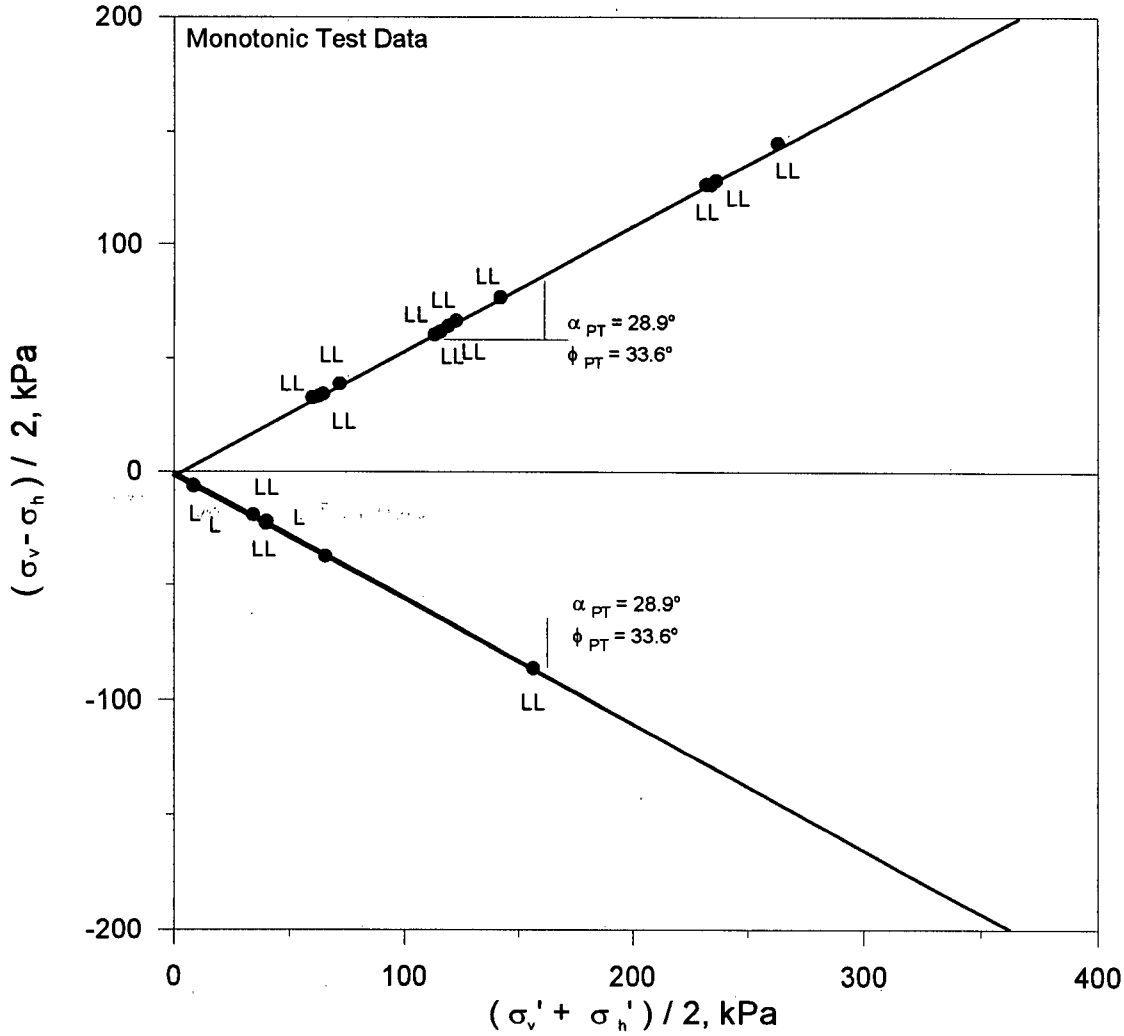

Fig 4.6 Effective stress states at phase transformation/steady state

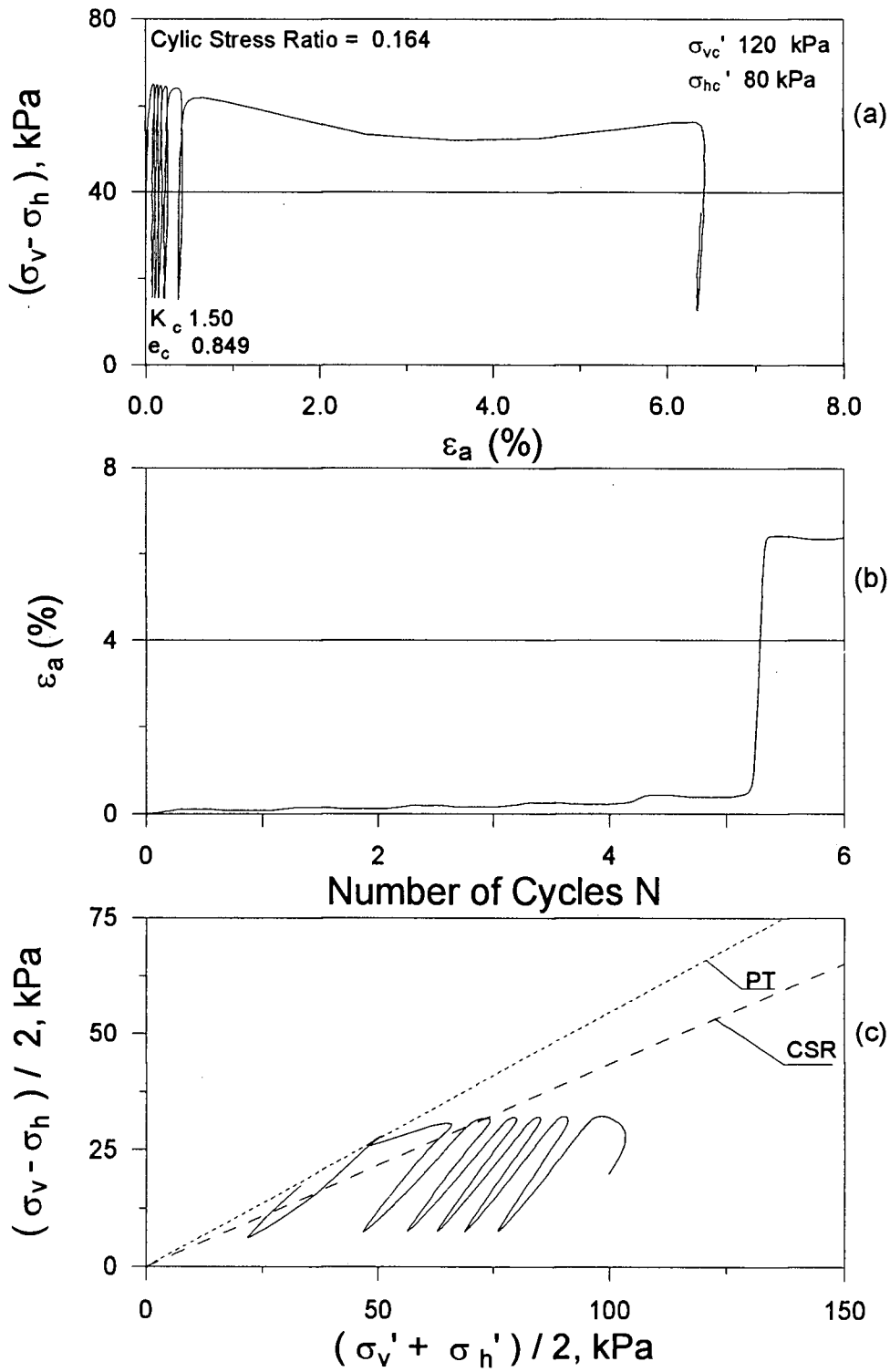

Fig 4.7 Liquefaction due to contractive deformation in compression during cyclic loading

develops in the sixth stress cycle. CSR and PT/SS lines noted in the static tests are also shown, and it may be noted that the initiation of contractive deformation and its arrest at the PT line correspond to the same mobilised friction angles under cyclic and static loading.

The cause of liquefaction due to contractive deformation in extension is illustrated for a typical cyclic test in Fig 4.8. The initial state is loose with hydrostatic σ'_{nc}= 100 kPa, D_{rc} = 39% and thus no static shear stress. Contractive deformation occurs in the seventh cycle. The triggering and the arrest of this deformation again occurs at approximately identical mobilised friction angles as under static loading.

The accumulation of strain, prior to liquefaction, is all on the extension side of the strain axis in Fig. 4.8(b). This contrasts with Fig. 4.7(b) where the static bias in compression has forced all of the strain to accumulate in the compressive mode

Cyclic stress levels that straddled the hydrostatic axis and had static shear in compression could result in strain accumulation initially in the extension or compression region depending on the degree of shear stress reversal.

Strain development due to excursion through states of σ'_{3c} = 0 illustrates the cause of liquefaction in Fig 4.9 for a typical test. The initial state of the sand represents σ'_{nc}= 400 kPa and K_c = 1.25. Cyclic loading induces stress reversals. Little strain develops until the stress path crosses the PT state (as noted in static tests) in the 9th compression cycle. Unloading of the compression pulse then causes a state of σ_3' = 0 and the following extension pulse develops the strain defined as liquefaction.

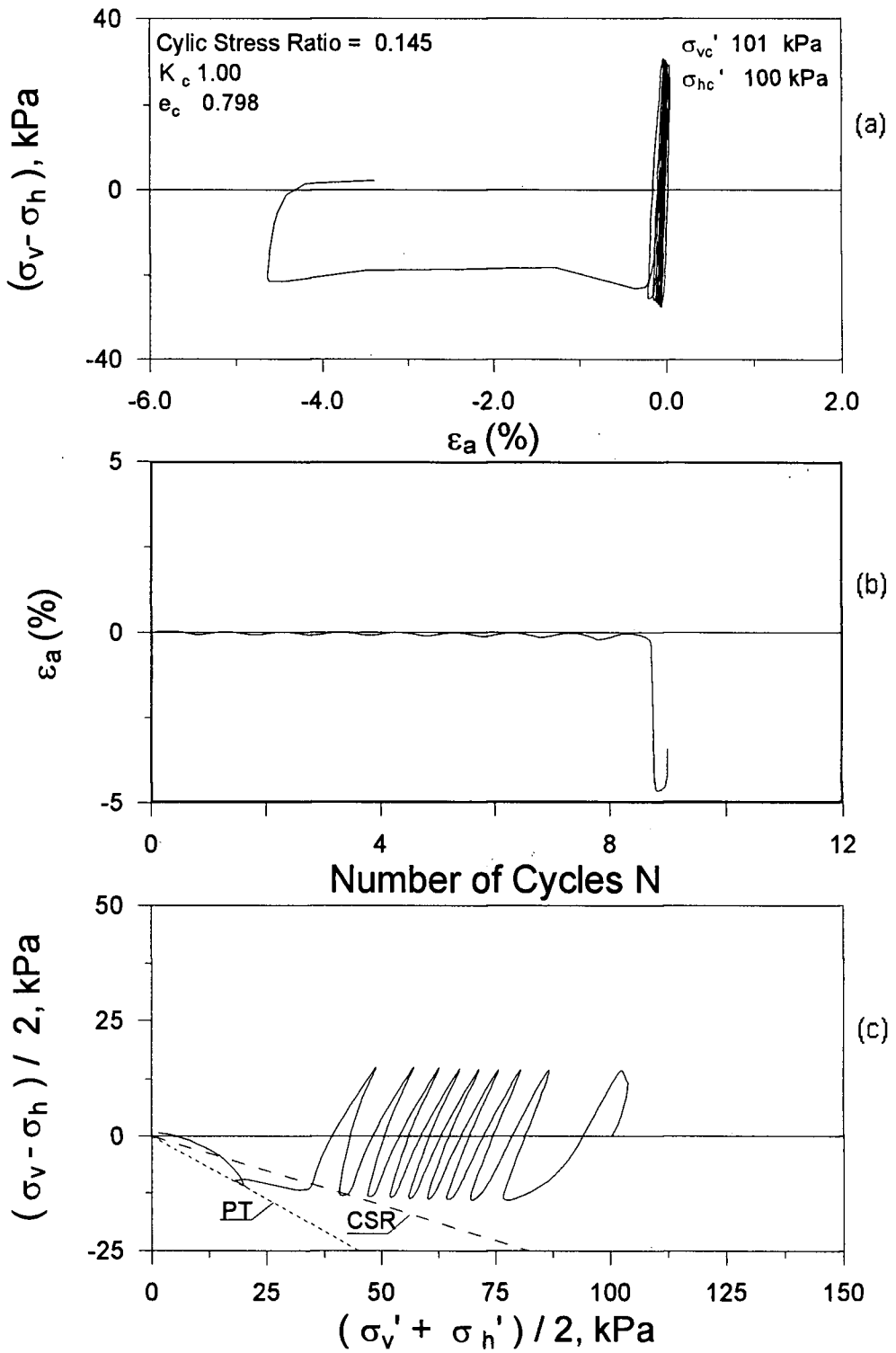

Fig 4.8 Liquefaction due to contractive deformation in extension during cyclic loading

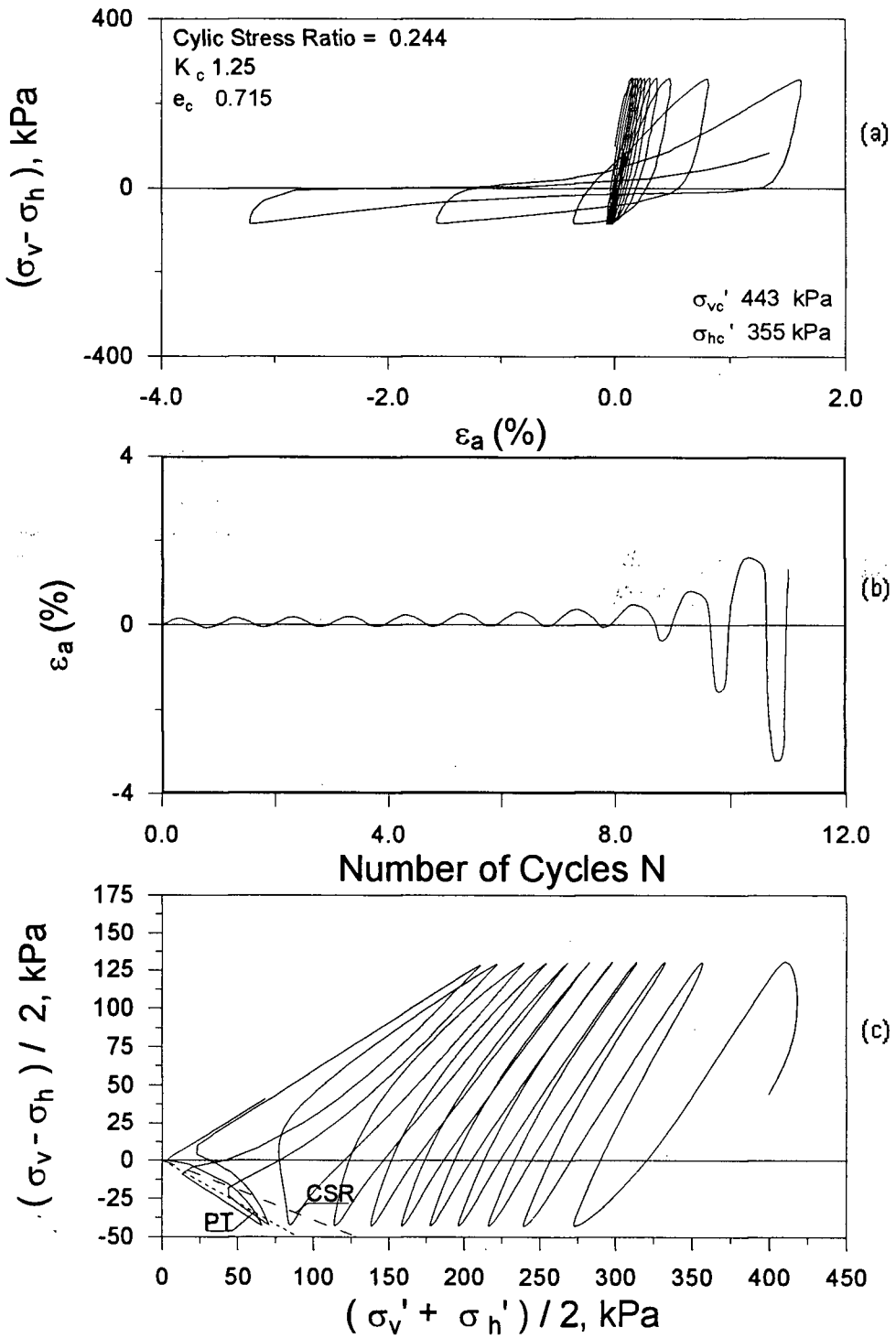

Fig 4.9 Liquefaction due to cyclic mobility with transient states of $\sigma'_3 = 0$ during cyclic loading

Neither the occurrence of contractive deformation nor excursions through transient states of $\sigma'_3 = 0$ is responsible for liquefaction due to cyclic loading in Fig 4.10. The initial state of the sand corresponds to $\sigma_{nc}' = 100$ kPa and $K_c = 2.01$. The cyclic loading pulse does not involve stress reversal. But the very first loading cycle causes the stress path to cross the PT line causing significant strain to develop. The axial strain after that point accumulates at a much decreasing rate with each cycle, every time the stress state makes excursions outside the PT line until the strain level defined as liquefaction is reached.

Linkage between static and cyclic behaviour

Several features of the undrained response are common to both static and cyclic loading. Fig. 4.11 illustrates by data points the effective stress conditions at which the contractive deformation initiates under cyclic loading. Not all, but only typical data is shown in the interest of clarity. The mobilized friction angle, Φ_{CSR} at which contractive deformation is triggered for example, in the loosest deposited sand, is essentially identical to that observed under static loading. CSR lines under static loading are shown as solid. This equality applies to both compression and extension modes of loading.

The friction angle $\Phi_{PT/SS}$ mobilized at PT/SS during cyclic loading may also be noted to be equal to that observed under static loading, regardless of the mode of loading (Fig. 4.12). Typical data for initial states that were not contractive under static loading, and hence would not be so under cyclic loading (Vaid and Chen 1985), are also shown in Fig. 4.12 in addition to those that responded contractively. Thus the $\Phi_{PT/SS}$ of

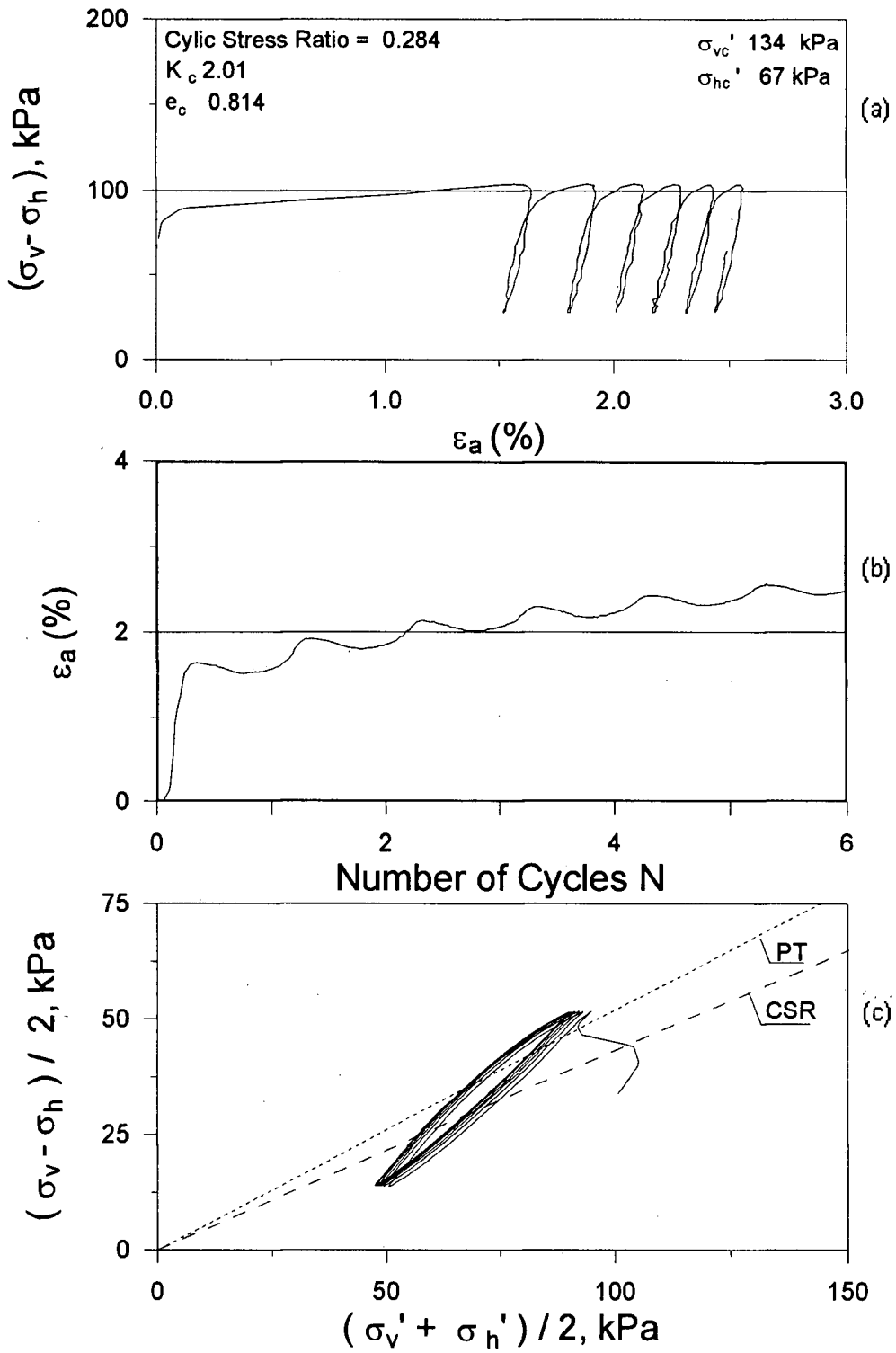

Fig 4.10 Liquefaction due to cyclic mobility without transient states of $\sigma'_3 = 0$ during cyclic loading

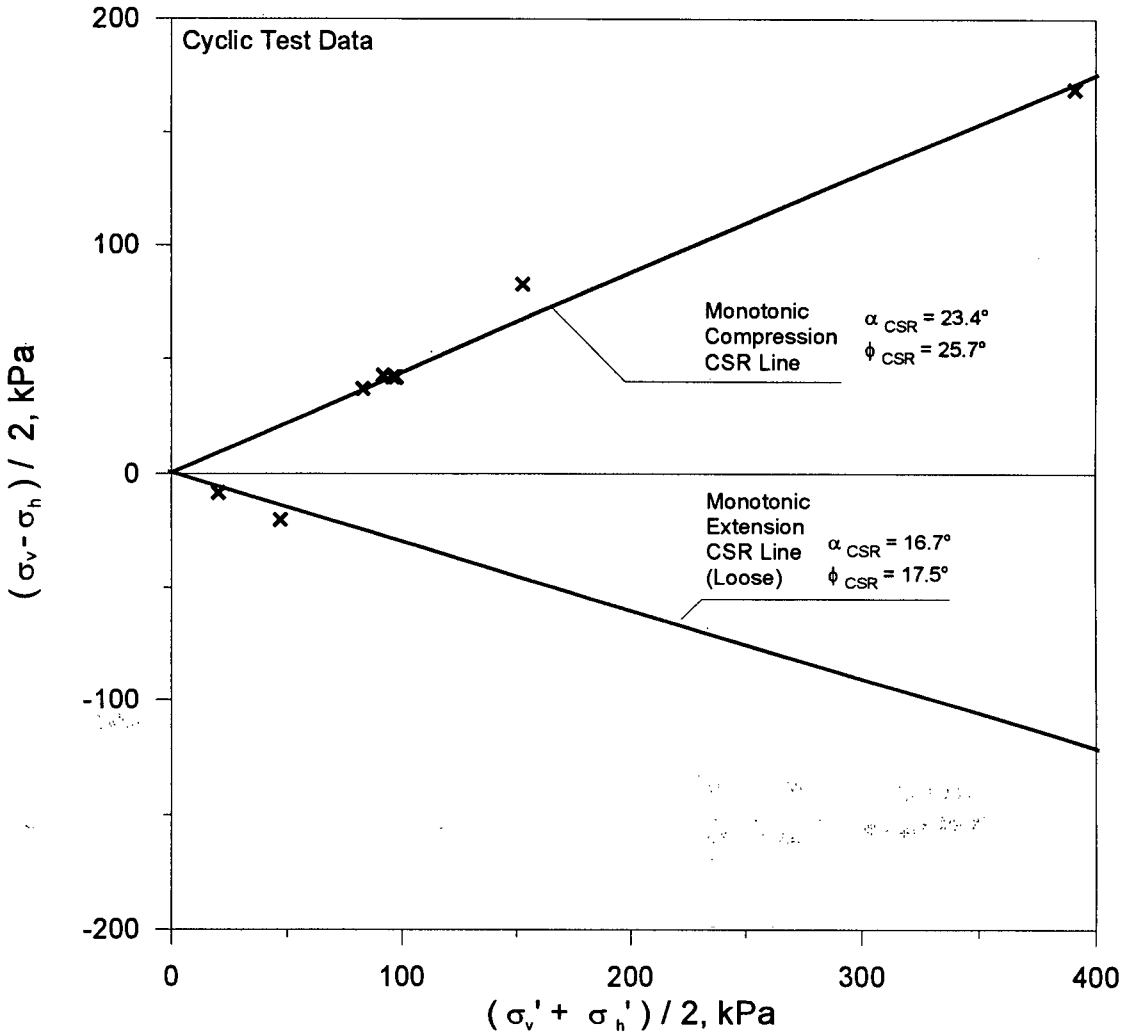

Fig 4.11 Effective stress states at triggering of strain softening during cyclic loading

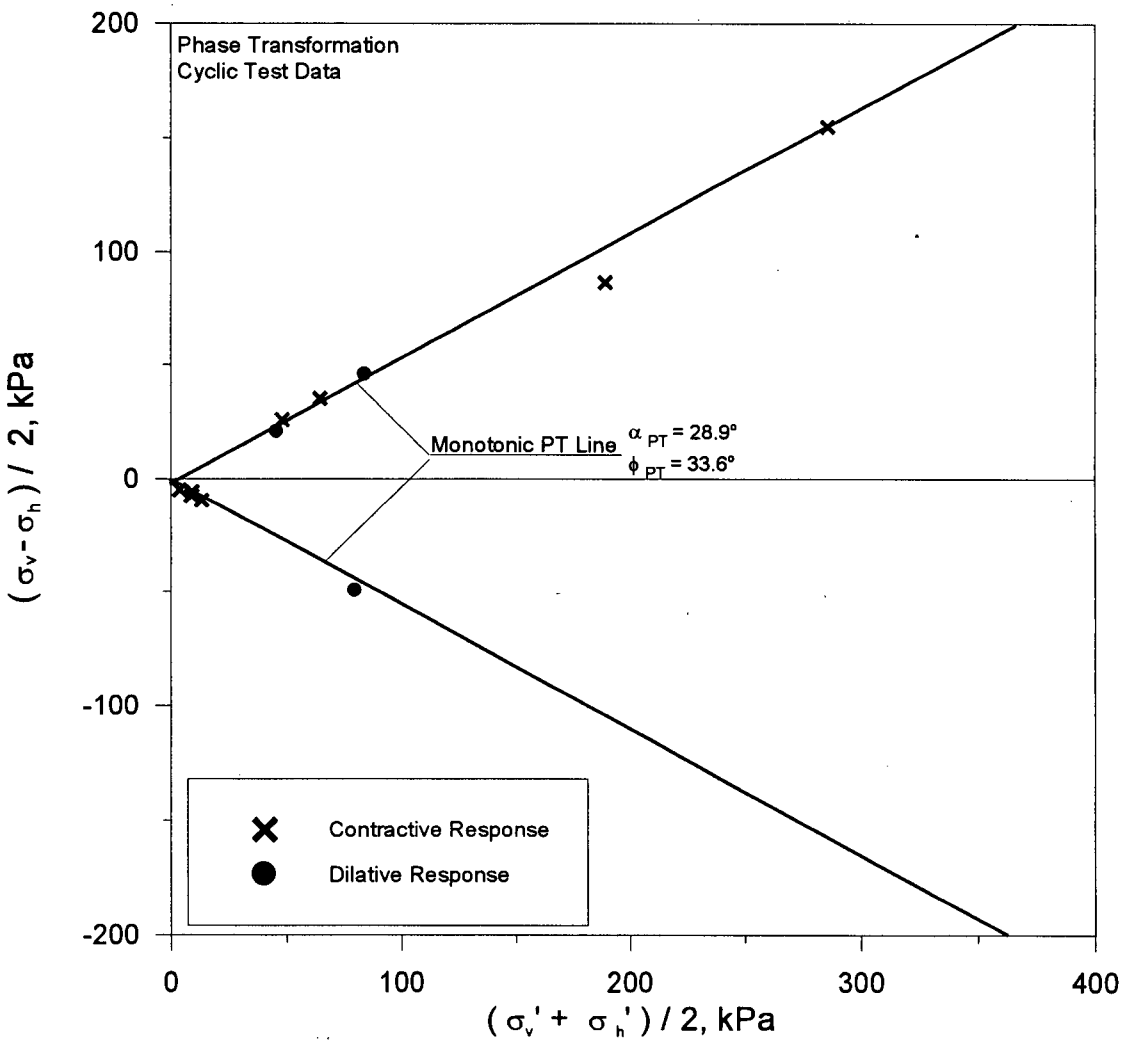

Fig 4.12 Effective stress states at phase transformation during cyclic loading

a sand appears to be a unique property of the material, independent of either the initial states or the mode of loading, as has been demonstrated in earlier studies on Fraser river sand (Vaid and Thomas, 1995) and other sands (Vaid and Chern, 1985; Vaid et al., 1990).

The mobilised undrained shear strength $S_{PT/SS}$ at PT/SS when contractive deformation occurred in compression during either static or cyclic loading is shown in Fig. 4.13 as a function of void ratio e_c and confining stress σ'_{nc}. Similar data under triaxial extension is shown in Fig. 4.14. For a given σ'_{nc} $S_{PT/SS}$ may be noted to be independent of the manner of undrained loading; static or cyclic. $S_{PT/SS}$ is not only a function of e_c but also of the magnitude of σ'_{nc}, and for a given e_c and σ'_{nc} it's value in extension is much smaller than that under compression. The difference is the largest for the loosest initial states at which $S_{PT/SS}$ in extension is only about one fifth of that in compression. Other sands also exhibit similar characteristics (Vaid et al., 1990).

Cyclic Resistance

Fig. 4.15 shows cyclic resistance data at σ_{nc}` = 100 kPa and K_c = 1.5 in the form of e_c Vs. Number of cycles to liquefaction. Each contour represents a constant amplitude of $\sigma_{d_{cy}} / 2\sigma_{3c}'$. Cyclic stress amplitudes were selected such that liquefaction occurred in less than 100 cycles. The mechanism of strain development leading to liquefaction is clearly identified. If contractive deformation was responsible for liquefaction then it is labelled CC for compression and CE for extension mode.

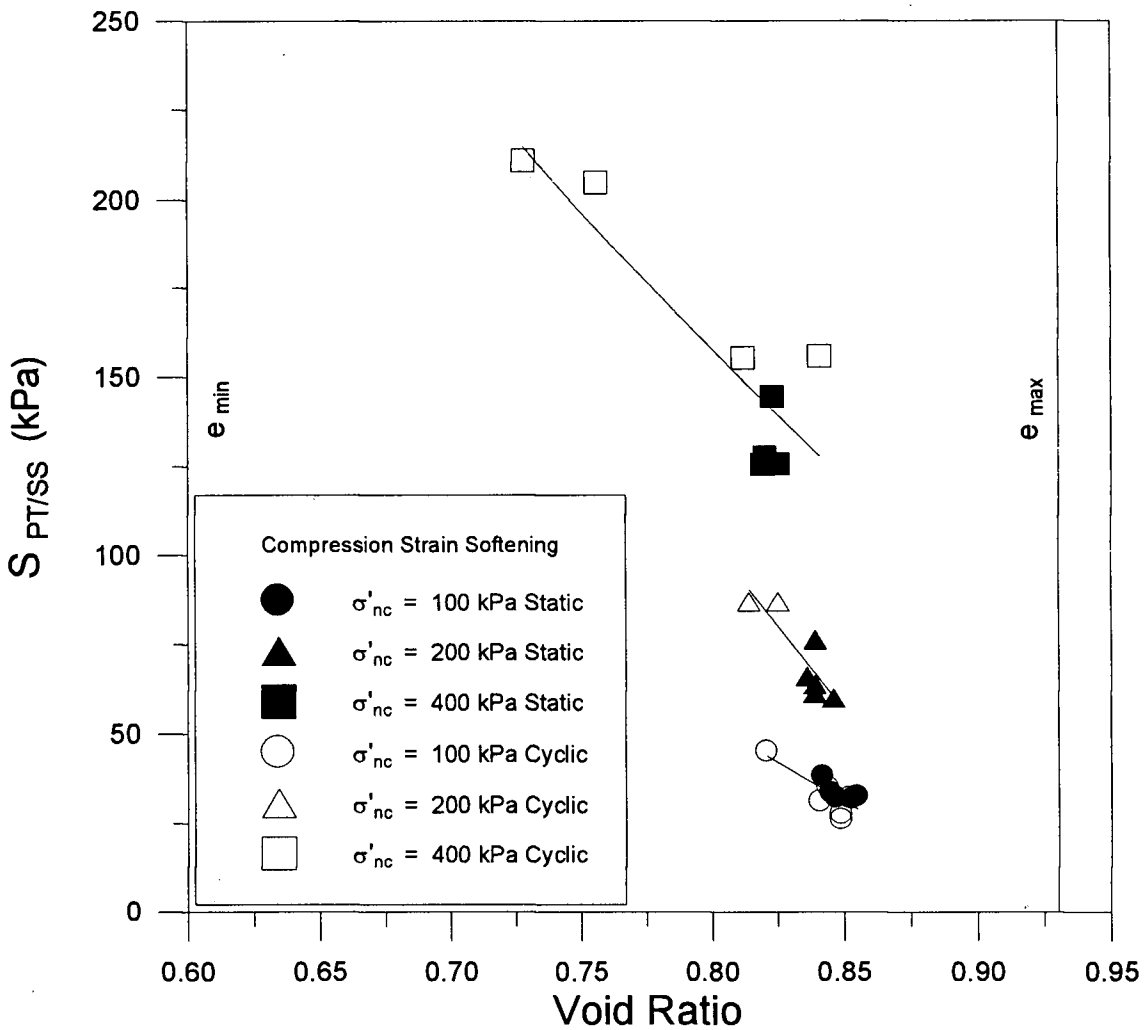

Fig 4.13 Undrained strength at phase transformation/steady state as a function of void ratio and confining stress in triaxial compression

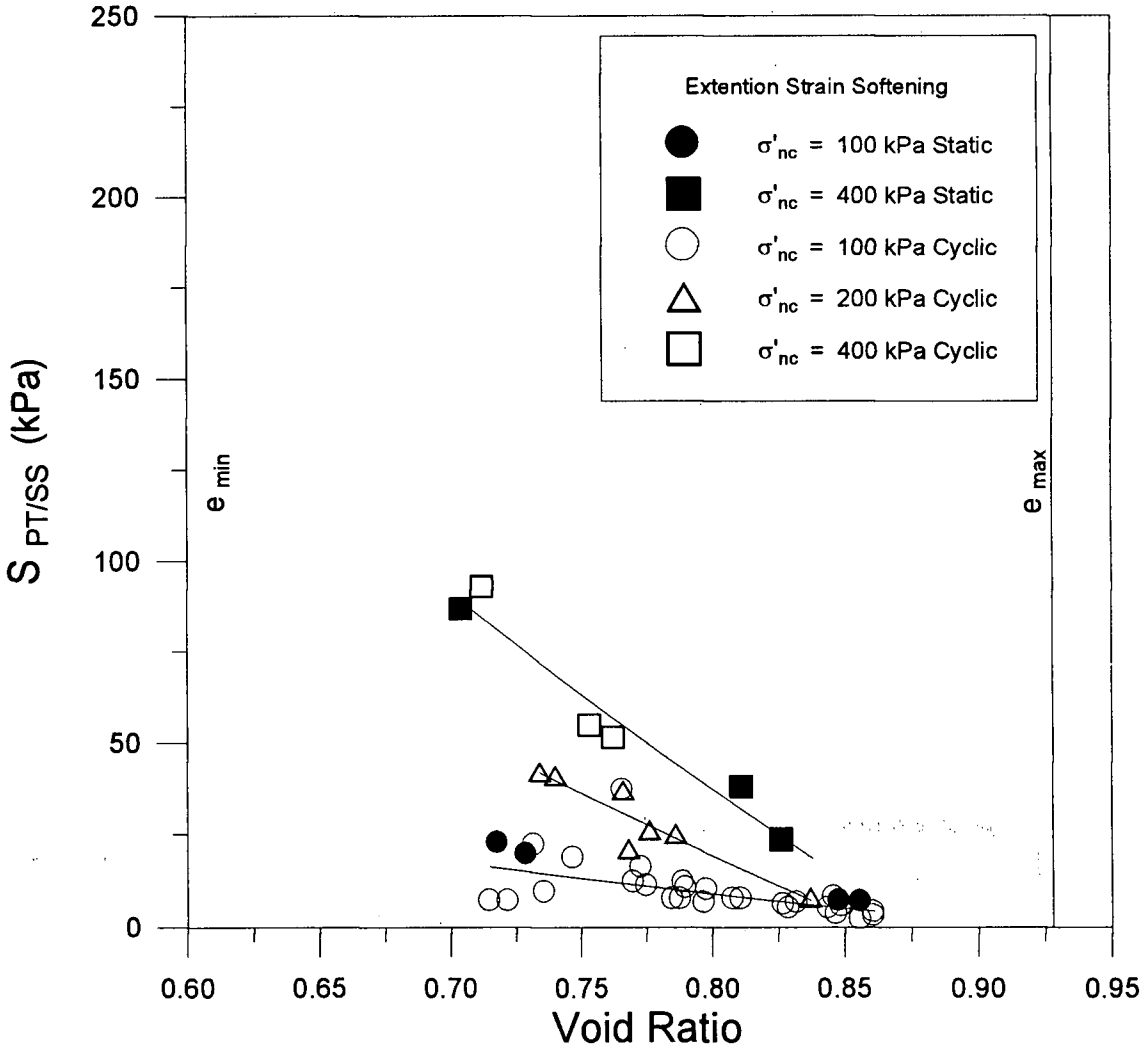

Fig 4.14 Undrained strength at phase transformation/steady state as a function of void ratio and confining stress in triaxial extension

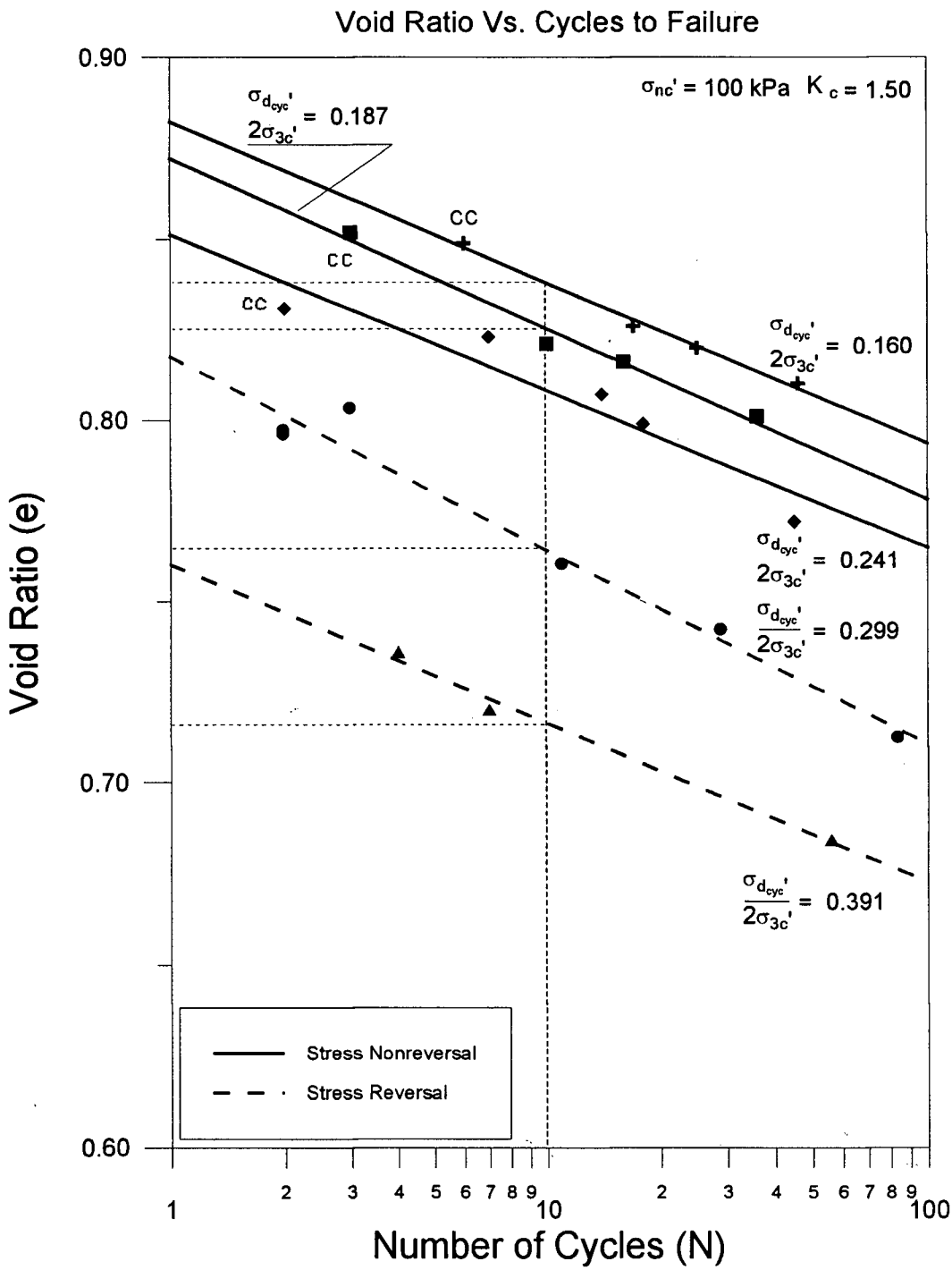

Fig 4.15 Cyclic resistance curves e_c vs N for 100 kPa, Kc = 1.50

Transient states of σ_3` = 0 was the cause of liquefaction due to cyclic mobility if shear stress reversal was involved during cyclic loading, as well as when no such stress reversal occurred.

Essentially linear behaviour between e_c and log(N) may be noted at each amplitude of constant $\sigma_{d_{cy}} / 2\sigma_{3c}'$. Relative density and corresponding cyclic resistance pairs at a specified number of cycles, which depend on the characteristics of a given earthquake, (10 selected herein) was picked up from the contour intersecting at the selected number of cycles, in order to yield the dependence of cyclic resistance on relative density at the chosen σ'_{nc} and K_c values. Contours similar to those in Fig. 4.15 at σ'_{nc} = 100 kPa, but at K_c values of 1.00, 1.25 and 2.00 are shown in Fig. 4.16 to Fig. 4.18. Data similar to that at σ'_{nc} = 100 kPa in Figs. 4.15 to 4.18 are included in appendix A for higher values of σ'_{nc} = 200 kPa and σ'_{nc} = 400 kPa

Contractive deformation was the cause of liquefaction during cyclic loading if for the selected initial state and cyclic stress level τ_{cy}, the following conditions were satisfied.

- The sand was contractive under static loading
- The cyclic shear stress amplitudes (τ_{cy} + τ_{st}) exceeded its $S_{PT/SS}$ in compression or extension and
- The number of stress cycles applied is enough to carry the effective stress state to the CSR line in compression or extension

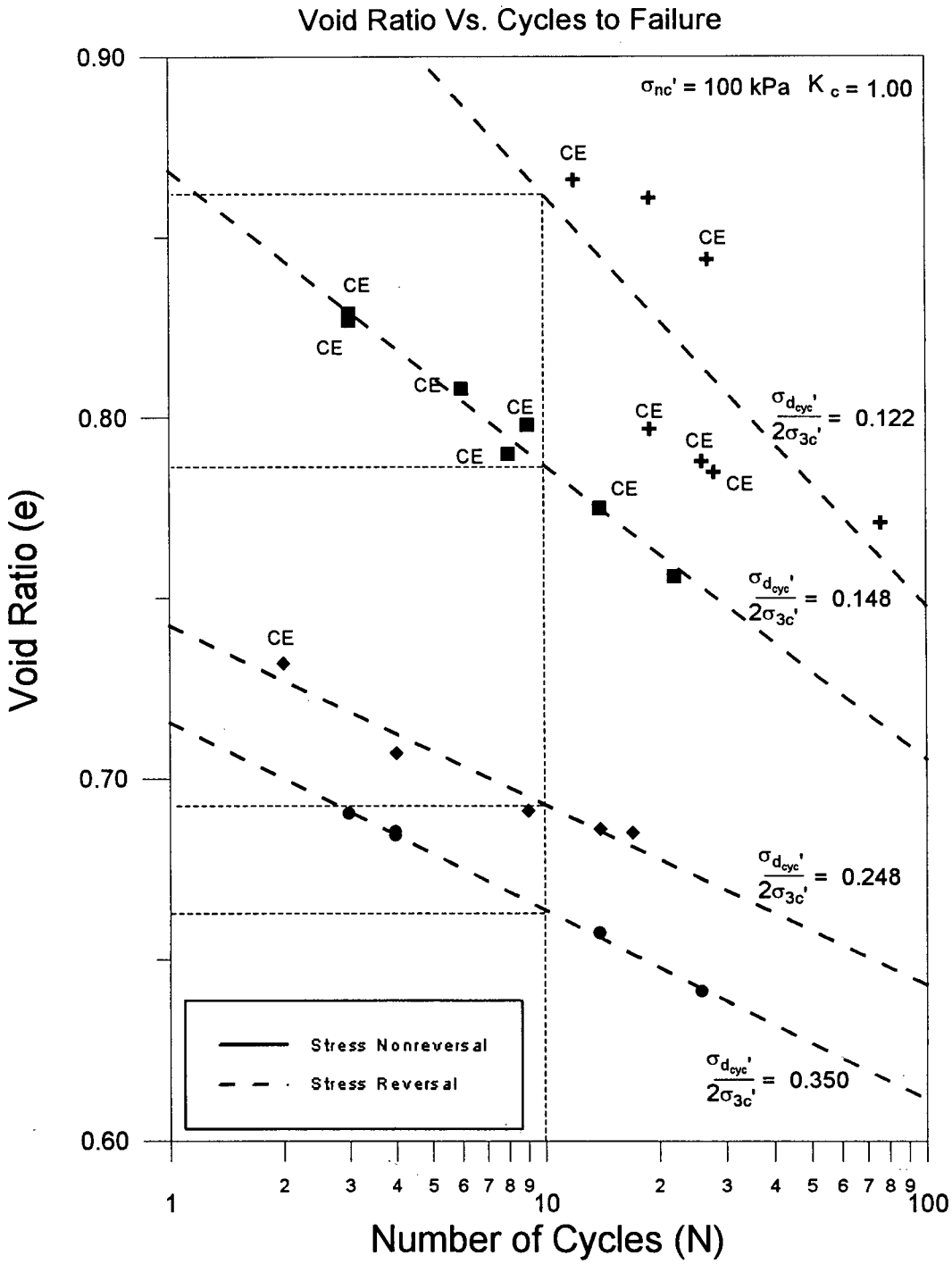

Fig. 4.16 Cyclic Resistance curves e_c vs N for 100 kPa, K_c =1.00

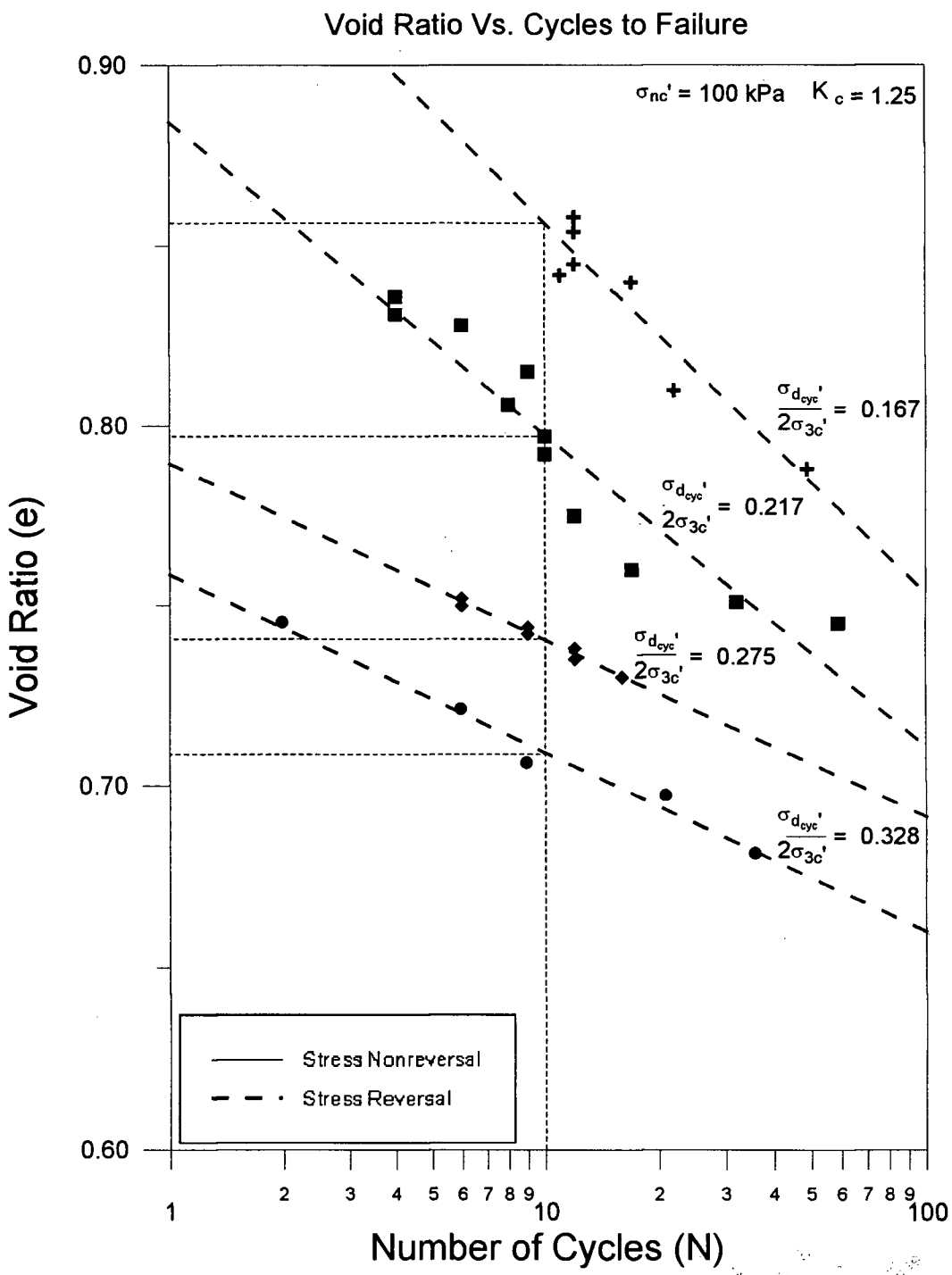

Fig. 4.17 Cyclic Resistance curves e_c vs N for 100 kPa, K_c =1.25

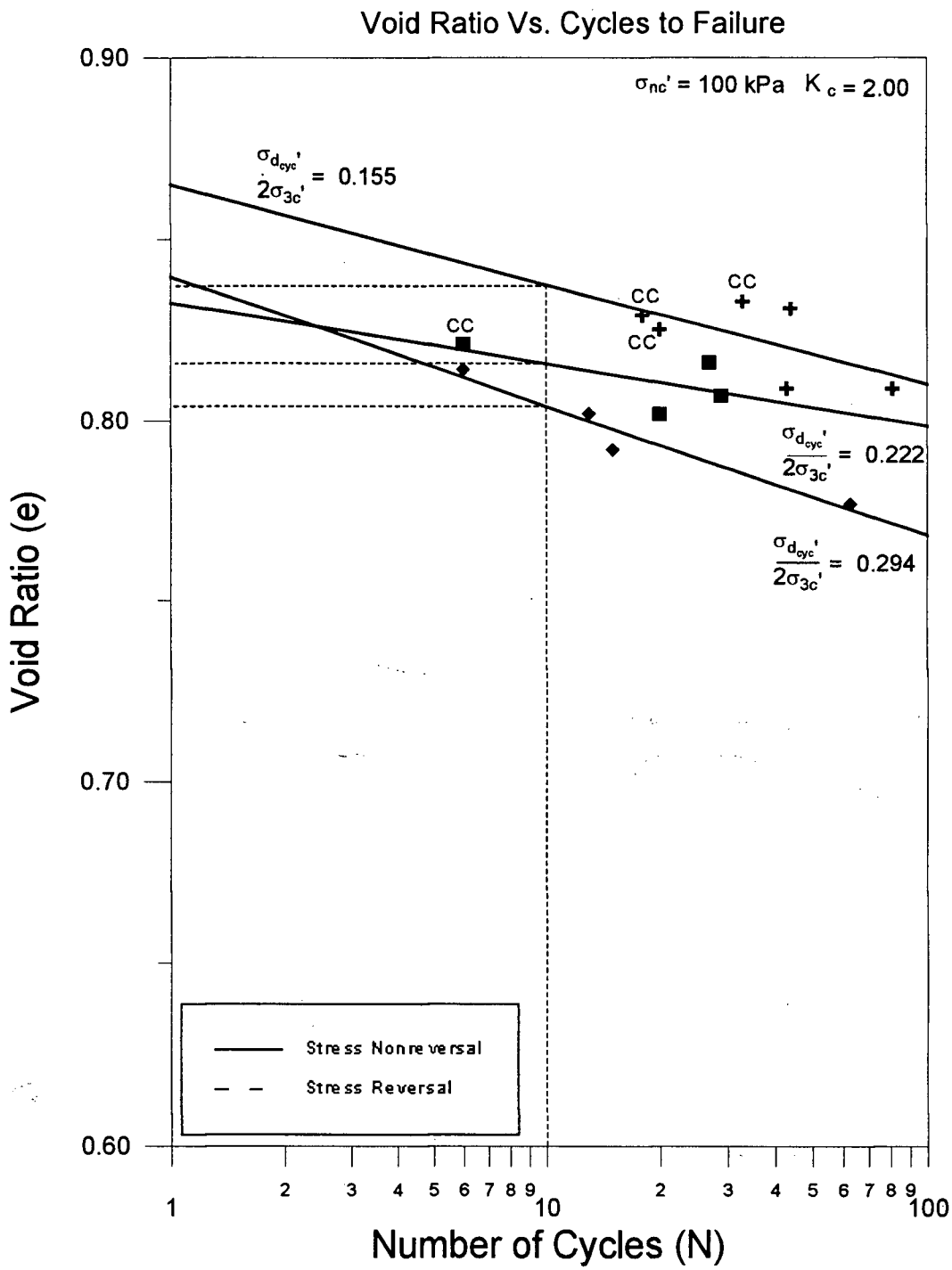

Fig. 4.18 Cyclic Resistance curves e_c vs N for 100 kPa, K_c =2.00

These requirements were first recognised and demonstrated by Vaid et al. (1989) for another sand. If any of the conditions stated above was not satisfied, then strain during cyclic loading developed due to cyclic mobility associated with or without encountering transient states of zero effective stress, depending on whether shear stress reversal occurred or not.

The resulting cyclic resistance curves of Fraser River sand derived from the data in Figs. 4.15 to 4.18 and in Appendix A, at σ_{nc}' = 100, 200 and 400 kPa and several levels of K_c (static shear) are plotted in Figs. 4.19 to 4.21. These figures completely describe the dependency of cyclic resistance on both confining stress and static shear stress levels, in addition to its dependency on relative density.

As pointed out previously, the minimum D_{rc} accessible to the sand in the loosest deposited state, and after the application of the range of confining and static shear stresses used was about 25% under the highest stress level. Thus the effect of static shear and confining stress levels on cyclic loading can only be considered for D_{rc} > 25%.

At any confining stress level, CRR vs D_{rc} relationship is profoundly influenced by the level of static shear. Under σ'_{nc} =100 kPa, (Fig. 4.19) an increase in cyclic resistance with static shear stress occurs only for D_{rc} greater than about 30%. At looser density states increase in static shear causes the maximum increase in resistance over the K_c = 1 value for small K_c levels, but the difference decreases with further increase in K_c, and at K_c = 2 the resistance in fact becomes even smaller than that at K_c = 1. It appears that at $D_{rc} \approx$ 30%, the increase is essentially independent of the static shear.

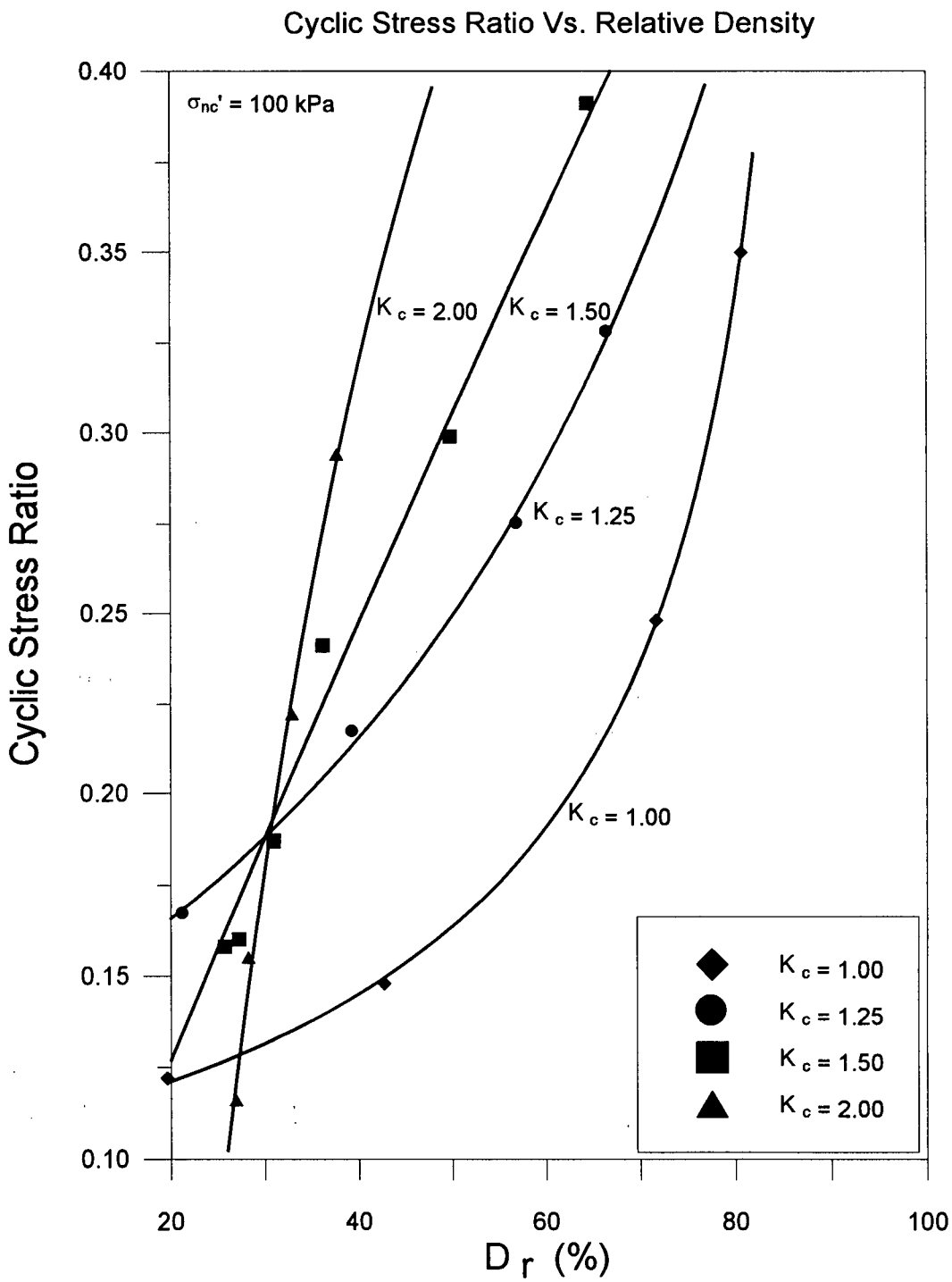

Fig 4.19 Cyclic resistance CRR vs D_r of Fraser river sand at σ_{nc}` = 100 kPa

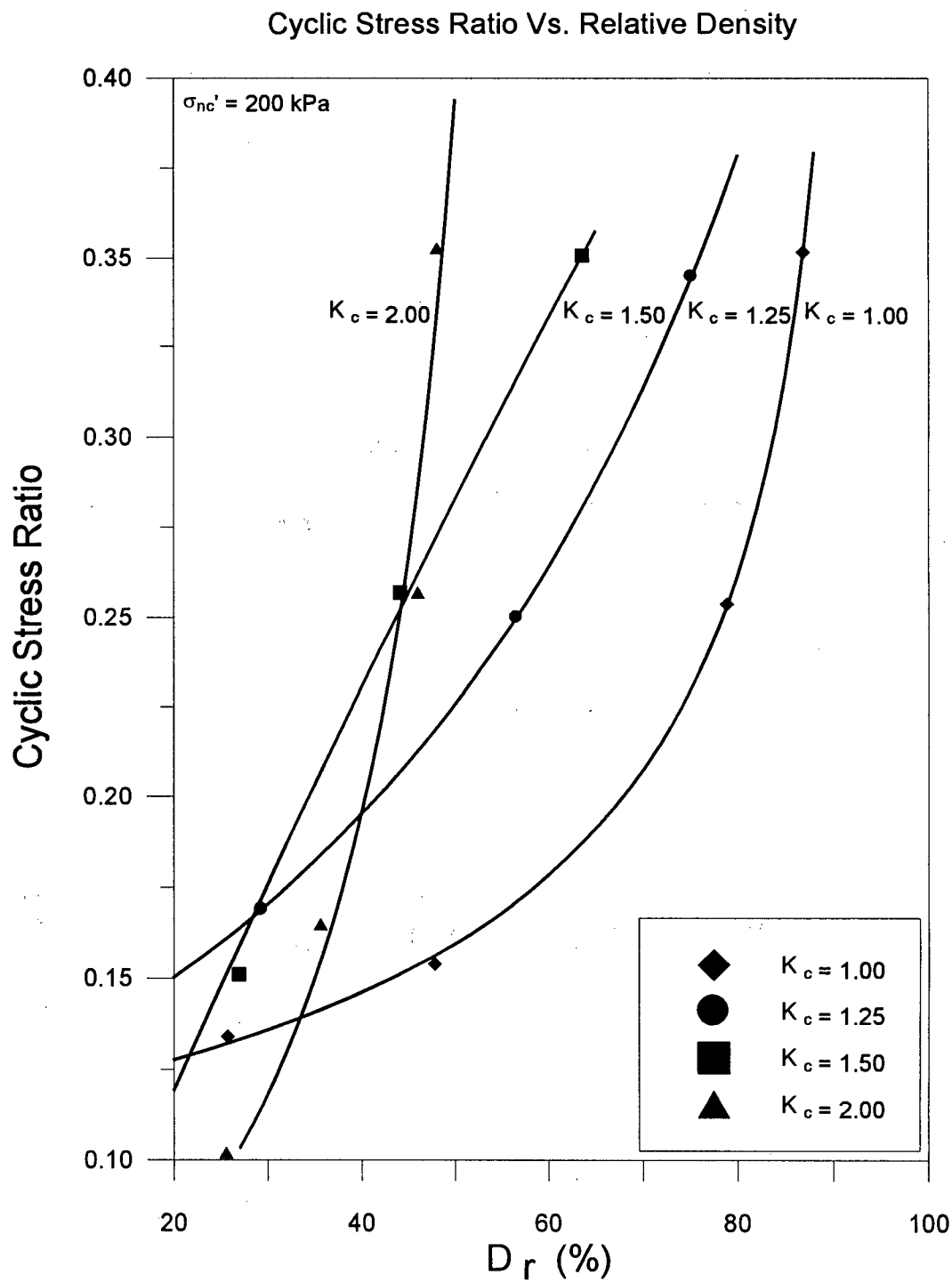

Fig. 4.20 Cyclic resistance CRR vs D_r of Fraser River sand at σ_{nc}` = 200 kPa

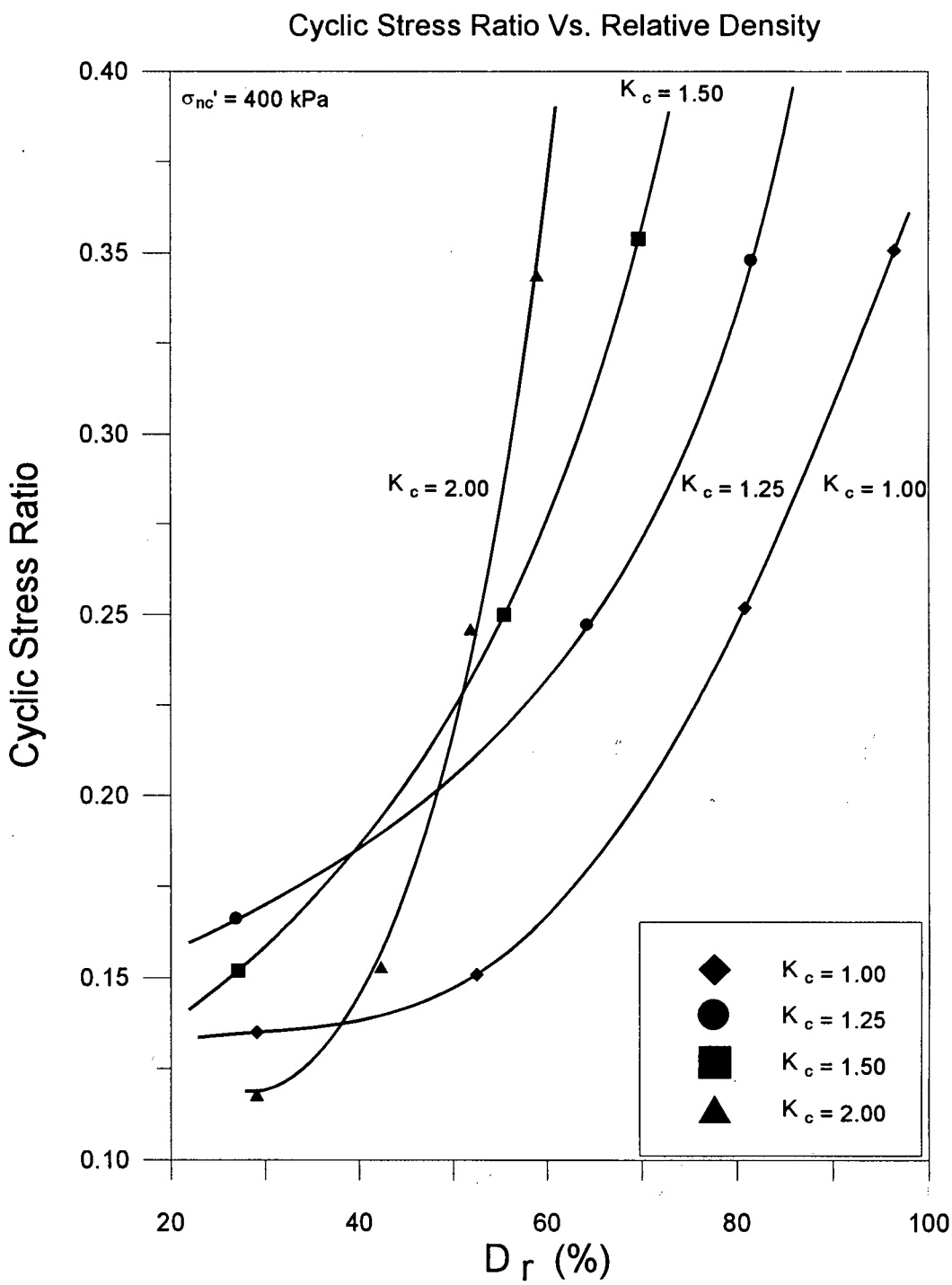

Fig. 4.21 Cyclic resistance CRR vs D_r of Fraser river sand at σ_{nc}` = 400 kPa

The behaviour at higher levels of σ'_{nc} = 200 and 400 kPa is essentially similar, except the cut off D_{rc} level beyond which the resistance always increases with Kc is higher at about 45% for σ'_{nc} = 200 kPa and 50% for σ'_{nc} = 400 kPa. Again at density states lower than these cut off values the cyclic resistance is higher with Kc > 1, except for the highest Kc used, when it decreases below the Kc = 1 value.

Effect of static shear and confining stress levels - K_σ, K_α factors

The results in Figs. 4.19 to 4.21 are cross plotted in Figs. 4.22 to 4.24 to yield correction factor K_σ*K_α that would be needed to extrapolate the reference $(CRR)_{100,\,0}$ to $(CRR)_{\sigma',\alpha}$ for the effects of static shear and confining pressure empirically. The data is plotted as K_σ*K_α vs α at several constant values of relative densities, loose to dense. Since σ'_{nc} = 100 kPa in Fig. 4.22, K_σ = 1 and thus the combined correction factor K_σ*K_α degenerates to K_α. Also superimposed in Figs. 4.22 to 4.24 are the suggested relationships by Seed and Harder (1990). At σ'_{nc} = 200 and σ'_{nc} = 400 kPa, the vertical ordinates in Figs. 4.23 and 4.24 have been suitably adjusted by the appropriate K_σ factors relevant to the σ'_{nc} level according to Seed and Harder (1990).

For the sand tested, the correction factors proposed by Seed and Harder grossly underestimate the cyclic resistance at all relative density states, and especially for the looser densities. For example, for the loose D_r = 35%, the observed K_α is > 1 at about 1.75 compared to the suggested value of < 1 at about 0.5 for high levels of K_c.

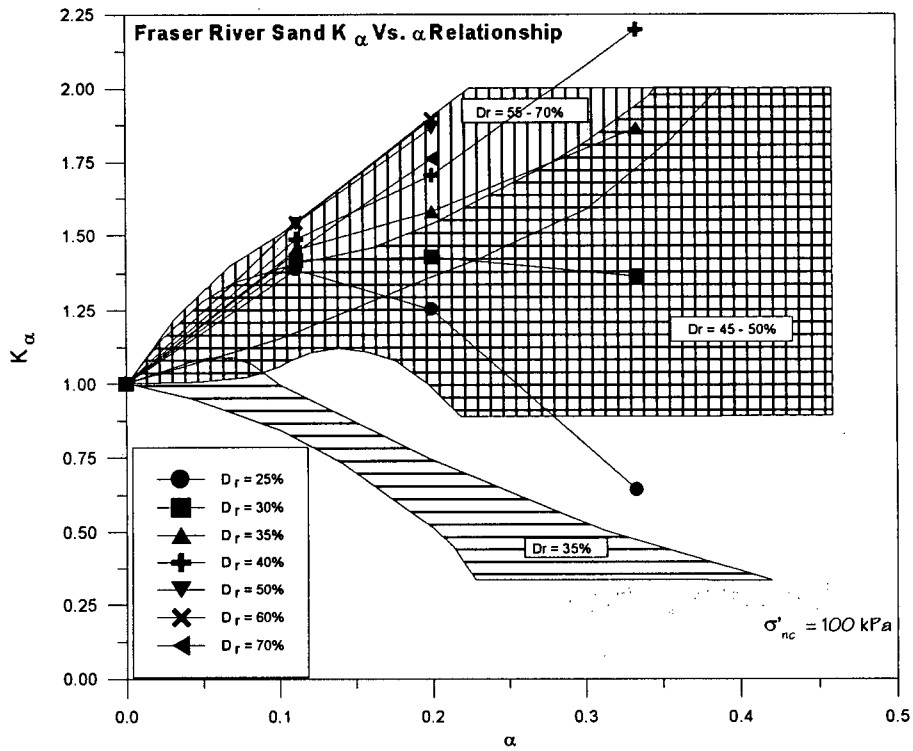

Fig. 4.22 K_α vs α for Fraser river sand at several density states

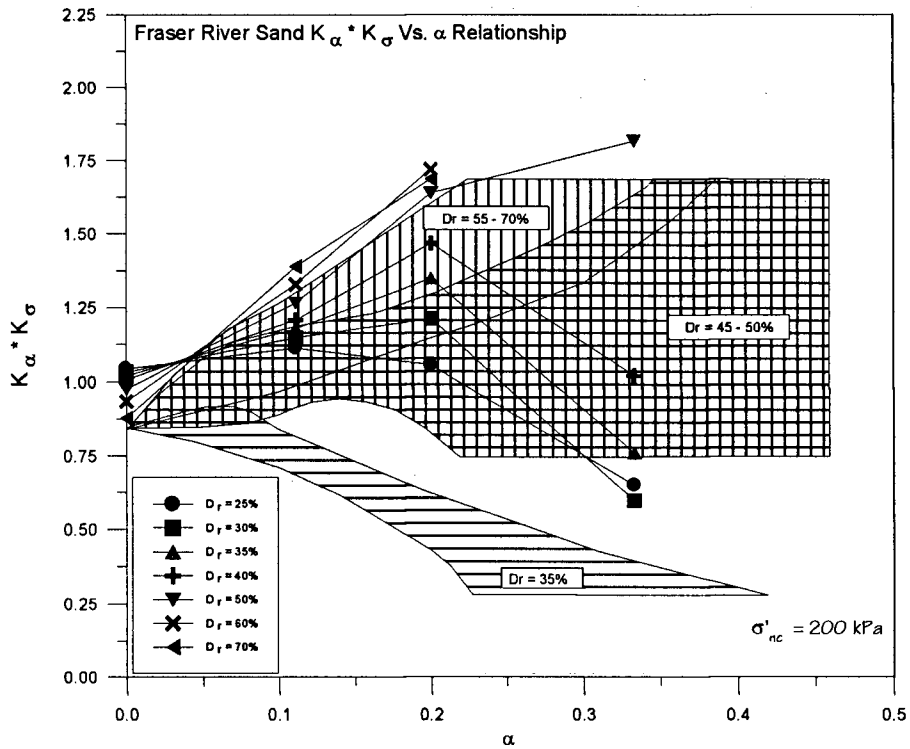

Fig. 4.23 The combined cyclic resistance factor, Kσ*Kα for Fraser river sand at σ'_{nc} = 200 kPa.

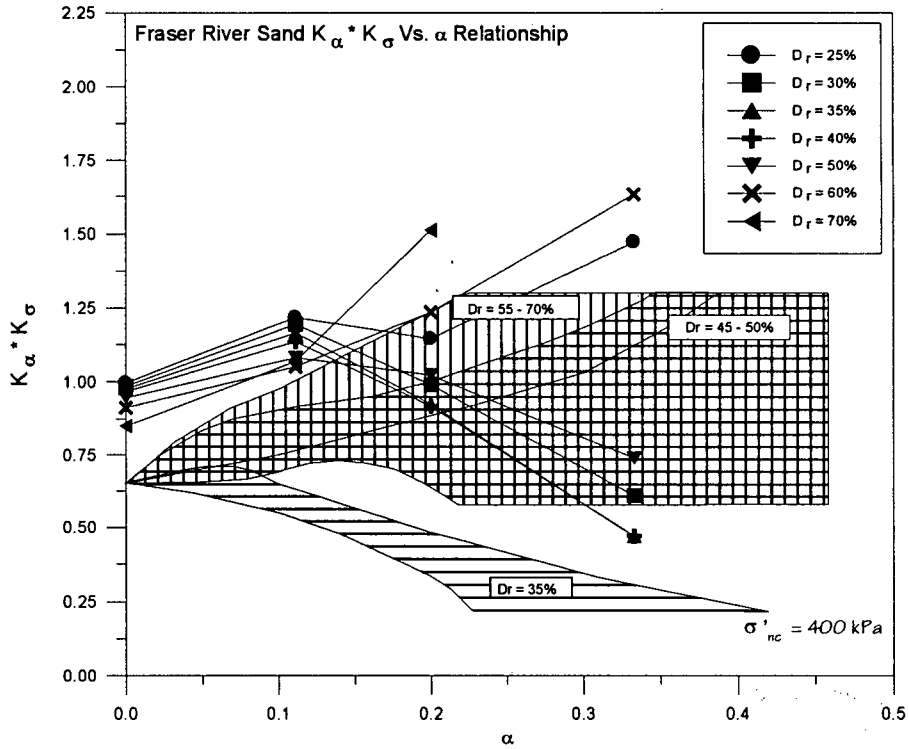

Fig. 4.24 The combined cyclic resistance factor, $K\sigma*K\alpha$ for Fraser river sand at σ'_{nc} = 400 kPa.

The measured K_α is less than one only for the loosest accessible state, when α is greater than about 0.25 as opposed to the suggested drop off below one at α in excess of about 0.08. At D_r greater than about 50%, the measured K_α are comparable to those proposed, regardless of the α level.

The K_σ*K_α factors at higher σ'_{nc} = 200 kPa again increase with increasing α up to about α = 0.11. With further increase in α, K_σ*K_α suffer a decrease only at the loosest state of D_r = 25%. The α level at which a decrease occurs in K_σ*K_α with further increase in α gets delayed as D_r increases to about 40%. Nevertheless, the measured K_σ*K_α values are invariably much higher than the values proposed by Seed and Harder, regardless of the α level. At Dr in excess of about 40%, the measured and predicted values are reasonably comparable. Similar comments may be applied to the behaviour at even higher σ'_{nc} = 400 kPa (Fig. 4.24). Under no circumstances, the measured K_σ*K_α factors are smaller than the proposed values regardless of the α level.

A direct comparison of measured and predicted cyclic resistance based on Seed and Harder (1990) is illustrated in Figs. 4.25 to 4.28. The shaded regions in these figures represent the predictions using Seed and Harder (1990) correction factors together with the reference data shown at σ'_{nc} = 100 kPa and a = 0°. For a fixed α, the measured resistance at σ'_{nc} = 400 kPa is significantly larger than predicted regardless of the D_r level. The discrepancy is the largest at looser density states, which in fact are the most prone to liquefaction. The under prediction becomes somewhat larger at lower σ'_{nc}. The difference between the measured and suggested factors gets smaller at denser states (D_r > 60%) as well.

Relationship similar to Fig. 4.25, but at higher $\alpha = 0.20$ level is shown in fig. 4.26, and again regardless of the D_r level, the measured values of CRR are substantially higher than those predicted using the currently suggested factors for modifying $(CRR)_{100,0}$.

Figs. 4.27 and 4.28 show comparisons similar to those in Figs. 4.25 and 4.26, but at fixed σ'_{nc} and two levels of α. The measured CRR may be noted to be substantially higher than those predicted values at each σ'_{nc}, regardless of α and D_r levels.

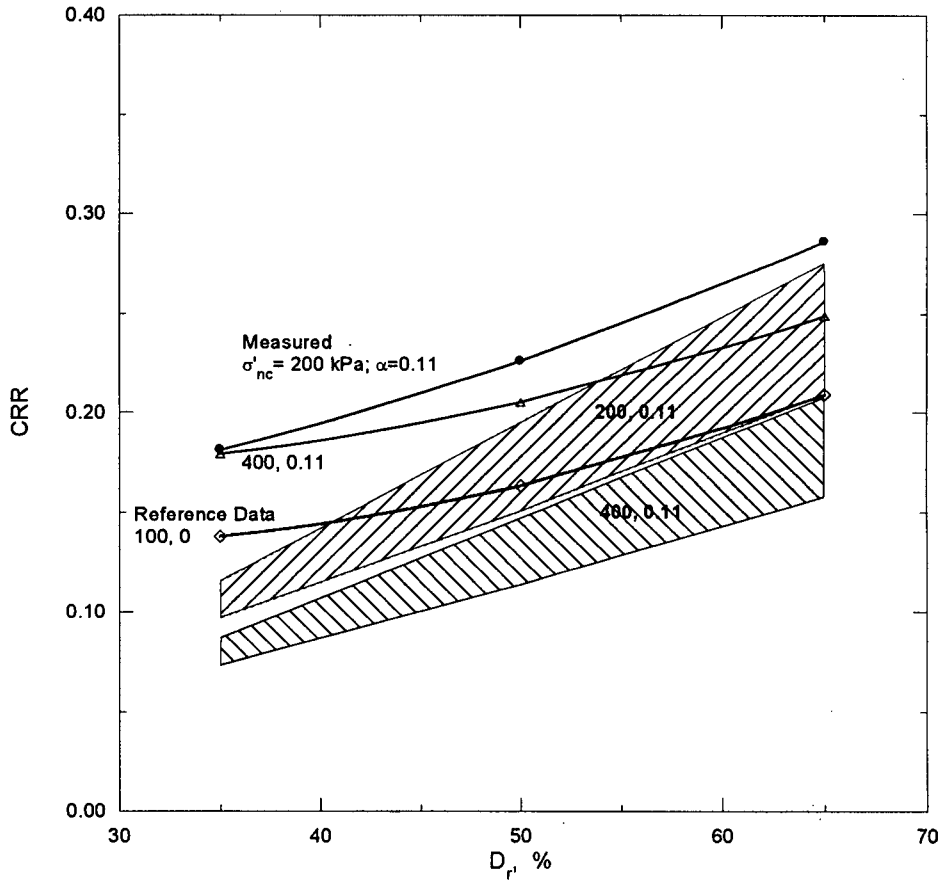

Fig. 4.25 Measured versus predicted cyclic resistance at fixed α = 0.11 level

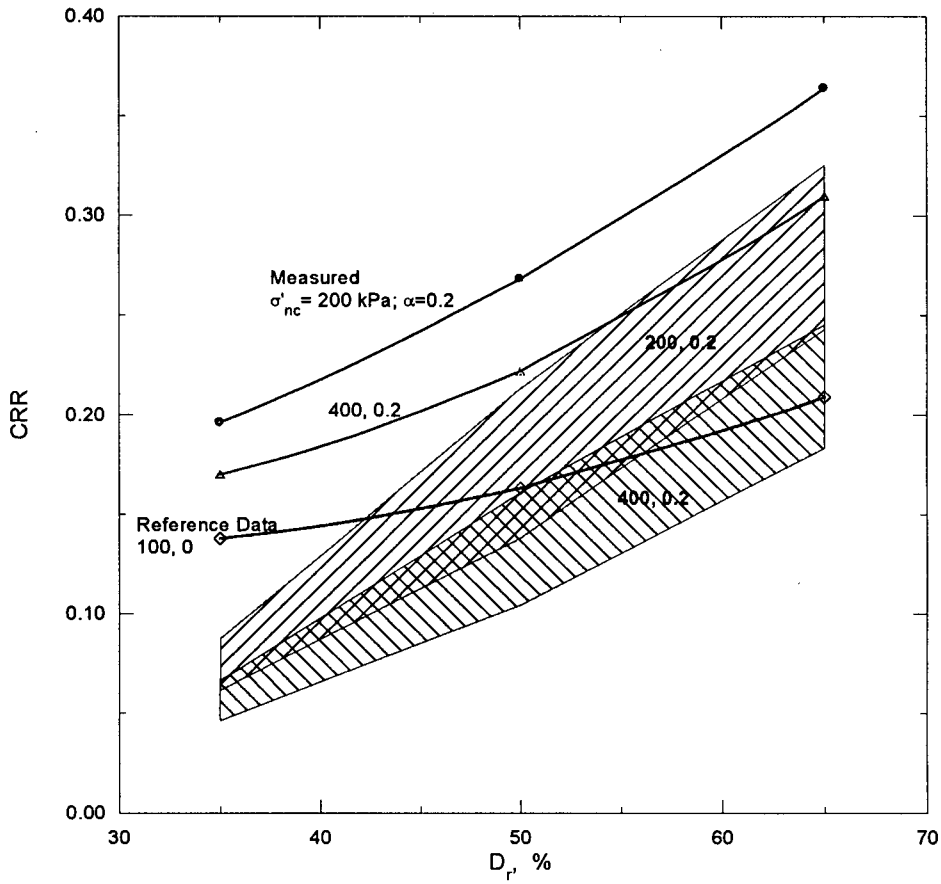

Fig. 4.26 Measured versus predicted cyclic resistance at fixed α = 0.20 level

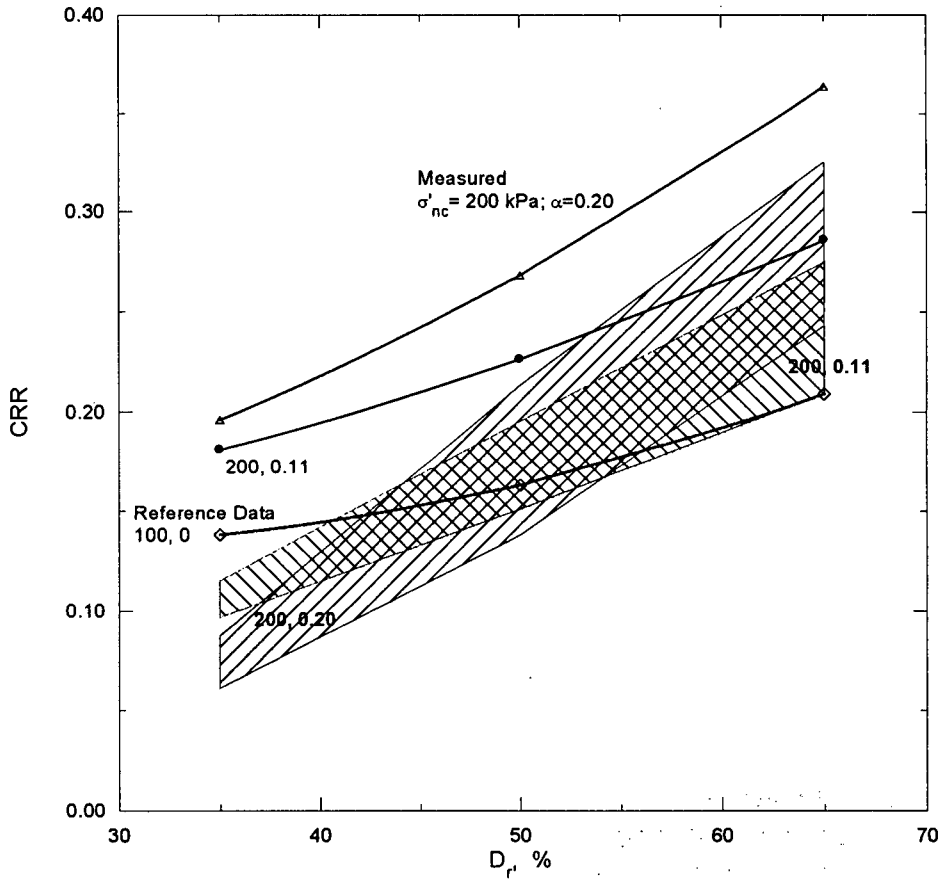

Fig. 4.27 Measured versus predicted cyclic resistance at fixed σ'_{nc} = 200 kPa level

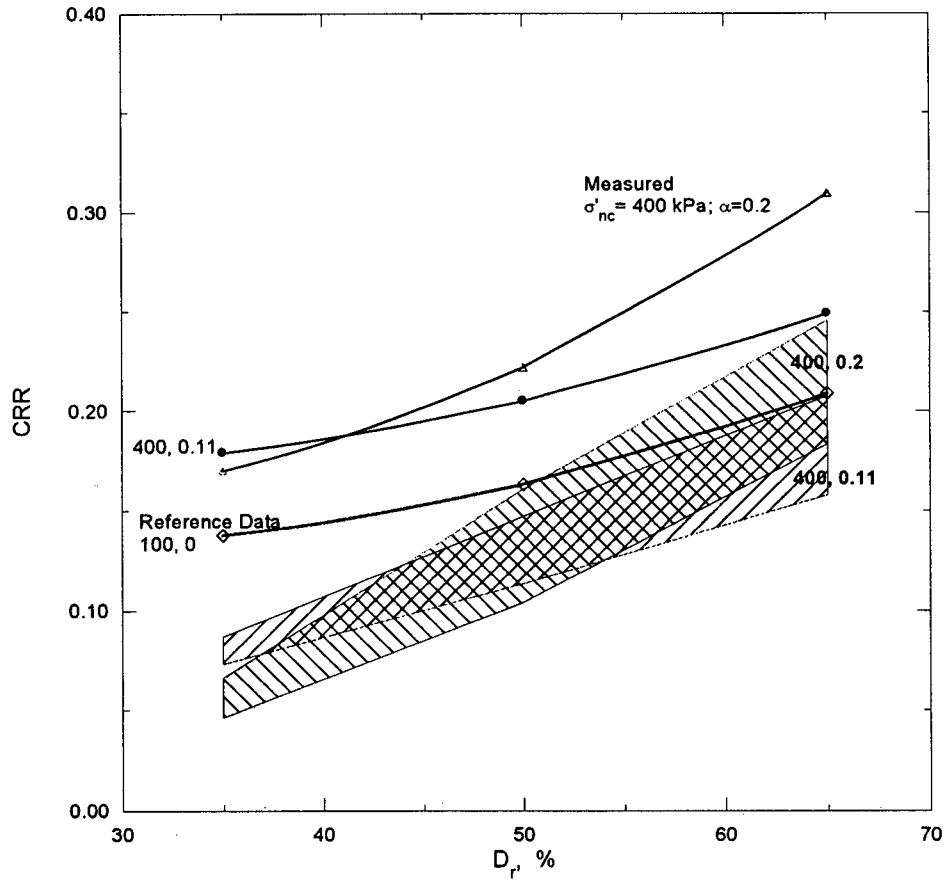

Fig. 4.28 Measured versus predicted cyclic resistance at fixed σ'_{nc} = 400 kPa level

CHAPTER 5

CONCLUSIONS

Undrained static and cyclic loading response of saturated Fraser River sand has been studied under triaxial loading conditions over a range of confining stresses, relative densities and initial static shear. The cyclic loading response was determined at three levels of confining stresses and four levels of static shear stress. The response was examined for each initial condition over a broad range of densities and cyclic stress ratios. The results of these tests lead to the following conclusions.

1. The static compression response of the sand was slightly contractive but only at the loosest deposition density. Increasing static shear stress increased the degree of contractivness, as did increasing the confining stress.

2. The static extension unloading response was contractive over a much greater range of densities than in compression.

3. The shear strength at phase transformation/steady state ($S_{PT/SS}$) is a function of the consolidated density, the mean normal confining stress and mode of loading. In extension the strength is reduced to about half the value in compression at higher densities, but at low densities it is only a fraction of the compression values. The span of void ratios over which the contractive response was noted in compression is much smaller than in extension. The

response is independent of the manner of loading, static and cyclic in both extension and compression. For a given deformation mode, it however is not a function of void ratio alone, but dependent in addition on the confining stress level.

4. In cyclic loading the effect of increasing the confining stress at a given static bias generally decreased the resistance to liquefaction. However at the loosest states the increase in confining stress had little effect.

5. The increase in the static shear stress at a given confining stress initially increased the cyclic resistance at low static shear levels, but further increase in static shear decreased it for the loosest state.

6. The rate of increase in the resistance to liquefaction as a function of relative density was much higher at the high static bias.

7. K_σ*K_α factor is grossly underestimated for the sand tested, by the K_α, K_σ factors proposed by Seed and Harder (1990) at all relative density states, regardless of the confining stress and static shear stress levels. The degree of conservatism implied by the current methods of taking confining and static shear stresses into account is too high, and most pronounced for loose density states. The Seed and Harder suggestions tend to approach the measured values as the density increases.

REFERENCES

Andersen, K. H., Pool, J. H., Brown, S. F. and Rosenbrand, W. F. (1980). "Cyclic and static laboratory tests and Drammen Clay," Journal of Geotechnical Engineering Division, ASCE, Vol. 106, No. GT5, pp. 499-529.

Brown, S. F., Lashine, A. K. F. and Hyde, A. F. I. (1975) "Repeated load triaxial testing of a silty clay," Geotechnique, Vol. 25, No. 1, pp. 95-114.

Casagrande, A. (1976). "Liquefaction and cyclic deformation of sands – a critical review." Harvard Soil Mechanics Series, No. 88, Cambridge, Mass., Jan.

Casagrande, A. (1975), "Liquefaction and cyclic deformation of sands, A critical review", Proceedings of the fifth American Conference on Soil Mechanics and Foundation Engineering, Buenos Aires, Vol. 5, pp 79-123

Castro, G. (1969). "Liquefaction of Sands," PhD Thesis, Harvard Univ., Cambridge, Mass.

Castro, G. (1975). "Liquefaction and cyclic mobility of saturated sands," Journal of the Geotechnical Engineering Division, ASCE, Vol. 101, GT-6, pp. 551-569.

Castro, G. and Poulos, S. J., (1977). "Factors affecting liquefaction and cyclic mobility." Proc. ASCE, Vol. 103, No. GT6, pp. 501-516.

Castro, G., Poulos, S. J., France, J.W., and Enos, J. L. (1982). "Liquefaction induced by cyclic loading," Geotechnical Engineers, Inc. Report Submitted to National Science Foundation, March.

Chern, J. C. (1981). "Effects of static shear on resistance to Liquefaction," M.A.Sc. Thesis, The University of British Columbia, Vancouver.

Chern, J. C., (1985), "Undrained response of saturated sands with emphasis on liquefaction and cyclic mobility", PhD Thesis, The University of British Columbia, Vancouver,

Garrison, R.E., Luternauer, J.L., Grill, E.V., MacDonald, R.D., and Murray, J.W., (1969). "Early Diagenetic Cementation of Recent Sands, Fraser River Delta, British Columbia Sedimentology," Vol. 12, pp. 27-46.

Hasegawa, T., Uchida, K. and Tateishi, T. (1981). "Dynamic strength of a soil subjected to initial shear stress," Trans. JSIDRE, No. 94, pp. 61-71.

Hasegawa, T., Uchida, K. and Tateishi, T. (1982). "Dynamic critical line of a soil subjected to initial shear stress," 17th Japan Conference on Soil Mechanics and Foundation Engineering, Naha, Okinawa, pp. 1589-1592.

Houston, W. H. and Herrmann, H. G. (1980). "Undrained cyclic strength of marine soils," Journal of Geotechnical Engineering Div., ASCE. Vol. 106, No. GT6, pp. 691-712.

Kuerbis, R. H. (1989). "Effects of gradation and fines content on the undrained response of sand," M.A.Sc. Thesis, The University of British Columbia, Vancouver.

Lee, K. L. and Seed, H. B. (1967). "Dynamic strength of anisotropically consolidated sand." Journal of the Soil Mechanics and Foundations Division, ASCE, Vol. 93, SM 5, pp. 169-190.

Lee, K. L., et al. (1975) "Properties of soil in the San Fernando hydraulic fill dams," Journal of Geotechnical Engineering, ASCE, Vol. 101, No. 8, pp. 801-821.

McRoberts, E. C. and Sladen, J.A., (1992). "Observations on static and cyclic sand – liquefaction methodologies," Can. Geotechnical Journal, Vol. 29, pp. 650-665.

Mohamad, R. and Dobry, R. (1986). "Undrained monotonic and cyclic strength of sand," Proc. ASCE, Vol. 112, No. GT10, pp. 941-958.

National Research Council (NRC). (1985), "Liquefaction of soils during earthquakes." Rep. No. CETS-EE-001 Nat. Acad. Press, Washington, D.C.

Negussey, D., Wijewickreme, W. K. D., and Vaid, Y. P., (1988), Constant-volume friction angle of granular materials., Canadian Geotechnical Journal, Vol 25, No. 1, pp 50-55.

Oda, M. (1972), "Initial fabrics and their relations to mechanical properties of granular material." Soils and Foundation, Tokyo, Japan, Vol. 12, No. 1, pp. 17-36

Ohara, S. and Matsuda, H. (1978). "Dynamic shear strength of saturated clay," Proc. JSCE, No. 274, pp. 69-78.

Seed, H. B. (1983). "Earthquake resistant design of earth dams." Proc. Symp. On Seismic Design of Embankments and Caverns, ASCE, pp. 41-64.

Seed, H. B. and Lee, K. L. (1966). "Liquefaction of saturated sands during cyclic loading." Journal of the Soil Mechanics and Foundation Division, ASCE, Vol. 92, SM 6, pp. 105-134.

Seed, H. B., Lee, K. L., Idriss, I. M. and Makdisi, F. (1973). "Analysis of the slides in the San Fernando dams during the earthquake of February 9, 1971," Report No. EERC 73-2, Earthquake Engineering Research Center, University of California, Berkeley California.

Seed, H. B., Mori, K. and Chan, C. K. (1975). "Influences of seismic history on the liquefaction characteristics of sands," Report No. EERC 75-25, Earthquake Engineering Research Center, University of California, Berkeley, California.

Seed, H. B., (1979), "Soil liquefaction and cyclic mobility evaluation for level ground during earthquakes", ASCE Journal of the Geotechnical Engineering division, Vol. 105, NO. GT2, pp. 201-255

Seed, R. B., and Harder, L. F., (1990). "SPT-based analysis of cyclic pore pressure generation and undrained residual strength." Seed Memorial Symp, BiTech Publ., Vancouver. Canada. pp. 351-376.

Toki, S. and Kitago, S. (1974). "Strength characteristics of dry sand subjected to repeated loading," Soils and Foundations, Vol. 14, No. 3, pp. 25-39.

Uchida, K. and Hasegawa, T., (1986). "Strength deformation characteristics of a soil subjected to an initial shear stress," Soils and Foundations, Vol. 26, No. 1, pp. 11-24.

Vaid, Y. P. and Chern, J. C.,, (1983a). "Effect of static shear on resistance to liquefaction." Soils and Foundations, Vol. 23, No 1 pp. 47-60.

Vaid, Y. P. and Chern, J. C., (1983b). "Mechanism of deformation during cyclic undrained loading of saturated sands", Soil Dynamics and Earthquake Engineering, Vol. 2 No. 3, pp. 171-176.

Vaid, Y. P. and Chern, J. C., (1985). "Cyclic and monotonic undrained response of sands", Proc. Advances in the Art of Testing Soils under cyclic loading conditions, Detroit, pp. 171-176.

Vaid, Y. P., Chung, E. K. F. and Kuerbis, R. (1989). "Preshearing and undrained response of sand." Soils and Foundation, Vol. 29, No. 4, pp. 49-61.

Vaid, Y. P., Chung, E. K. F. and Kuerbis, R. (1990). "Stress path and steady state." Canadian Geotechnical Journal, Vol. 27, No. 1 pp. 1-7.

Vaid, Y. P., Fisher, J. M., Kuerbis, R. H., and Negussey, D., (1990), "Particle gradation and liquefaction", ASCE Journal of Geotechnical Engineering, Vol 116, No. 4, pp. 698-703.

Vaid, Y. P. and Finn, W. D. L., (1978). "Static shear and liquefaction potential", ASCE Journal of the Geotechnical Engineering division, Vol. 105, No. GT10, pp. 1233-1246.

Vaid, Y. P. and Negussey, D. (1984). "Relative density of pluviated sand samples," Soils and Foundations, Vol. 24, No. 2, pp. 101-105.

Vaid, Y. P. and Negussey, D. (1988). "Preparation of reconstituted sand specimens." In Advanced triaxial testing of soils and rocks. American Society for Testing and Materials, Special Technical Publication 977, pp. 119-131.

Vaid, Y.P. and Sivathayalan, S (1996), "Static and cyclic liquefaction potential of Fraser Delta sand in simple shear and triaxial tests", Canadian Geotechnical Journal, Vol 33, No.2, pp. 281-289.

Vaid, Y. P. and Sivathayalan, S. (1996). "Errors in estimates of void ratio of laboratory sand specimens". Canadian Geotechnical Journal, Vol 33, No. 6, pp. 1017-1020.

Vaid, Y. P. and Thomas, J., (1995), "Liquefaction and post liquefaction behaviour of sand", ASCE Journal of Geotechnical Engineering, Vol 121, No. 2, pp 163-173.

Yasuhara, K., Yamanouchi, T. and Hirao, K. (1982). "Cyclic strength and deformation of normally consolidated clay," Soils and Foundations, Vol. 22, No. 3, pp. 77-91.

Yoshimi, Y. and H. Oh-Oka (1975). "Influence of degree of shear stress reversal on the liquefaction potential of saturated sand," Soils and Foundations, 15, No. 3 pp. 27-40

Appendix A

Cyclic Resistance curves e_c vs N of Fraser river sand at σ'_{nc} = 200 and 400 kPa.

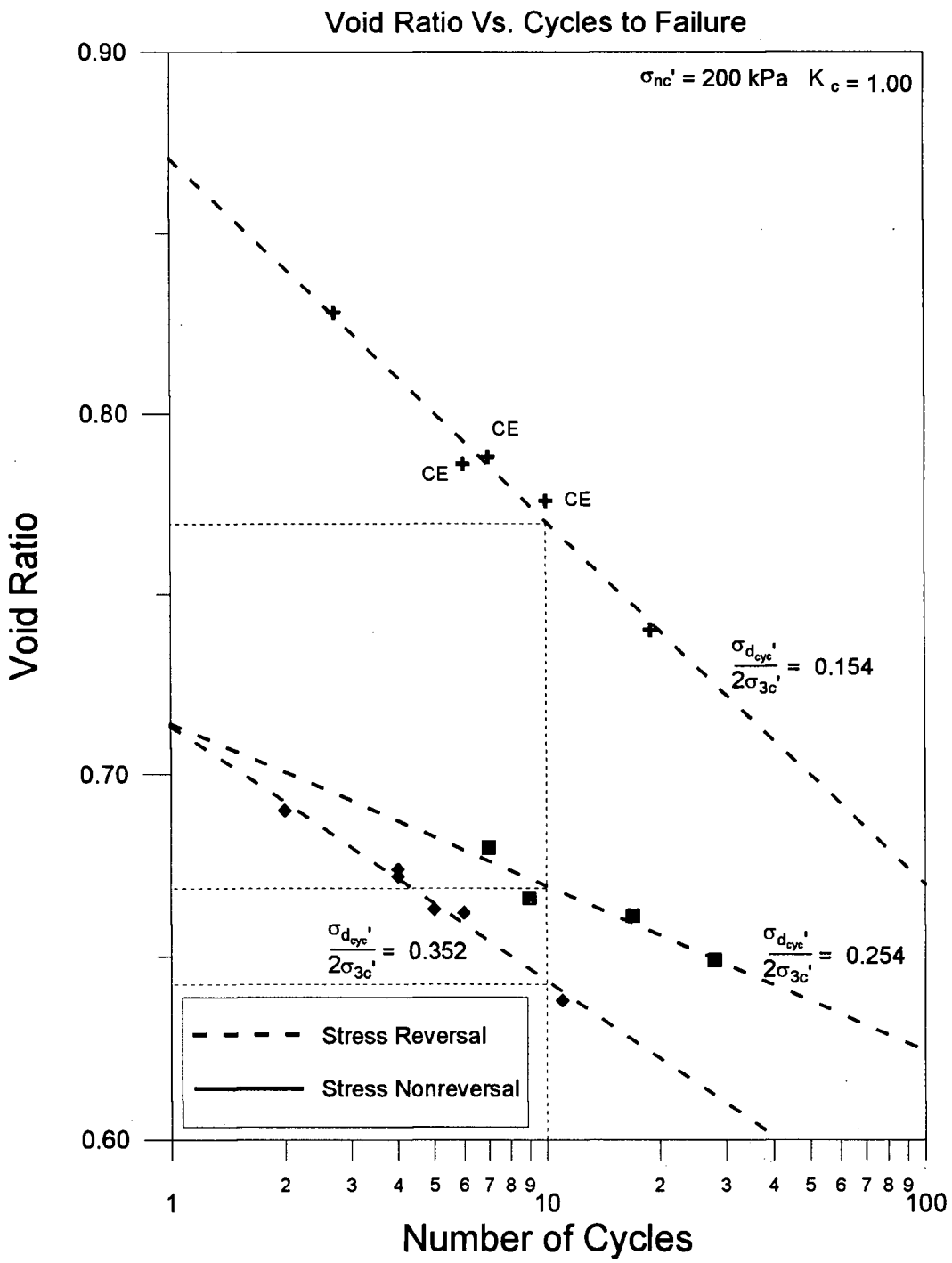

Fig. A1 Cyclic resistance curves e_c vs N for σ'_{nc} = 200 kPa and K_c = 1.00

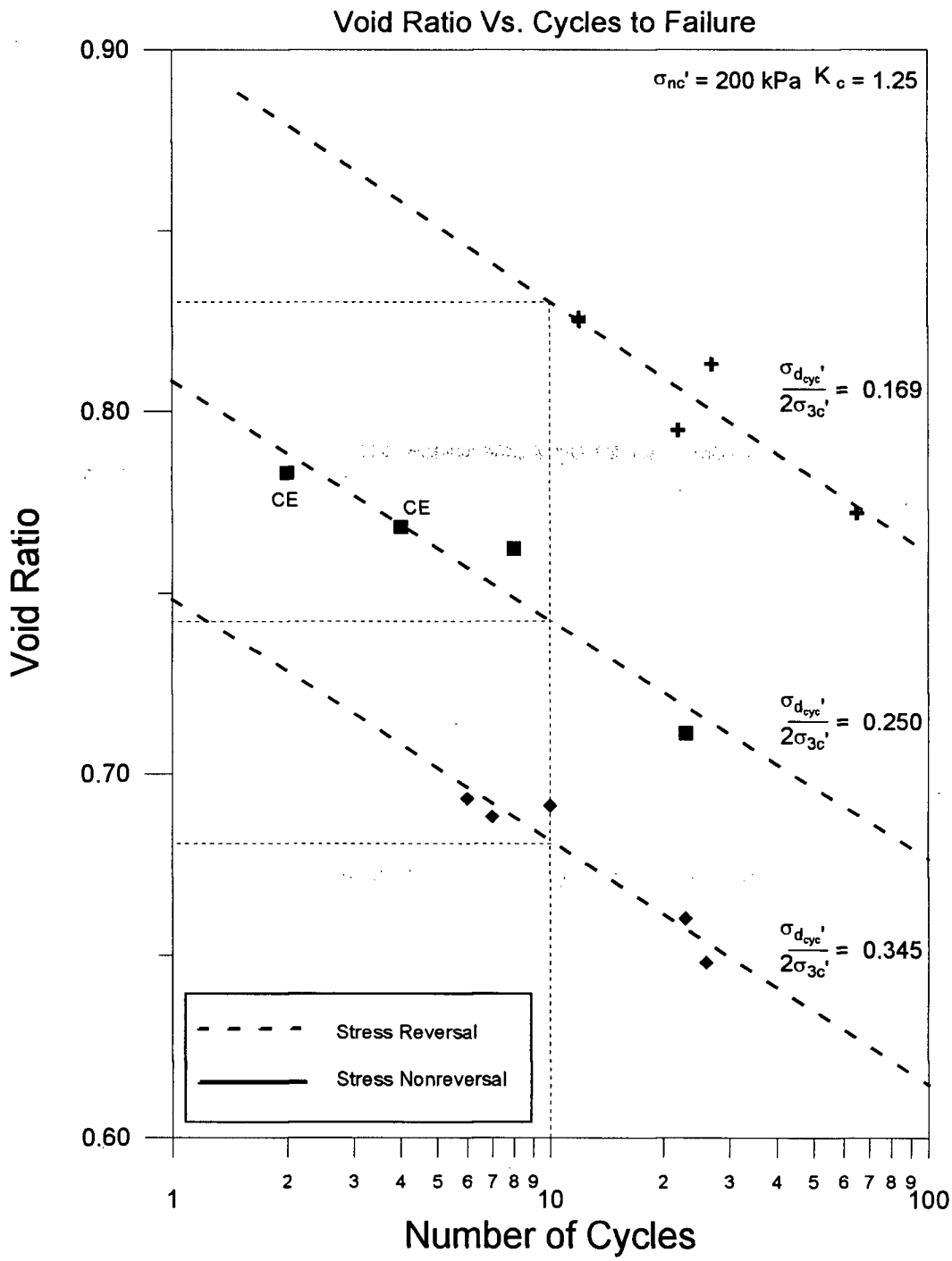

Fig. A2 Cyclic resistance curves ec vs N for σ'_{nc} = 200 kPa and K_c = 1.25

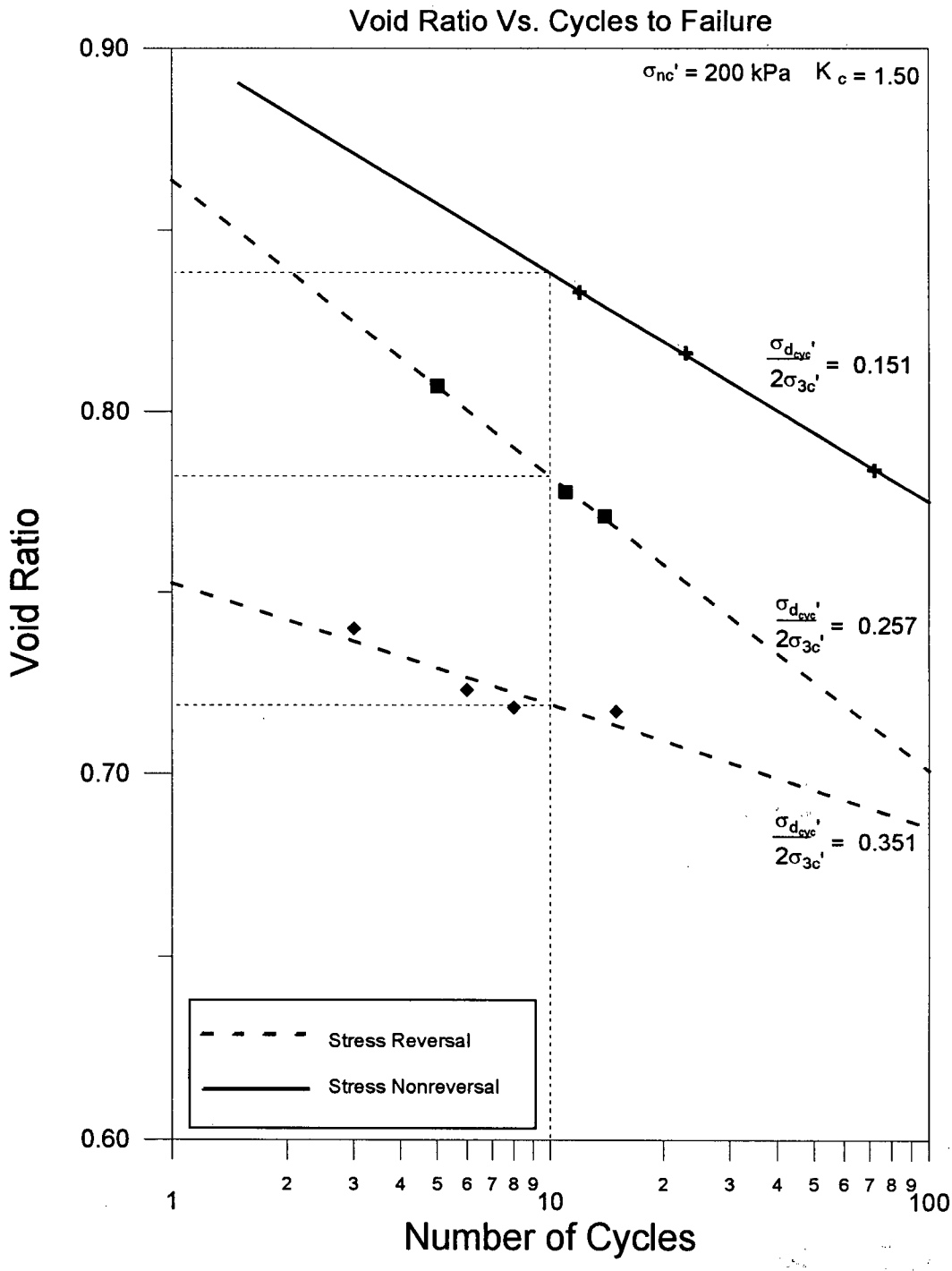

Fig. A3 Cyclic resistance curves ec vs N for σ'_{nc} = 200 kPa and K_c = 1.50

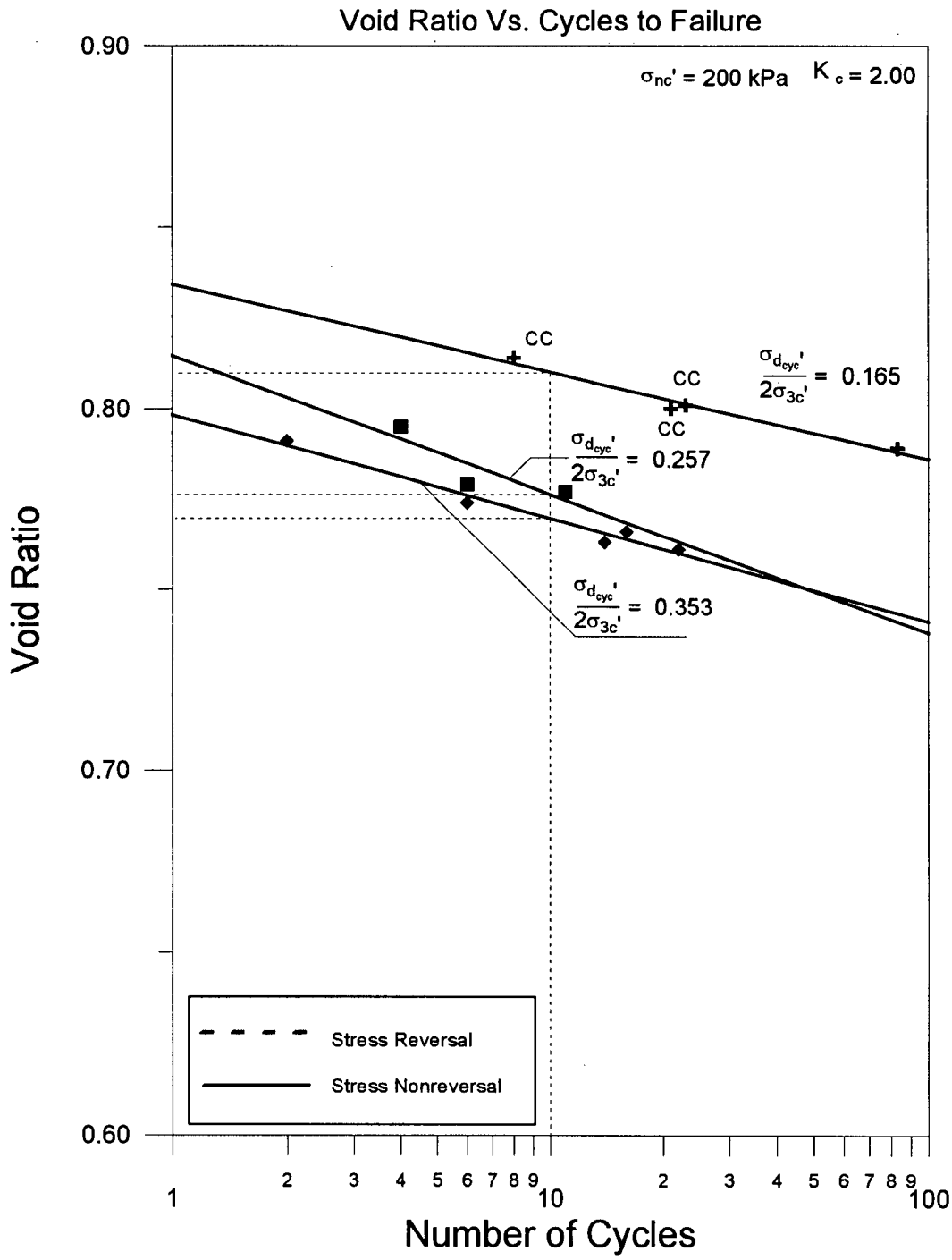

Fig. A4 Cyclic resistance curves ec vs N for σ'_{nc} = 200 kPa and K_c = 2.00

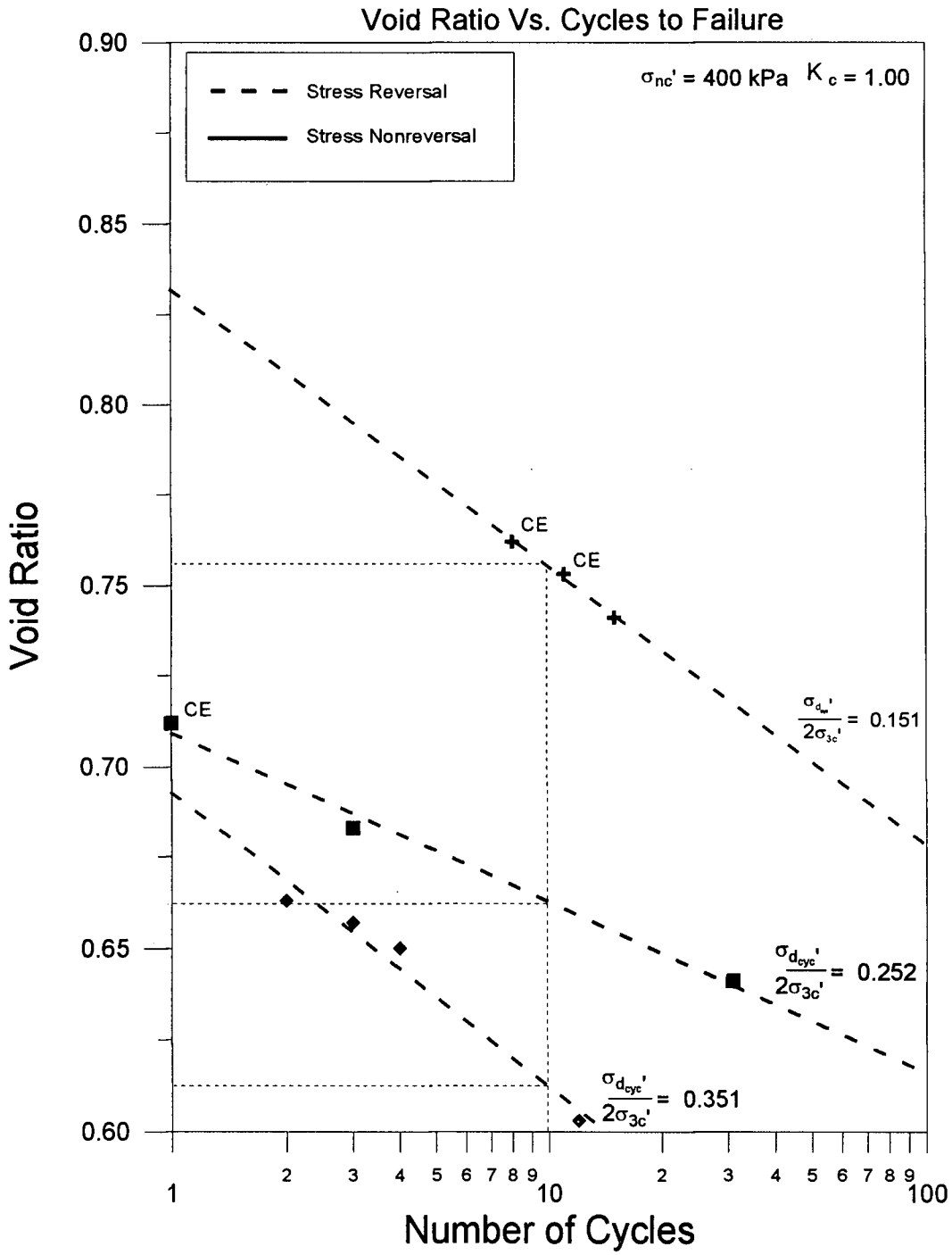

Fig. A5 Cyclic resistance curves ec vs N for σ'_{nc} = 400 kPa and K_c = 1.00

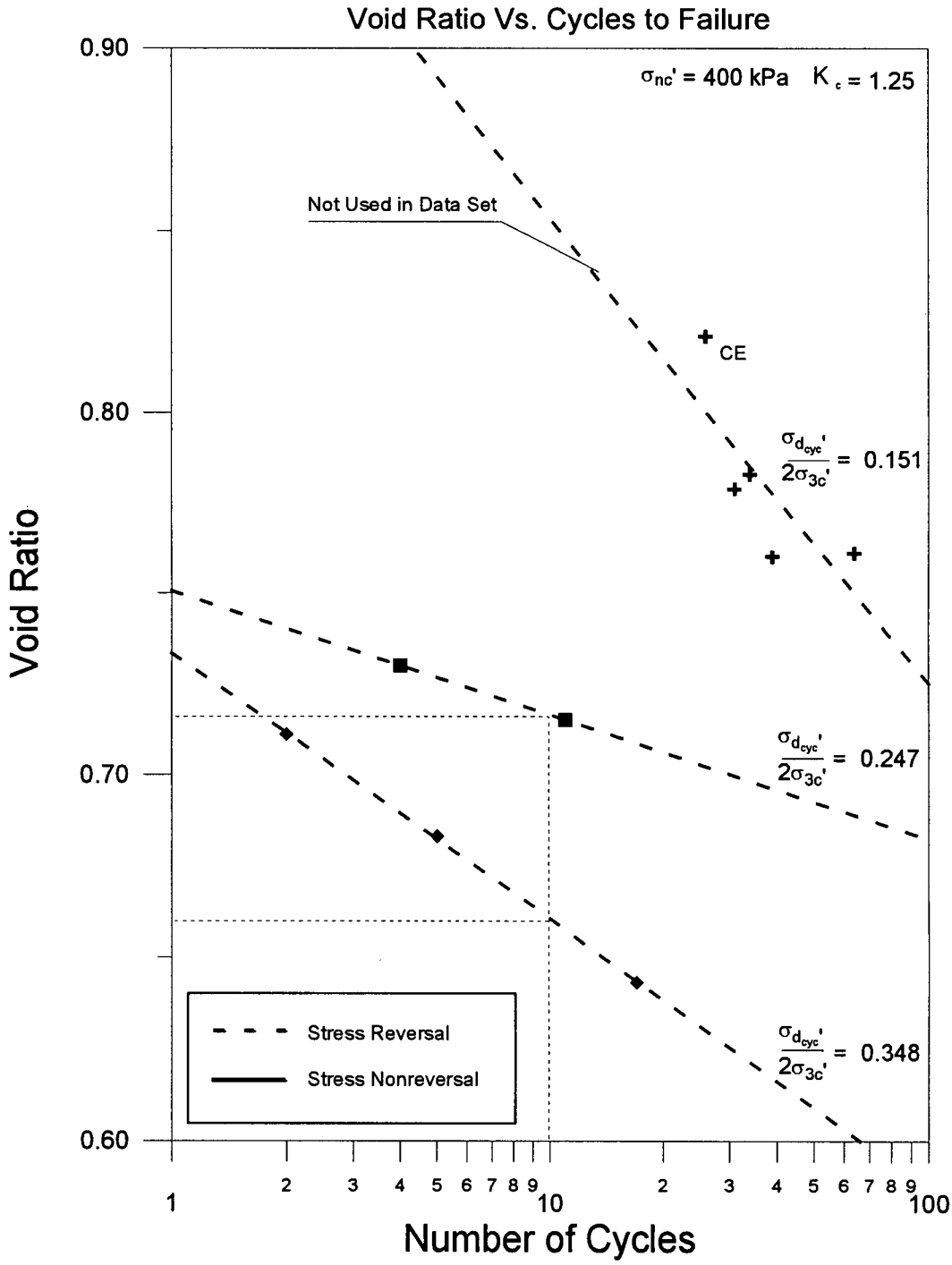

Fig. A6 Cyclic resistance curves ec vs N for σ'_{nc} = 400 kPa and K_c = 1.25

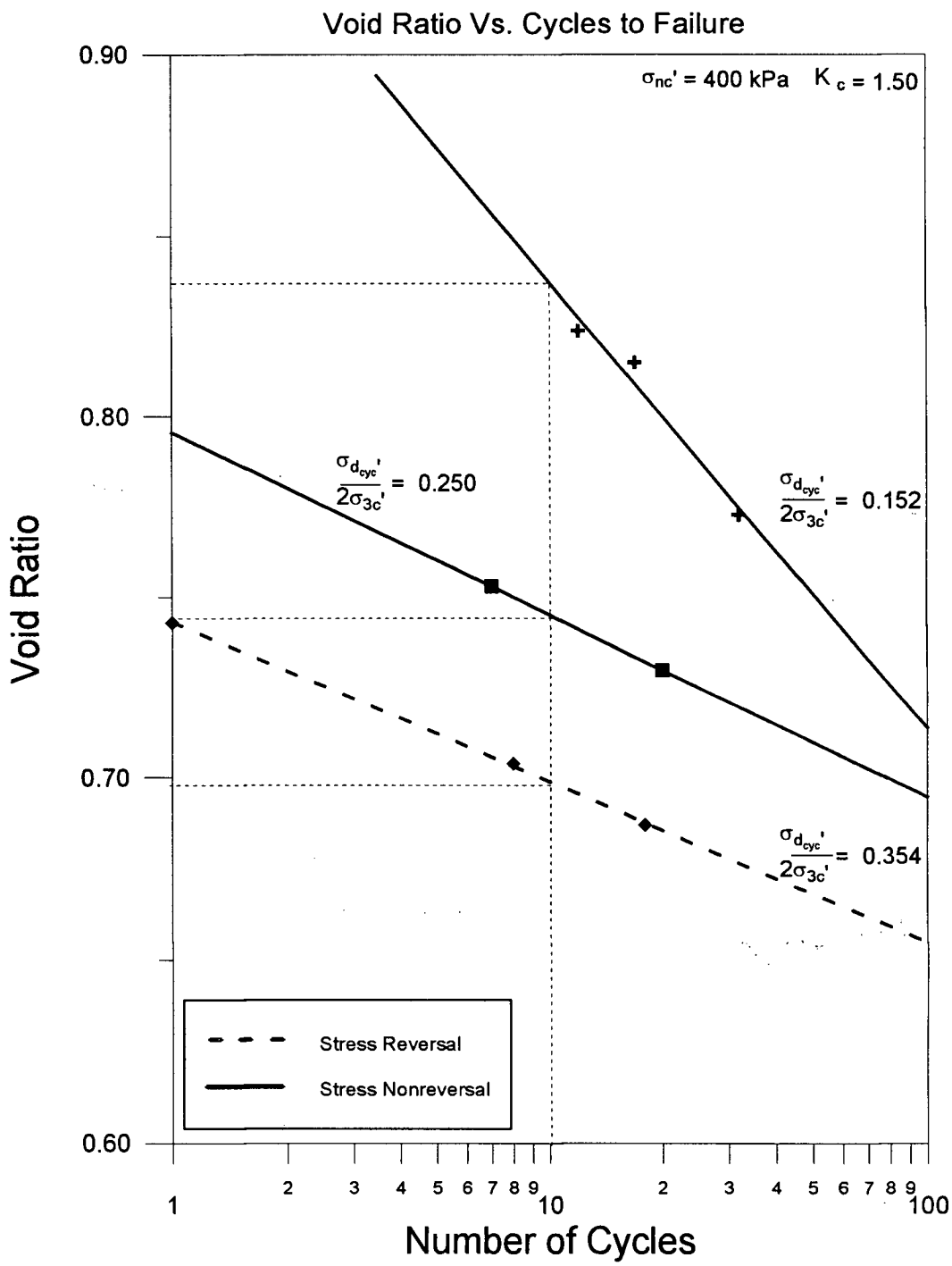

Fig. A7 Cyclic resistance curves ec vs N for σ'_{nc} = 400 kPa and K_c = 1.50

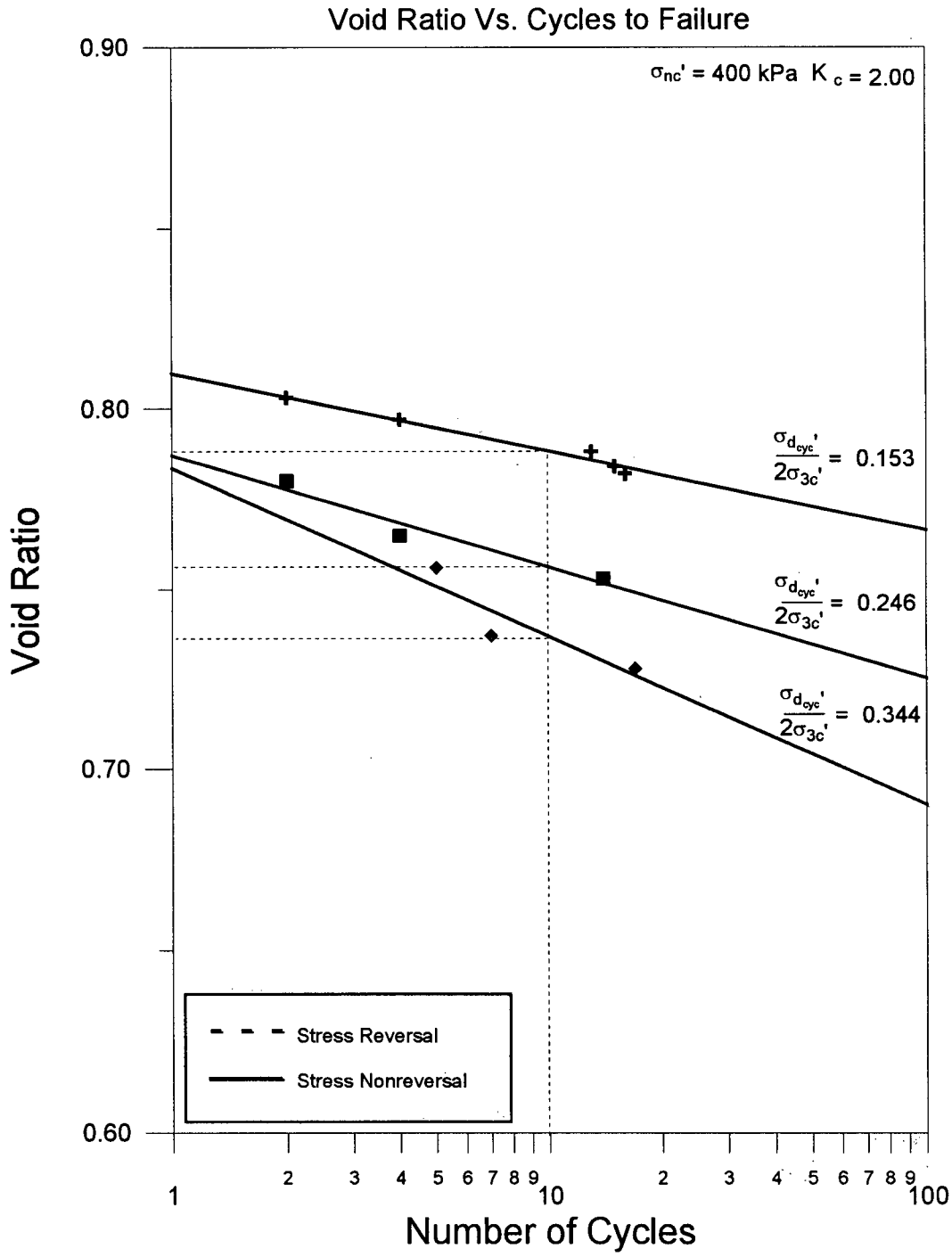

Fig. A8 Cyclic resistance curves ec vs N for σ'_{nc} = 400 kPa and K_c = 2.00